

NORTHWESTERN UNIVERSITY

Small Molecule Activation by Metalloporphyrin Complexes Isolated within Metal-Organic
Frameworks

A DISSERTATION

SUBMITTED TO THE GRADUATE SCHOOL
IN PARTIAL FULFILLMENT OF THE REQUIREMENTS

for the degree

DOCTOR OF PHILOSOPHY

Field of Chemistry

By

Audrey Theresa Gallagher

EVANSTON, ILLINOIS

December 2017

© Copyright by Audrey Theresa Gallagher 2017, except where otherwise noted.

All Rights Reserved

ABSTRACT**Small Molecule Activation by Metalloporphyrin Complexes Isolated in Metal-Organic Frameworks**

Audrey Theresa Gallagher

Contained in the following dissertation are detailed investigations regarding the thermodynamics of small molecule activation by metalloporphyrin complexes isolated within metal-organic frameworks (MOFs). Chapter 1 provides a description of the role metalloporphyrin complexes play in biological systems and the challenges associated with studying small molecule activation by metalloporphyrin sites in both the protein's native structure as well as molecular model complexes. This chapter culminates with a description of how an alternative material platform, a MOF, offers the opportunity to access species that have confounded isolation and thorough investigations in molecular form.

Chapters 2 and 3 focus on the study and characterization of low-coordinate metalloporphyrin O₂ adducts featuring iron and cobalt, respectively. Importantly, these results provide the first structurally-characterized five coordinate Fe–O₂ and Co–O₂ porphyrin species, further highlight the importance of axial ligation in biological O₂ transport and storage, and demonstrate the ability of a MOF to enable isolation and study of species that are highly unstable in molecular form. Chapter 4 employs the same approach to isolate a four-coordinate manganese(II) porphyrin complex and examine its reactivity with O₂ using a myriad of characterization techniques. X-ray diffraction experiments reveal for the first time a peroxomonaganese(IV) porphyrin species, which exhibits a side-on, η^2 binding mode. Further, quantification of the interaction of O₂ with manganese(II), iron(II), and cobalt(II) porphyrin complexes demonstrate that O₂ binding

enthalpy increases with increasing reductive capacity of the $M^{II/III}$ redox couple. Chapter 5 details the comprehensive characterization of highly-labile carbonyl adducts of cobalt porphyrin complexes. Importantly, this work provides the first crystallographic characterized example of a noniron first-row transition metal porphyrin complex. The combination of these four chapters provides not only key biological insight regarding the thermodynamics of small molecule activation by metalloporphyrin centers, but also, unprecedented characterization, particularly in the form of single crystal X-ray diffraction analysis, of species that have only been observed transiently in molecular form. Chapters 6 and 7 suggest next directions in the form of potential synthetic-pathways that can lead to the isolation and study of reactive metalloporphyrin complexes capable of carrying out group atom transfer chemistry. The combination of the results reported herein demonstrate that the sequestration of metalloporphyrin moieties within the solid-state architecture of MOFs provides access to a wide a range of novel coordination complexes.

ACKNOWLEDGEMENTS

I first thank my research advisor, Professor Dave Harris, who has been the single most important contributor to my success in graduate school. I am grateful both for the opportunity to build a research group under his guidance as well as the invaluable lessons he has taught me ranging from chalkboard lessons on ligand-field theory to the art of give a motivational (and of course, cheesy) speech. In addition to his roles as an academic advisor, I'd like to thank Dave for assembling "The Team" for whom I am happy to have spent half a decade (all of which will be acknowledged below). I would also like to thank Professor Danna Freedman not only for serving as one my committee members over the course of these five years but also, for being an invaluable mentor, particularly in my early years of graduate school. Lastly, I owe thanks to Professor Kenneth Poppelmeier, the third member of my thesis committee, for his support during my qualifying exam, original research proposal, and thesis defense.

In the long list of people who have contributed to my intellectual and scientific development, there are two who I owe particular acknowledgment of gratitude. First, I thank Professor John Anderson. While I am sure John would cringe at the prospect of being personally recognized here, he deserves credit for teaching me an immeasurable amount of chemistry both during and after his time in the lab, and for doing so with an admirable amount of patience. On another note, I am also grateful to John for reminding of the importance of humility by providing me with opportunity to be the brunt of the vast majority of his jokes (although I'd like to think I got a couple in myself from time-to-time). Secondly, I would like to thank Professor Joseph Zadrozny. I am happy to have had Joe as both a mentor and a friend during graduate school. Joe's positive attitude, enthusiasm for science, and philosophical rants made every day

interesting, entertaining, and even at times (believe it or not), fun.

There are few people that have had to put-up with me for more years than anyone. I would like to thank my family, particularly my parents Tim and Linda Gallagher. Whose support, love, and guidance is the single greatest contribution to any and all of my achievements. I also cannot forget my three favorite siblings, Aaron Gallagher, Andrew Gallagher, and Michelle Gallagher. Thank for you for being my first and best friends. I would also like to thank Paul Sanstead, whose proximity, shared experience, and support of the past five years has been tremendous contributor to my happiness during graduate school.

Lastly, I would like to thank those members of the Harris and Freedman group conglomerate (Hardman or Frarris, whichever suits you) who have been constant during my graduate experience. From the Harris group, Professor John Anderson, Jordan DeGayner, Arash Banisafar, Kang Du, Alex Gaudette, Professor Ie-Rang Jeon, and Maggie Kelty. From the Freedman group Samantha Clarke, Dr. Michael Graham, Dr. James Walsh, Prof. Joe Zadrozony and Scott Coste (left pillar) and Majed Fataftah (right pillar). I will certainly miss all of you.

To my grandparents, Lee and Gerry Gallagher

Table of Contents

ABSTRACT.....	3
ACKNOWLEDGEMENTS.....	5
LIST OF FIGURES	10
Chapter 1: Introduction.....	12
1.1 Metalloporphyrin Centers in Biology and Molecular Model Complexes	12
1.2 Metal-Organic Frameworks.....	13
1.3 Porphyrin Zirconium-Based Metal Organic Framework.....	14
1.4 Sequestration of Metalloporphyrin Sites in Metal-Organic Frameworks.....	16
Chapter 2: A Five-Coordinate Heme Dioxygen Adduct Isolated within a Metal-Organic	18
2.1 Introduction.....	19
2.2 Results and Discussion	21
2.3 Conclusion	26
Chapter 3: Dioxygen Binding at a Four-Coordinate Cobaltous Porphyrin Site in a Metal-Organic Framework: Structural, EPR and O ₂ adsorption analysis	28
3.1 Introduction.....	29
3.2 Results and Discussion	30
3.3 Conclusion	36
Chapter 4: A Structurally Characterized Peroxomanganese(IV) Porphyrin via Reversible O ₂ Binding Within a Metal-Organic Framework.....	38
4.1 Introduction.....	39
4.2 Results and Discussion	42
4.3 Conclusions.....	51
Chapter 5: CO Binding at a Four-Coordinate Cobaltous Porphyrin Site in a Metal-Organic Framework: Structural, EPR, and Gas Adsorption Analysis.....	53
5.1 Introduction.....	54
5.2 Results and Discussion	56
5.3 Conclusion	66
Chapter 6: Efforts Towards the Generation of a High-Valent Iron(V) Nitride in a Metal-Organic Framework	72
6.1 Introduction.....	72
6.2 Results and Discussion	74
6.3 Conclusion	77
Chapter 7: O ₂ Binding to a Chloride Ligated Heme Complex in Metal-Organic Framework	78
7.1 Introduction.....	78

7.2 Results and Discussion	79
7.3 Conclusion	80

List of Figures

Figure 1.1 Schematic diagram of a metal-organic framework.....	14
Figure 1.2 Crystal Structure of PCN-224.....	15
Figure 2.1 Reaction of PCN-224Fe with O ₂ at -78 °C to form PCN-224FeO ₂ displayed in the form of single crystal X-ray structures	21
Figure 2.2 O ₂ adsorption data for PCN-224Fe.....	23
Figure 2.3 Mössbauer spectra of PCN-224Fe and PCN-224FeO ₂	25
Figure 3.1 Reaction of PCN-224Co with O ₂ at 85 K to form PCN-224CoO ₂ displayed in the form of single crystal X-ray structures	31
Figure 3.2 X-Band EPR spectra for PCN-224Co and PCN-224CoO ₂	33
Figure 3.3 O ₂ adsorption data for PCN-224Co	34
Figure 4.1 UV/Visible spectra for PCN-224, PCN-224Mn, and PCN-224Mn in toluene.....	42
Figure 4.2 Diffuse reflectance infrared spectra of PCN-224Mn and PCN-224MnO ₂	43
Figure 4.3 Reaction of PCN-224Mn with O ₂ to form PCN-224MnO ₂ displayed in the form of single crystal X-ray structures	45
Figure 4.4 X-band EPR data for PCN-224Mn activated and suspended in toluene and toluene/pyridine solvent mixtures.....	47
Table 4.1 Selected EPR parameters corresponding to simulated EPR spectra for PCN-224Mn species	47
Figure 4.5 X-band EPR spectra for PCN-224Mn and PCN-224MnO ₂	48
Figure 4.6 O ₂ adsorption data for PCN-224Mn	50
Figure 5.1 Variable temperature diffuse reflectance spectra for PCN-224Co and CO.....	55
Figure 5.2 Reaction of PCN-224Co with CO at 8 K to form PCN-224Co(CO) ₂ displayed in the form of single crystal X-ray structures	56
Table 5.1 Selected crystallographic parameters for variable temperature single crystal X-ray diffraction analysis collected on PCN-224Co in the presence of CO.....	58

Figure 5.3 Reaction scheme displaying the reversible binding of CO to PCN-224Co to form mono- and di- carbonyl adducts.....	58
Figure 5.4 Variable temperature X-band EPR spectra for activated PCN-224Co ^{II} before and after the addition of CO.....	60
Figure 5.5 Experimental and simulated X-band EPR spectra for PCN-224Co ^{II} dosed with ca. 1 atm CO at 125 K and 12 K.....	61
Table 5.2 Variable temperature parameters corresponding to simulated EPR spectra for PCN-224Co ^{II} in the absence and presence of CO.....	61
Figure 5.6 CO adsorption data for PCN-224Co.....	63
Figure 6.1 Frontier orbitals of an iron(V) nitride in four and three-fold symmetry	72
Figure 6.2 Mössbauer spectra and corresponding fit parameters for PCN-224FeCl, PCN-224FeN ₃ , and the thermolysis product of PCN-224FeN ₃	74
Figure 6.3 Infrared spectra for PCN-224FeCl, PCN-224FeN ₃ , and the thermolysis product of PCN-224FeN ₃	75
Figure 7.1 Depiction of a 4-coordinate, imidazole, and chloride ligated heme center with the corresponding $\Delta E_{1/2}$ (V vs SCE) for each species.....	78
Figure 7.2 Mössbauer spectra and corresponding fit parameters of PCN-224FeCl and PCN-224Fe ^{II} Cl ⁻ at 80 K.....	79

Chapter 1: Introduction

1.1 Metalloporphyrin Centers in Biology and Molecular Model Complexes

Metalloporphyrin centers are intimately involved in a number of biological processes including O₂ transport and storage, electron transport, catalysis, sensing, cell adhesion, and neurotransmission.¹ The ubiquity of metalloporphyrin-based proteins in biology have rendered them an intense topic of investigation, with a goal of elucidating structure, function, and mechanistic insight into their various biological functions. The versatility of these proteins is largely dependent upon the ability of the reaction center to discriminate and selectively activate small molecule substrates, particularly diatomic gaseous signaling molecules such as O₂, CO, and NO.¹ As such, significant research efforts have focused on understanding the factors that influence small molecule activation and how this gives rise to the diverse biological processes carried out by metalloporphyrin-based proteins. A crucial consideration towards understanding these systems involves elucidating the impact the electronic structure of both the metal center and gaseous molecule has on the thermodynamics of substrate activation.

In nature, the metalloporphyrin sites are embedded within a protein superstructure, which serves to prohibit the metalloporphyrin active sites from engaging in unwanted side reactivity.² However, the complexity of the surrounding protein matrix restricts access to the metalloporphyrin center and therefore limits the study of substrate activation within the protein's native structure. Owing to this limitation, the last several decades have seen a number of researchers turn towards the development of molecular model complexes featuring a porphyrinate ligand that mimics the local coordination environment of the active site.³ The simplicity of molecular model complexes provides a method to directly probe changes to the

metal center upon substrate binding using straight forward and conventional characterization techniques.

Towards this aim, a number of researchers have sought to study small molecule activation using molecular metalloporphyrin model complexes.⁴ Indeed, these efforts have resulted in a myriad of physical characterizations and have improved our understanding into the nature of substrate activation by metalloporphyrin centers. Nevertheless, these studies have often not been straightforward due to interference from solution effects such as bimolecular reactions, axial ligand ligation, and solvent/solute interactions involving the porphyrin ligand.⁵ As such, the study of small molecule activation by metalloporphyrin centers is often limited to spectroscopic characterization at low temperature, primarily within frozen gas matrices. A key challenge, particularly in regards to the study of gaseous substrate binding, involves the inability to access low-coordinate unsaturated molecular metalloporphyrin centers in solution, which impedes gas binding and a thorough investigation into the thermodynamics of substrate activation.

One way to overcome these challenges is to embed reaction centers within a porous extended solid. Here, the rigid superstructure provided by the solid-state architecture immobilizes the metal centers, preventing participation in deleterious side reactivity. Further, anchoring the metalloporphyrin centers within a solid-state structure enables gas-phase reactions, thereby eliminating the formation of unwanted side products or interference from solvent molecules. An ideal platform for this study is an emerging class of materials known as metal-organic frameworks (MOFs).

1.2 Metal-Organic Frameworks

Metal-organic frameworks (MOF) are a porous crystalline class of materials composed of metal-

based nodes, typically single ions or clusters of ions, connected through organic bridging ligands to form highly ordered, crystalline lattices (Figure 1.1). Owing to their large internal surface areas and design flexibility, these materials have been investigated for a variety of applications including gas storage,⁶ gas separation,⁷ sensing,⁸ ionic and electronic conductivity,⁹ drug delivery¹⁰ and catalysis.¹¹ While MOFs have been extensively studied for these various applications, they have received considerably less attention for the investigation of small molecule activation at unsaturated metal centers. Nevertheless, they are an ideal platform for this study as their porous structure enables removal of exogenous solvent and therefore, heterogeneous gas phase reaction chemistry. Further, their inherent crystallinity provides a means to probe substrate activation by the metal center using X-ray diffraction techniques.

1.3 Porphyrin Zirconium-Based Metal Organic Framework

The emerging field of MOF chemistry has been accompanied by an advent of novel structural architectures featuring a diverse range of ligand sets and inorganic nodes. A subclass of metal-organic frameworks that are of particular interest are those featuring porphyrinic organic struts and Zr^{IV} oxo-cluster-based inorganic nodes.¹² Indeed, over ten distinct structures featuring

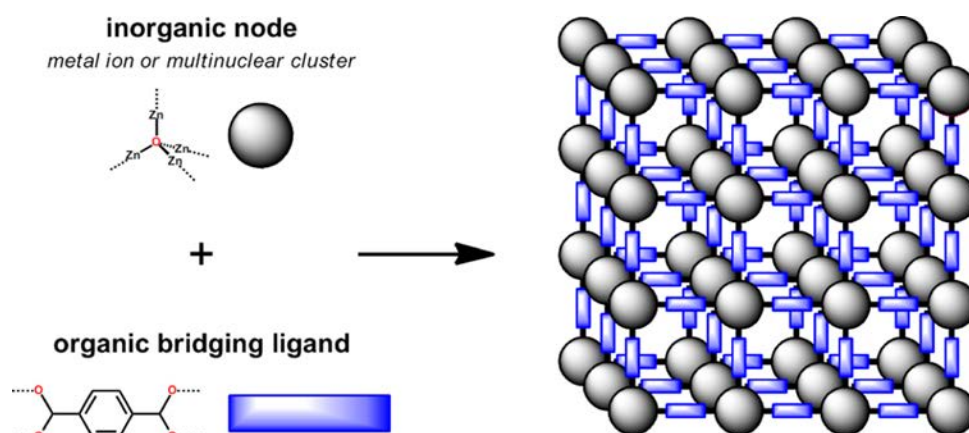


Figure 1.1 Schematic diagram of a metal-organic framework featuring the inorganic nodes (grey spheres) and organic bridging ligands (blue rod) that form a 3D highly order porous structure.

porphyrinic zirconium MOFs have been reported. The significance of these structure types relates to both the biological and catalytic activity of metalloporphyrins as well as the stability of the Zr^{IV} oxo-cluster-based inorganic node. The development of structure types featuring Zr^{IV} oxo-cluster-based inorganic nodes, first reported in the UiO-66 family of MOFs, is a notable advancement in the field of MOF chemistry.¹³ This cluster imparts increased stability to the frameworks especially when compared to other MOFs, enabling the exploration of a wide range of chemistry that require more extreme reaction conditions.¹⁴ While porphyrin-based MOFs have been utilized for a variety of purposes, including gas sorption,¹⁵ catalysis,¹⁶ photosensitization,¹⁷ and photovoltaics,¹⁸ the use of the rigid architecture of MOFs to study small molecule activation of by metalloporphyrin complexes is a novel application.

For the purposes of our study, we utilize the Zr^{IV} -based metal-organic framework PCN-224, owing to several key attributes (Figure 1.2).^{12e} First, PCN-224 features tetracarboxyphenylporphyrin linkers, providing a platform in which the porphyrin centers can

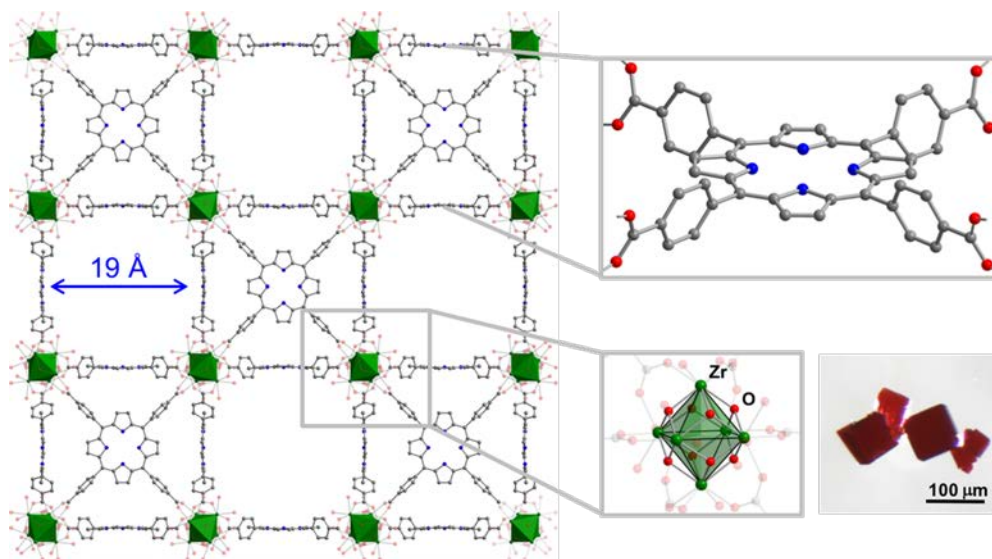


Figure 1.2 Crystal structure of PCN-224 featuring the organic porphyrin bridging ligand and Zr^{IV} cluster. Single crystals of PCN-224 are shown in the bottom right corner. Adapted from reference 12e.

be isolated in a porous, extend solid. The inorganic nodes of this framework consist of highly robust Zr_6O_8 clusters, rendering PCN-224 stable over a wide pH and temperature range. Additionally, we have modified the synthetic procedure to enable the isolation of large single crystals of PCN-224, providing facile structural characterization by single-crystal X-ray diffraction. This is an imperative requirement as the complexes of interest have eluded crystallographic characterization in molecular form. Furthermore, the structure of PCN-224 features large channels with a diameter of 19 Å, which facilitates heterogeneous reactions between gaseous substrates and metalloporphyrin centers. Finally, metalation of PCN-224 with Fe^{III} , Co^{II} , and Ni^{II} ions has already been reported, providing an important precedent for insertion of metal ions into the porphyrin binding pocket.

1.4 Sequestration of Metalloporphyrin Sites in Metal-Organic Frameworks

By embedding metalloporphyrin centers in modifiable 3D MOFs, this strategy offers the opportunity to access species that have confounded isolation and thorough investigations in molecular metalloporphyrin complexes. Importantly, this strategy lies at the interface of molecular and materials chemistry and offers key advantages of both. The general ease of characterization as well as the synthetic tunability of MOFs parallels the simplicity of molecular systems, where site-specific access to the metal center enables a direct study on the impact of substrate activation by the metalloporphyrin center. This method also overcomes the challenges associated with studying these complexes in molecular form, where the immobilization of the metal centers into a solid-state material platform allows study of gaseous substrate binding in the absence of competitive solution-based side reactivity. Further, MOFs permit the study and isolation of coordinatively unsaturated, redox active metal centers that not only lends itself to an

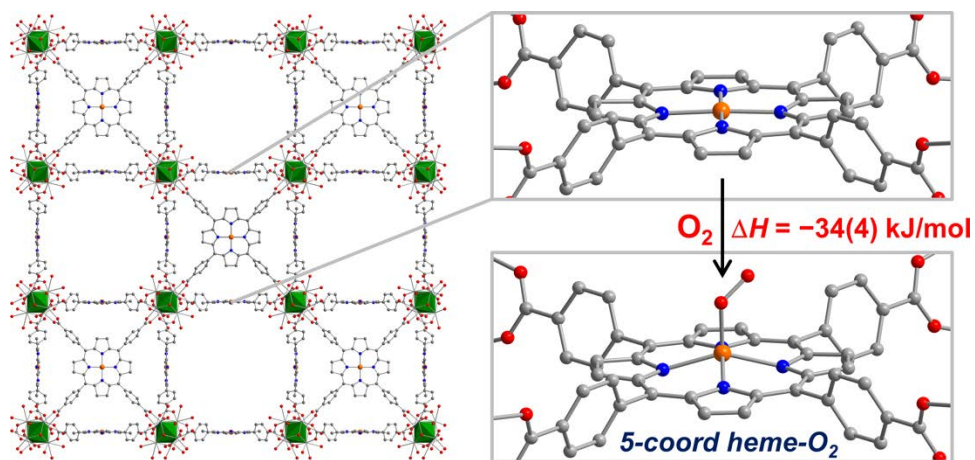
investigation of the role metalloporphyrin centers play in biological systems, but also a step towards the development of materials for selective gas binding. While substrate activation by metalloporphyrin centers has been studied extensively over the course of the past 30 years, this strategy allows a more thorough and comprehensive investigation into the understanding of substrate activation by metalloporphyrin centers, as well as access to fundamentally new coordination compounds that have eluded characterization in molecular form.

Chapter 2: A Five-Coordinate Heme Dioxygen Adduct Isolated within a Metal-Organic

Reprinted with permission from:

Anderson, J. S.; Gallagher, A. T.; Mason, J. A.; Harris, T. D. *Journal of American Chemical Society* **2014**, *136*, 16489–16492.

Copyright 2014 American Chemical Society.



2.1 Introduction

Metalloproteins featuring iron porphyrin, or heme, prosthetic groups are ubiquitous in nearly all forms of life. The heme functionality is intimately involved in a variety of biological processes, including O₂ transport and storage, electron transport, catalysis, and sensing.¹ Specifically, O₂ transport and storage mediated by the proteins hemoglobin and myoglobin, respectively, is essential to mammalian life.² The critical roles of heme proteins have rendered them a topic of intense study, primarily in order to understand the structural and electronic features that govern their functionality. Toward this end, tremendous concerted efforts have focused on the development of synthetic heme molecular model complexes that can mimic the reversible O₂ binding characteristic of globin proteins.³

The study of molecular heme dioxygen model complexes has been hampered by their instability as mononuclear complexes. In the absence of a protein superstructure, heme complexes typically undergo irreversible oxidation via bimolecular condensation reactions, ultimately forming oxo-bridged Fe^{III}₂ complexes.⁴ This obstacle prompted the development of sterically protected “picket-fence” porphyrins, which served to prevent bimolecular decomposition reactions and enabled isolation of the first examples of thoroughly characterized heme-O₂ adducts.^{3,5} These systems also enabled studies aimed toward understanding the role of axial histidine donors, present in both hemoglobin and myoglobin, in O₂ binding.⁶ Along these lines, a longstanding challenge has been the isolation and characterization of five-coordinate, or “base-free,” heme-O₂ adducts. Indeed, comparison of the O₂ binding affinity of such a species with their six-coordinate analogues would help to further elucidate the function of the axial ligand in biological heme centers. Nevertheless, despite the elegant design of other elaborate

porphyrin scaffolds,² observation of five-coordinate heme-O₂ adducts has been limited to spectroscopic evidence at low temperature, primarily within frozen gas matrices, as these species invariably undergo bimolecular decomposition or O₂ dissociation under ambient conditions.⁷

As an alternative to the above methods for isolating five-coordinate heme-O₂ adducts, we hypothesized that a heme-containing metal-organic framework (MOF) would provide an ideal platform for the isolation and study of these species, as the solid-state structure of the MOF should prevent bimolecular condensation reactions and obviate the need for solvent to enable gas-phase reactions. MOFs are particularly well-suited for this challenge over other solid-state materials, owing to their porous structure, high degree of synthetic tunability, and amenability to single-crystal diffraction studies. Moreover, while a number of research groups have found success in explorations of MOF reactivity, the vast majority of these reports have centered on catalytic activity rather than the isolation and study of reactive species.⁸ Encouragingly, numerous porphyrinic MOFs have already been reported, including those with open porphyrin ligands that can be post-synthetically metallated.⁹ Herein, we report the incorporation of a coordinatively unsaturated ferrous heme center into a MOF, and its reaction with O₂ to give a five-coordinate heme-O₂ complex. This species is structurally characterized for the first time, and combined spectroscopic and O₂ adsorption experiments reveal key features of its electronic structure and O₂ affinity.

2.2 Results and Discussion

The recently reported Zr-based porphyrinic MOF PCN-224 exhibits several attributes that are well-suited for the isolation and study of reactive species, including remarkable stability to acid and base and capacity for post-synthetic porphyrin metallation (see Figure 1).¹⁰ Using a slight modification of the reported preparation, large cubic crystals of PCN-224, suitable for single-crystal X-ray diffraction analysis, were prepared. Subsequently, following a procedure similar to that for preparation of molecular (TPP)Fe^{II} (TPP = 5,10,15,20-tetraphenylporphyrin dianion),¹¹ single crystals of PCN-224 were heated under nitrogen in a DMF solution containing excess anhydrous FeBr₂ and 2,6-lutidine to give the ferrous heme-containing compound PCN-224Fe^{II} (**1**) (see Figure 2.1).

Single-crystal X-ray diffraction analysis of **1** revealed a structure that exhibits a four-coordinate heme center residing square planar coordination environment. The Fe-N distance of 1.982(4) Å is close to that of 1.966 Å reported for (TPP)Fe^{II}.¹² No significant residual electron density

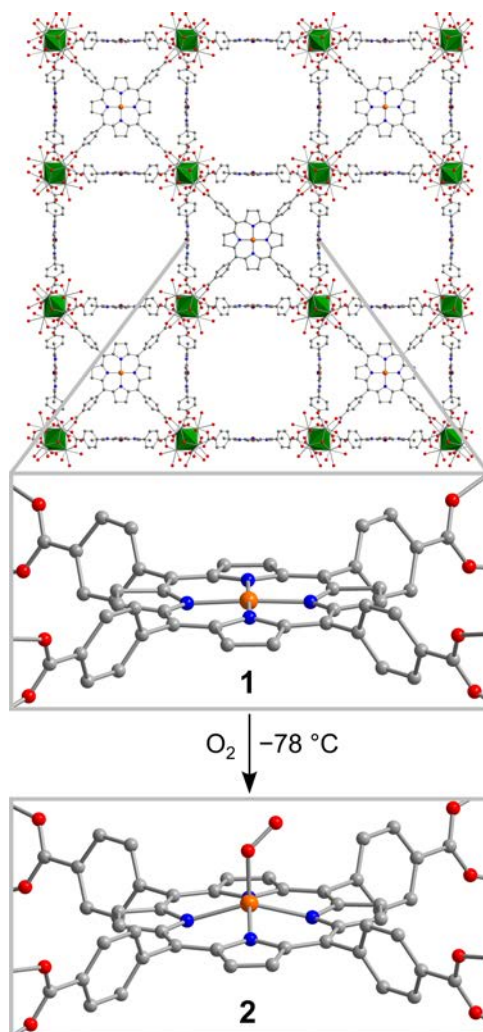


Figure 2.1 Reaction of PCN-224Fe (**1**) with O₂ at -78 °C to form PCN-224FeO₂ (**2**). Green octahedra represent Zr atoms; orange, blue, red, and gray spheres represent Fe, N, O, and C atoms, respectively; hydrogen atoms are omitted for clarity. Selected interatomic distances (Å) and angles (°) for **2**: Fe-O 1.79(1), O-O 1.15(4), Fe...N₄ plane 0.526(2), Fe-O-O 118(4), N-Fe-O 104(1).

corresponding to an axial ligand could be located in the difference Fourier map. Note that while a number of heme-containing MOFs have been previously reported,^{9fhiil} to our knowledge, **1** represents the first example of a MOF with coordinatively unsaturated ferrous heme centers.¹³ In addition to single-crystal X-ray analysis, complete metallation of the bulk crystalline material with Fe^{II} was confirmed by IR, diffuse reflectance UV-Vis, and trace metals analysis. Furthermore, N₂ adsorption data collected for a desolvated sample of **1** at 77 K provided a Brunauer-Emmett-Teller (BET) surface area of 2369 m²/g. This value is close to those reported for other metallated forms of PCN-224 and confirms that high porosity is maintained upon metallation of PCN-224 with Fe^{II}.

Upon exposure of desolvated **1** to 1 atm of dry O₂ at ambient temperature, no significant changes were observed in the IR and diffuse reflectance UV-Vis spectra. This result is in stark contrast to behavior previously observed in molecular ferrous heme complexes with axial imidazole ligands, which readily bind O₂ at room temperature.³ In contrast, carrying out this experiment with single crystals of **1** at -78 °C resulted in an immediate color change from purple to dark red-brown. Subsequent analysis of X-ray diffraction data collected at 100 K revealed the formation of a new compound, PCN-224FeO₂ (**2**), featuring an O₂ ligand coordinated to the heme iron center (see Figures 2.1). The structure of the heme unit in **2** consists of a five-coordinate Fe center residing in a square pyramidal coordination environment, with the O₂ ligand coordinated to the Fe center in an η¹, end-on binding mode. The Fe-O distance of 1.79(1) Å is in the range of 1.75-1.90 Å previously reported for molecular six-coordinate heme-O₂ adducts, which are best described as featuring an Fe^{III}-superoxide composition.¹⁴ Additionally, while the O-O distance of 1.15(4) Å and the Fe-O-O angle of 118(4)° are consistent with those previously

reported, these metrics must be regarded with caution due to crystallographic disorder of the O₂ about a 4-fold axis. The Fe^{III} center is displaced out of the plane formed by the four pyrrole nitrogen atoms by 0.526(2) Å along the Fe-O bond, consistent with displacement distances typically observed for five-coordinate metalloporphyrin complexes.¹⁵

To the best of our knowledge, compound **2** represents the first structurally characterized example of a five-coordinate, “base-free” heme-O₂ adduct. In fact, coordinatively unsaturated terminal metal-O₂ adducts in any ligand environment are exceedingly

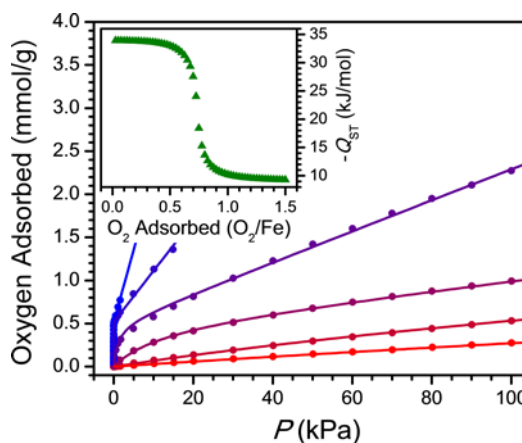


Figure 2.2 O₂ adsorption data for **1** at 141, 156, 195, 226, 273, and 298 K (blue to red gradient). Circles represent data, and solid lines correspond to fits using a dual-site Langmuir model. Inset: O₂ isosteric heat of adsorption curve for **1** as a function of amount adsorbed.

rare, with only three structurally characterized examples in molecular complexes of Cu¹⁶ and Pd.¹⁷ Indeed, to our knowledge, **2** represents the first structurally characterized example of an Fe-O₂ species with an Fe coordination number less than six. Here, the stability of this complex towards irreversible oxidation is almost certainly provided by the rigid solid-state MOF scaffold, which precludes bimolecular condensation reactions.

The surprising lack of reactivity of **1** with O₂ at room temperature prompted us to examine the thermodynamics of O₂ binding using gas adsorption measurements. Consistent with the reactivity described above, the O₂ isotherm obtained for **1** exhibits an initial sharp uptake at temperatures below 195 K (see Figure 2.2). The slope of this uptake decreases upon warming to 226 K, and the isotherm becomes nearly linear with pressure upon warming further to 298 K. To

quantify the O₂ binding, isotherm data at temperatures of 141, 156, 195, 226, 273, and 298 K were independently fit using a dual-site Langmuir model as previously described.¹⁸ These fits revealed binding enthalpies of $-29(2)$ and $-10.0(2)$ kJ/mol, which we assign to O₂ binding at the Fe centers and physisorption on the remainder of the MOF surface, respectively. Consistent with this assignment, treatment of the 141, 156, and 195 K isotherm data with the Clausius-Clapeyron equation provided an initial isosteric heat of adsorption of $-34(4)$ kJ/mol at low coverage, which ultimately drops to a plateau of $-10(2)$ kJ/mol at loadings greater than 0.7 mmol/g, the value expected for a 1:1 Fe:O₂ stoichiometry (see Figure 2, inset). Note that, to our knowledge, this represents only the second measurement of O₂ adsorption at a coordinatively unsaturated Fe center within a MOF.¹⁹

The observed O₂ binding enthalpy at low coverage of $-34(4)$ kJ/mol in **1** is substantially lower than those of 63-65 kJ/mol previously reported for Fe centers in myoglobin and molecular heme complexes with axial imidazole ligands.³ We initially hypothesized that this difference may stem from a high-spin electronic configuration for Fe^{III} in **2**, in contrast to the low-spin configuration invariably observed in six-coordinate species. To further probe this possibility, Mössbauer spectra were collected for a pulverized crystalline sample of **1**, both in the absence and presence of O₂. At 100 K, the spectrum of **1** in the absence of O₂ exhibits a quadrupole doublet with an isomer shift of $\delta = 0.580(2)$ mm/s and a quadrupole splitting of $\Delta E_Q = 1.417(6)$ mm/s, both consistent with previously reported values for four-coordinate D_{4h} ferrous heme centers (see Figure 2.3).²⁰ Upon addition of 1 atm of dry O₂ to this sample at -78 °C, the subsequent Mössbauer spectrum at 100 K showed complete consumption of **1** and concomitant formation of primarily **2** with a small amount of high-spin Fe^{III} impurity. Compound **2** exhibits a

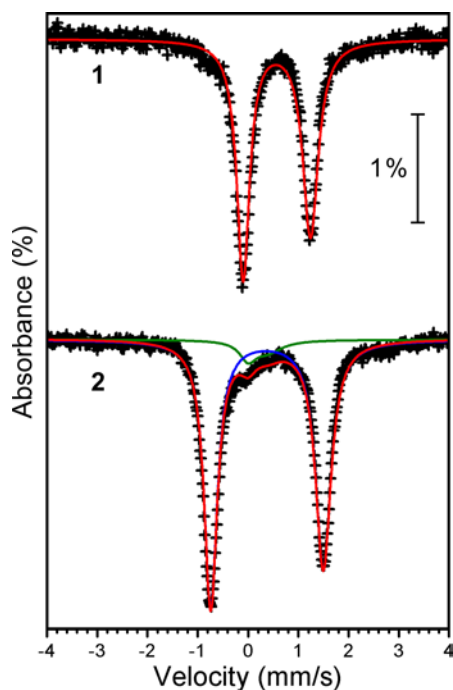


Figure 2.3 Mössbauer spectra of **1** and **2**, collected for pulverized crystalline samples at 100 K. Filled black circles represent experimental data, and solid lines correspond to fits to the data.

quadruple doublet with an isomer shift of $\delta = 0.378(2)$ mm/s and a quadrupole splitting of $\Delta E_Q = 2.24(1)$ mm/s, which can be unambiguously assigned to a low-spin ferric heme center.^{20,21} Indeed, these parameters are very similar to those previously reported for six-coordinate heme-O₂ adducts, all of which are also low-spin.²⁰ Moreover, the low-spin configuration is consistent with that suggested by a low-temperature NMR study of a five-coordinate heme-O₂ adduct.^{7a} In stark contrast to previously reported six-coordinate heme-O₂

adducts, the spectrum of **2** undergoes a gradual release of O₂ upon warming, converting cleanly back to **1** at 250 K. This observation is consistent with the relatively weak O₂ binding enthalpy determined from gas adsorption analysis.

The observation of low-spin configurations for both **2** and six-coordinate heme-O₂ adducts systems eliminates the possibility of spin state differences as the source of highly dissimilar enthalpies of O₂ binding. Furthermore, the temperature independence of binding enthalpy at low temperature, as ascertained through the O₂ adsorption experiments, suggests that a thermally-induced spin state transition is not operative in **2**. Therefore, electron donation from an axial ligand appears to be the primary source of differences in O₂ binding. Despite this supposition, the enhanced electron density at Fe in six-coordinate imidazole-ligated heme complexes

apparently does not engender significant π backbonding, as the CO stretching frequency in heme-CO adducts has been shown to be relatively invariant to coordination number.²² Alternatively, since the binding of O₂ effects a redox reaction at both Fe and O₂ centers, we hypothesize that the difference in binding strengths may be correlated to the relative redox potentials of four- and five-coordinate ferrous heme centers. Indeed, inspection of reported redox potentials for the Fe^{II}/Fe^{III} couple reveals a difference of ca. 0.250 V between four-coordinate and imidazole-ligated five-coordinate heme complexes.²³ The potential difference, when substituted into the Nernst equation, corresponds to a difference in free energy of 24 kJ/mol. This value, while a rudimentary approximation, nevertheless is very close to the observed estimated difference in O₂ binding enthalpy of 30(5) kJ/mol between **2** and six-coordinate imidazole-ligated analogues. Thus, this analysis suggests that a critical role of axial imidazole ligation in six-coordinate heme-O₂ species may be to generate a heme center with a sufficiently reducing Fe^{II/III} couple to enable strong O₂ binding at ambient conditions.

2.3 Conclusion

The foregoing results demonstrate the ability of a MOF to enable the isolation of a five-coordinate heme-O₂ complex, a species that has previously eluded structural and thorough spectroscopic characterization in molecular form. A combination of structural and spectroscopic experiments reveals unequivocally that this species comprises a low-spin Fe^{III} center coordinated to a superoxide ligand in an end-on, η^1 geometry. Moreover, variable-temperature O₂ adsorption studies show that O₂ binding in this species is much weaker than that observed in six-coordinate analogues. This observation further highlights the critical importance of the axial histidine ligand on heme sites in globin proteins, as the absence of this ligand would lead to ineffectual O₂

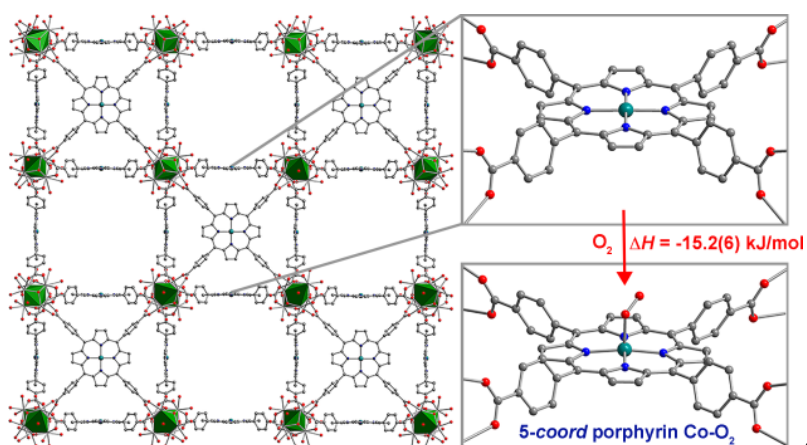
transport properties due to a drastically weakened O₂ binding enthalpy. Taken together, these results provide an illustration of how the solid-state structure of a MOF can provide a platform to isolate and study unstable species that cannot be isolated in molecules.

Chapter 3: Dioxygen Binding at a Four-Coordinate Cobaltous Porphyrin Site in a Metal-Organic Framework: Structural, EPR and O₂ adsorption analysis

Reprinted with permission from:

Gallagher, A. T.; Kelty, M. L.; Park, J. G.; Anderson, J. S.; Mason, J. A.; Walsh, J. P. S; Collins, S. L.; Harris, T. D. *Inorganic Chemistry Frontiers* **2016**, 3, 536-540.

Copyright 2016 Royal Society of Chemistry



3.1 Introduction

Dioxygen adducts of molecular metalloporphyrin complexes have generated much interest for decades, owing to their relevance as models of proteins that carry out biological processes such as O₂ transport and catalytic oxidation chemistry.¹⁻³ In particular, porphyrin iron, or heme, complexes serve as molecular models of the O₂-binding proteins hemoglobin and myoglobin.^{4,5} In addition to hemes, cobalt porphyrin complexes have also garnered significant interest, owing largely to the fact that the doublet electronic ground state of both their deoxy- and oxy- forms lends itself to electron paramagnetic resonance (EPR) analysis.⁶⁻⁸

Studies of molecular metalloporphyrin dioxygen adducts, in particular those involving Fe, have been limited by the propensity of these complexes to undergo deleterious bimolecular condensation reactions to form thermodynamically favoured and kinetically inert oxo-bridged dinuclear species.^{9,10} These challenges have been partially overcome through introduction of bulky substituents onto the porphyrin scaffold in order to block access to one or both axial coordination sites of the metal center. Nevertheless, even in the presence of sterically encumbered porphyrin ligands, an axial ligand such as imidazole is necessary in order to prevent bimolecular condensation or dioxygen dissociation. Consequently, the characterization of five-coordinate, base-free oxyheme¹¹⁻¹⁴ and oxycobalt porphyrin¹⁵⁻²¹ complexes in molecular form has been largely limited to spectroscopic studies in frozen solvent matrices at low temperature.

We recently reported the post-synthetic metalation of the porphyrinic zirconium MOF PCN-224 with Fe^{II} to give a four-coordinate ferrous heme complex within the compound

PCN-224Fe^{II}.²² Subsequent addition of dry O₂ to this species at -78 °C gave a five-coordinate heme dioxygen adduct that was characterized by single-crystal X-ray diffraction and several spectroscopic methods. Moreover, O₂ adsorption measurements on activated PCN-224Fe^{II} revealed an Fe-O₂ binding enthalpy of -34(4) kJ/mol. This value is nearly half of that commonly observed in ferrous heme model complexes and in myoglobin,^{2,23-25} and demonstrates the importance of an axial ligand in biological O₂ binding. Herein, we extend this work to cobalt by examining the O₂ binding of a four-coordinate cobaltous porphyrin within PCN-224 through single-crystal X-ray diffraction, EPR spectroscopy, and O₂ adsorption measurements. Specifically, we show that O₂ binds the coordinatively unsaturated Co center to give a five-coordinate Co^{III} superoxo species and that O₂ binding at a four-coordinate Co^{II} center is considerably weaker than has been observed in analogues with axial ligands, in line with our previous findings regarding four-coordinate Fe^{II}.

3.2 Results and Discussion

The compound PCN-224Co was reported previously, as synthesized by carrying out the MOF assembly reaction from 5,10,15-20-tetrakis(carboxyphenyl)porphyrin cobalt(II).²⁶ We synthesized PCN-224Co through a different route, by post-synthetic metalation of the free-base porphyrin-containing PCN-224.²⁶ Here, soaking cubic single-crystals of PCN-224 with excess anhydrous CoCl_2 in DMF in the presence of excess 2,6-lutidine at 150 °C for 12 h resulted in the insertion of a Co^{II} ion into the porphyrin cavity to give, after activation, the compound PCN-224Co (1). Quantitative Co metalation of this material was confirmed by diffuse-

reflectance UV/Visible spectroscopy and trace metals analysis (see Experimental Section). In addition, an N_2 adsorption isotherm collected for **1** at 77 K provided a BET surface area of 3070(70) m^2/g . This surface area is similar to other values reported for PCN-224 derivatives,^{22,26} and therefore

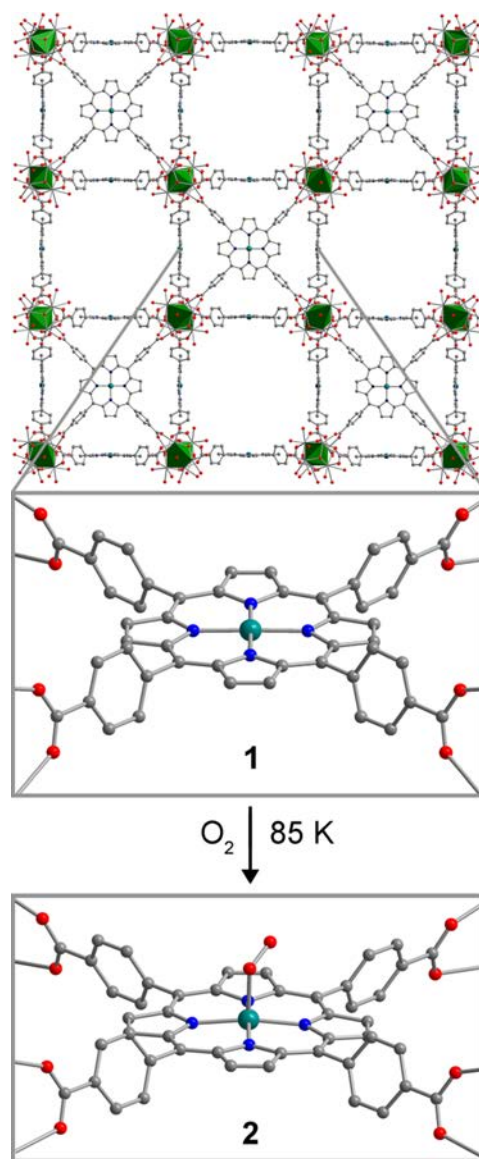


Figure 3.1 Reaction of PCN-224Co (**1**) with O_2 at 85 K to form PCN-224Co O_2 (**2**). Green octahedra represent Zr atoms; teal, blue, red, and gray spheres represent Co, N, O, and C atoms, respectively; hydrogen atoms are omitted for clarity. Selected interatomic distances (Å) and angles (°) for **2**: Co-O 1.93(4), Co-N 1.974(5), O-O 1.30(4), Co \cdots N $_4$ plane 0.15(4), Co-O-O 121(2).

confirms that microporosity is retained upon post-synthetic metalation. This result provides another example of post-synthetic metalation of a MOF with cobalt.²⁷⁻³²

Upon metalation of PCN-224 with Co, the compound retains its single crystallinity, enabling characterization of **1** by single-crystal X-ray diffraction. The structure of **1** features a four-coordinate Co^{II} center that lies squarely within the N₄ plane formed by the four pyrrole nitrogen atoms of the porphyrin ligand, along a crystallographic four-fold rotation axis (see Figure 3.1). The Co-N distance of 1.936(5) Å is in the range of 1.931-1.944 Å observed for molecular four-coordinate cobalt porphyrin complexes,³³ although considerably shorter than the distance of 2.156(1) Å reported in the related MOF Hf-PCN-221(Co).³⁴ No significant residual electron density was present in the difference Fourier map, confirming the absence of ligation in the Co axial coordination sites.

A thin-walled quartz capillary containing a single crystal of PCN-224Co was exposed to 1 atm of dry O₂, cooled to 77 K and sealed under reduced pressure. Subsequent X-ray analysis of data collected at 85 K revealed the formation of a new species, PCN-224CoO₂ (**2**). The structure of **2** displays a five-coordinate Co center in a square-pyramidal coordination environment, with the O₂ ligand coordinated to the Co center in an η¹, end-on binding mode (see Figure 3.1). The Co-O distance of 1.93(4) Å falls in the range of 1.92-1.93 Å previously reported for six-coordinate molecular Co-O₂ adducts, which have been described as Co^{III} superoxo (O₂⁻) species.^{35,36} The O-O distance of 1.30(4) Å and the Co-O-O angle of 121(2)° are also consistent with previously reported molecular species. Note, however, that these values should be regarded with caution owing to disorder associated with the crystallographic four-fold symmetry at the Co center. The Co^{III} center is displaced from the mean plane of the four pyrrole nitrogen atoms by

0.15(4) Å, with a corresponding elongated Co-N distance of 1.974(5) Å, and these metrics are consistent with five-coordinate, low-spin Co^{III} porphyrin species in molecular form.^{37,38} Notably, the displacement of the Co center is significantly smaller than that previously observed in the analogous MOF-based Fe species, which featured a displacement of 0.526(2) Å. This difference may be attributed to the smaller ionic radius of low-spin Co^{III} relative to low-spin Fe^{III}.³³ To our knowledge, **2** provides the first example of a structurally-characterized Co-O₂ adduct with a Co coordination number less than six.

In order to further probe the electronic structure of **1** and **2**, continuous-wave X-band EPR spectra were collected on activated crystalline samples at 15 K. In a quartz tube under static vacuum, **1** exhibits an axial spectrum that is split into an eight-line pattern, with this splitting arising due to hyperfine coupling of the unpaired electron to the $I = 7/2$ ⁵⁹Co nucleus (see Figure 3.2, upper). To model these data, spectral simulations were carried out using the program Easyspin³⁹ and the Hamiltonian $\hat{H} = \mu_B H \cdot g \cdot S +$

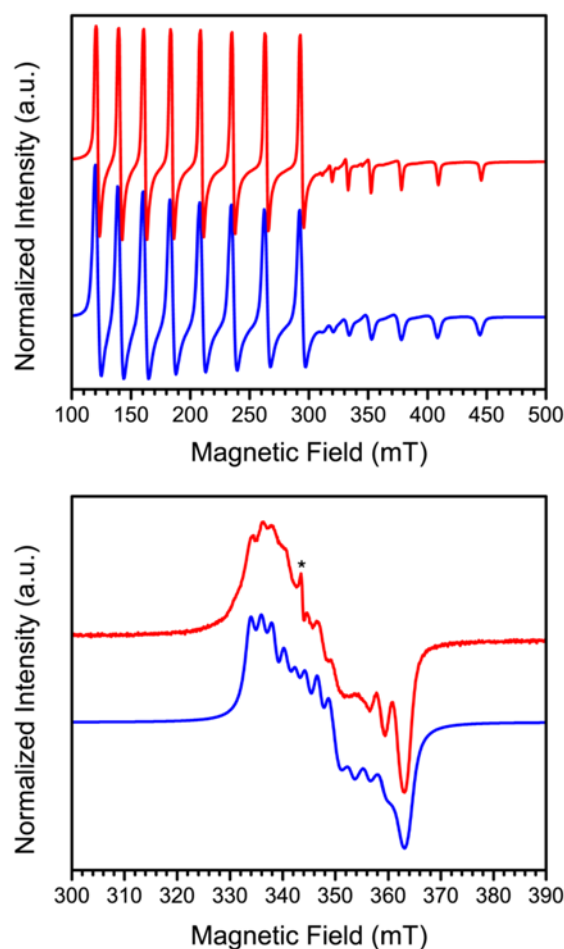


Figure 3.2 X-Band EPR spectra for **1**, collected at 15 K, under static vacuum (upper) and dosed with 1 atm O₂ at ambient temperature (lower). Red and blue lines correspond to experimental data and simulations, respectively, and the asterisk denotes a small amount of $S = 1/2$ impurity with $g = 2.00$. Microwave frequency = 9.632 GHz; microwave power = 6.31 mW.

$I_{\text{Co}} \cdot A_{\text{Co}} \cdot S$, where μ_{B} is the Bohr magneton, H is the applied dc magnetic field, g the g -tensor, S and I_{Co} are the electronic and ^{59}Co nuclear spins, respectively, and A_{Co} is the tensor for hyperfine coupling to the ^{59}Co nucleus. The spectrum was best modeled with values of $S = 1/2$, $g_{\perp} = 3.271$, $g_{\parallel} = 1.783$, $A_{\perp\text{Co}} = 1122$ MHz, and $A_{\parallel\text{Co}} = 480$ MHz, with the parallel direction taken to be the axis normal to the porphyrin N_4 plane. Here, the $S = 1/2$ ground state and large g_{\perp}/g_{\parallel} ratio are consistent with previous reports of four-coordinate Co^{II} porphyrin complexes that were doped into solid-state diamagnetic matrices to prevent axial ligation.¹⁸⁻²¹ Moreover, the deviation of g_{\perp} from the free electron value of 2.0023 in cobalt porphyrin complexes is directly correlated to the axial perturbation of the Co center along the parallel direction,^{3,42-43} and the large deviation observed here for **1** corroborates the four-coordinate environment of the Co center as indicated by X-ray crystallography.

The lower panel of Figure 3.2 shows the spectrum of the oxygenated derivative **2**, formed by dosing a sample of **1** with 1 atm of O_2 at ambient temperature followed by cooling to 15 K, which exhibits a rhombic spectrum with a significantly decreased degree of hyperfine coupling. The spectral features exist over a much smaller field range than in **1**, indicative of reduced g -anisotropy. Simulating the spectrum according to the isotropic spin Hamiltonian given above provides the following parameters: $S = 1/2$, $g_x = 2.016$, $g_y = 1.973$, $g_z = 1.900$, $A_{x\text{Co}} = 60$ MHz, $A_{y\text{Co}} = 80$ MHz, and $A_{z\text{Co}} = 0$ MHz (unresolved). The rhombicity of this spectrum is consistent with a bent Co-O-O angle, which precludes a symmetry rotation axis.

This model is compatible with those previously invoked for molecular porphyrin Co-

O₂ adducts, in which one of the two singly occupied π^* orbitals of O₂ forms a σ bond with the Co d_z^2 orbital to form a doubly occupied molecular orbital, while the other orbital remains singly occupied and non-bonding.^{44,45} Accordingly, **2** is best described as Co^{III}-O₂^{-•}, *i.e.* a low-spin Co^{III} center bound by an $S = 1/2$ superoxo ligand. Indeed, this electronic structure is consistent with previous studies of dioxygen adducts of porphyrin Co complexes that feature axial ligands at the Co center or solute and/or solvent

molecules that engage in π interactions with the porphyrin ligand.⁴⁶

In order to examine the thermodynamics of O₂ binding in PCN-224Co, O₂ adsorption data were collected at selected temperatures. As depicted in Figure 3.3, the O₂ isotherm for **1** collected at 113 K exhibits an initial step uptake at low pressure. As temperature is increased, the slope of this steep region decreases until the isotherm becomes nearly linear at 195 K. In

order to quantitate the O₂ binding, isotherm data at temperatures of 113,

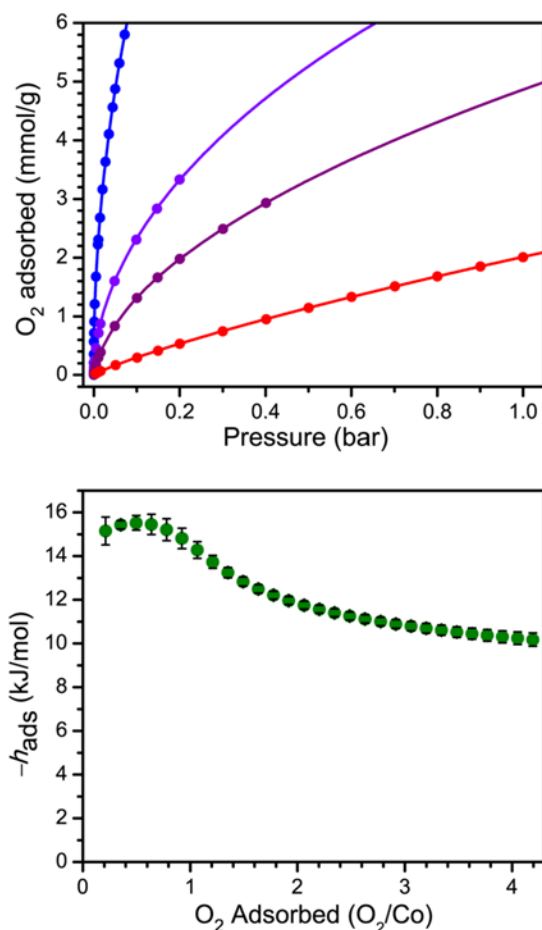


Figure 3.3 Upper: O₂ adsorption data for **1** at 113, 141, 156, and 195 K (blue to red gradient). Circles represent data, and solid lines correspond to fits using a dual-site Langmuir-Freundlich model. Lower: O₂ differential enthalpy of adsorption curve for **1** as a function of amount adsorbed. Green circles represent data, and error bars are shown in black.

141, 156, and 195 K were each fit to a dual-site Langmuir-Freundlich model.^{22,47} Subsequent treatment of the variable-temperature isothermal data with the Clausius-Clapeyron equation revealed a differential enthalpy of adsorption of $h_{\text{ads}} = -15.2(6)$ kJ/mol at low O₂ loading, followed by a gradual drop near 1:1 O₂/Co to a plateau at $h_{\text{ads}} = -10.2(3)$ kJ/mol. We respectively assign these distinct values to O₂ binding at the four-coordinate Co^{II} center and physisorption to the remainder of the MOF surface. The adsorption enthalpy of $-15.2(6)$ kJ/mol is slightly lower than that of -17.8 kJ/mol reported for O₂ binding at a five-coordinate ($\mu_4\text{-O}$)Co^{II} tetracarboxylate unit in PCN-9.⁴⁸

The Co-O₂ binding enthalpy of $h_{\text{ads}} = -15.2(6)$ kJ/mol at low coverage is considerably weaker than values previously reported for cobalt porphyrins that feature axial ligands, both in Co-substituted globin proteins and in molecular model complexes.^{49,54} These values range from -33 kJ/mol for a 1-methylimidazole-bound capped Co complex⁵³ to -68 kJ/mol for cobalt octaethylporphyrin supported on a highly oriented pyrolytic graphite (HOPG) surface, where the HOPG acts as an axial ligand.⁵⁴ Indeed, the binding enthalpy of $h_{\text{ads}} = -15.2(6)$ kJ/mol observed for **1** + O₂ falls in the range of 22-46% of these values. This difference is similar but even more pronounced than that observed for the O₂ binding of the four-coordinate heme in PCN-224Fe^{II}, which was approximately half of the values commonly observed for hemes with axial ligands,²² and further underscores the importance of axial ligand electron donation to the metal center to enable O₂ transport and storage.

3.3 Conclusion

The foregoing results illustrate the ability of a metalloporphyrinic MOF to enable the

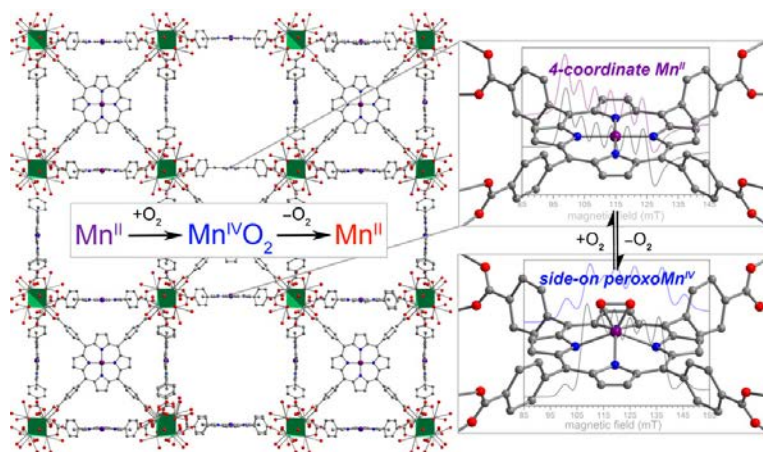
crystallographic characterization of a porphyrin Co-O₂ species, as well as the quantitation of O₂ binding at a four-coordinate, base-free cobaltous porphyrin site. X-band EPR spectra reveal the electronic structure of the oxycobalt species to best be described as a low-spin Co^{III} center coordinated to an $S = 1/2$ superoxo ligand. Variable-temperature O₂ adsorption measurements provide a Co-O₂ binding enthalpy of $h_{\text{ads}} = -15.2(6)$ kJ/mol, considerably lower than what is observed in analogous complexes with axial ligands. These results are consistent with those previously reported for O₂ binding at a MOF-based four-coordinate heme species, and further demonstrate the importance of axial ligands in O₂ binding in tetragonal metal complexes. Future work will focus on employing cobalt porphyrin units to carry out oxygen-atom transfer chemistry.

Chapter 4: A Structurally-Characterized Peroxomanganese(IV) Porphyrin via Reversible

O₂ Binding within a Metal-Organic Framework

Gallagher, A. T.; Lee, J. Y; Kathiresan, V.; Anderson, J. S.; Hoffman, B. M.; Harris, T. D.

submitted.



4.1 Introduction

The activation of O₂ by metalloproteins is central to a wide range of biological processes, including bond activation, O₂ transport, metabolism, and the regulation of reactive oxygen species.¹ In many of these processes, metal complexes of O₂²⁻, or peroxide, represent reactive intermediates that are generated during the catalytic cycles of enzymatic reactions.^{1a-c,2} For instance, C–H bond activation by heme-containing enzymes involves peroxoiron intermediates.^{1a-c,2ab,d} In addition, water oxidation by the oxygen-evolving complex in Photosystem II^{2e} and the degradation of superoxide ion by manganese superoxide dismutase^{2a} are postulated to proceed through a peroxomanganese intermediate. The prominence and unusual reactivity of peroxoiron and manganese species in biology has motivated efforts to synthesize and characterize synthetic molecular model complexes, largely in order to elucidate the structure, physical properties, and chemical reactivity of these intermediates.^{2b,3} Indeed, tremendous progress has been made in the synthesis and study of both peroxoiron and manganese complexes. For instance, a number of mononuclear heme⁴ and non-heme⁵ peroxoiron complexes have been isolated, including two examples^{5a,b} with structural characterization. In addition, several mononuclear peroxomanganese species have been isolated,^{6,7,8} with two recent structurally-characterized examples featuring Mn^{IV}.⁹

Despite these advances, significant challenges remain in the isolation of peroxomanganese complexes that display reversible O₂ binding under ambient conditions, an important function often found in biological systems.¹⁰ Toward this end, manganese(II) porphyrin complexes present an attractive platform, owing to their ability to carry out the two-electron reductive activation of O₂¹¹ and thus form high-valent peroxomanganese complexes.¹² To date, one

crystal structure of an O₂ coordinated to a manganese porphyrin has been reported. This complex, formed by addition of KO₂ to (TPP)Mn^{II} (H₂TPP = 5,10,15,20-tetraphenylporphyrin), was shown to feature a Mn^{III} ion coordinated to a peroxo ligand in a side-on, η² binding mode.^{7a} While [(TPP)Mn(O₂)]⁻ provides an important structural example of the peroxo binding mode, the presence of Mn^{III} renders O₂ loss unfavourable, as it would necessitate the formation of a high-energy Mn^I species. In contrast, peroxomanganese(IV) complexes, as formed by reaction of Mn^{II} with O₂, have been probed by numerous spectroscopic techniques, including EPR,^{12a,c,e} vibrational,^{12l,n} NMR,^{12k} and UV/Visible^{12a,c} spectroscopies, in addition to computational methods.^{12d,i} Although these investigations support a side-on peroxomanganese(IV), this geometry has not been confirmed by a crystal structure. Furthermore, the thermal instability of the peroxomanganese(IV) species has limited their characterization and hindered a thorough investigation of their structure and properties.

A key limitation in the study of O₂ binding in molecular metalloporphyrins is the propensity for these species to form oxo-bridged complexes via irreversible bimolecular condensation reactions.¹³ For instance, in Fe^{II} and Co^{II} complexes, highly elaborate ligands such as the sterically protected “picket-fence” porphyrins were necessary to prevent bimolecular decomposition reactions and enable the isolation and thorough characterization of six-coordinate Fe and Co–O₂ adducts, which feature axial imidazole or thiolate ligands.¹⁴ In contrast, analogous axially-ligated Mn^{II} complexes do not bind O₂, which has been attributed to the preference for five-coordinate geometry in porphyrinic Mn ions.^{12bg} Consequently, no peroxomanganese(IV) porphyrin species have been isolated or studied under ambient conditions.

As an alternative to employing molecular systems, one can envision isolating a

peroxomanganese(IV) complex within a porphyrinic metal-organic framework (MOF). Here, the porous, solid-state structure of the MOF prevents bimolecular condensation reactions and enables introduction of gas-phase substrates in the absence of exogenous solvent. Furthermore, whereas the inherent reactivity of the peroxomanganese(IV) complexes has precluded crystallographic characterization, the crystallinity of MOFs provides an ideal platform to carry out single-crystal X-ray diffraction analysis. Illustrative of this approach, we have previously shown that the porphyrinic MOF PCN-224¹⁵ can be employed to study low-coordinate O₂ adducts^{16,17} and labile carbonyl complexes.¹⁸ Herein, we comprehensively examine O₂ binding to Mn^{II} in PCN-224 using a host of physical methods. Taken together, these experiments unambiguously establish the presence of a side-on peroxomanganese(IV) species, and the O₂ binding is shown to be reversible even at ambient temperature.

4.2 Results and Discussion

Synthesis of PCN-224Mn^{II}. The porphyrinic MOF PCN-224 was synthesized as previously described.¹⁵ Subsequent metalation of the porphyrin with Mn^{II} was carried out by heating single crystals of PCN-224 under N₂ in a DMF solution containing excess MnBr₂ and 2,6-lutidine, followed by evacuation at 150 °C for 12 h, to give the compound PCN-224Mn^{II} (**1**). Complete metalation of the porphyrin within the bulk crystalline material was confirmed by solid-state diffuse reflectance UV/Visible spectroscopy and trace

metals analysis (see Figure 4.1 and Experimental Section). Furthermore, N₂ adsorption data collected for a desolvated sample of **1** at 77 K provided a Brunauer-Emmett-Teller surface area of 2455 m²/g, close to the accessible surface reported for other metalated variants of PCN-224,^{15,16,17,19} thereby confirming the retention of porosity upon metalation and the successful removal of solvent molecules from the pores. While several manganese porphyrin-containing MOFs have been reported, to our knowledge,²⁰ **1** represents the first example of a MOF that features a four-coordinate Mn^{II} porphyrin complex.

The diffuse reflectance UV/Visible spectrum obtained for an activated sample of **1** exhibits similar peak maxima to the absorption spectrum of **1** suspended in toluene, but nevertheless

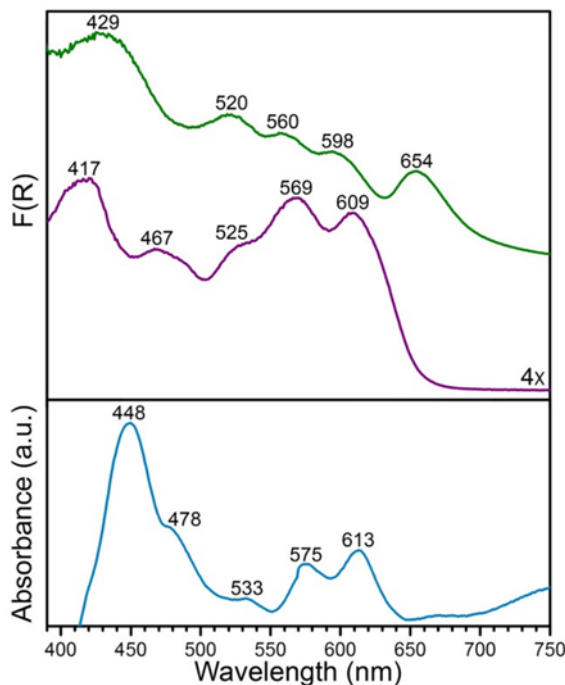


Figure 4.1 Solid-state diffuse reflectance UV/Visible spectra for PCN-224 (green) and its manganese(II)-metalated form **1** (purple), plotted as the Kubelka-Munk function F(R). For comparison, the absorption spectrum for a toluene suspension of **1** (blue) is shown, highlighting changes in the peak positions with and without toluene.

features key differences (see Figure 4.1).

Most notably, the spectrum reported for **1** in toluene displays a Soret band at 448 nm, while spectrum of activated **1** features a Soret band at 417 nm. These differences can possibly be attributed to the rigorous four-coordinate nature of the Mn center in **1**, compared to a slight distortion from local D_{4h} symmetry at Mn in the toluene solution imposed by Mn–toluene interactions as has been observed

for the molecular analogue, (TPP)Mn (see crystallography discussion below).^{8b,16} More specifically, these changes may be attributed to the difference in mixing of metal- and porphyrin-based π orbitals in the two complexes, as changes in degree of mixing are known to influence the resulting adsorption spectra of metalloporphyrin complexes.²¹ In the case of the rigorously in-plane Mn center, the maximal overlap of Mn $d_{xz,yz}$ and porphyrin π^* orbitals may account for the changes in the features in the electronic spectrum of **1**.

Infrared Spectroscopy. As an initial investigation into the interaction between Mn^{II} and O_2 , a desolvated sample of **1** was exposed to ca. 1 atm of dry O_2 and monitored by diffuse reflectance infrared Fourier transform spectroscopy (DRIFTS). The addition of O_2 to **1** at 298 K was accompanied by the appearance of three new vibrations, situated at 801, 984, and 1017 cm^{-1} (see Figure 4.2), indicative of conversion to a Mn– O_2 complex in the compound PCN-224Mn O_2

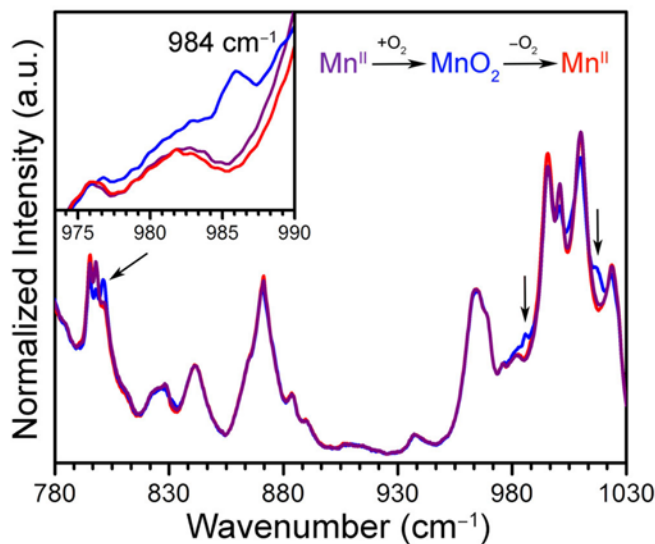


Figure 4.2 DRIFTS spectra for **1** at 298 K under static vacuum (purple), upon addition of O_2 (blue), and after subsequent purging with Ar (red). The inset shows an expanded view of the spectra, highlighting the $\nu_{\text{O-O}}$ vibration of the dioxygen adduct in **2** at 984 cm^{-1} .

(2). The vibrations at 801 and 1017 cm^{-1} have been previously attributed to a lowering of local symmetry from D_{4h} to C_{2v} at Mn^{II} upon O_2 binding.¹²¹ This symmetry reduction occurs due to a displacement of Mn from the N_4 plane of the porphyrin upon the addition of an axial ligand, in this case O_2 . Moreover, the feature at 984 cm^{-1} is identical within error to the formerly assigned $\nu_{\text{O-O}}$ vibration from a mixture of the molecular complex $(\text{TPP})\text{Mn}^{\text{II}}$ and O_2 , as isolated in a frozen Ar matrix at 15 K.¹²¹ Remarkably, in contrast to molecular systems, where the deoxymanganese(II) complex was only partially regenerated after purging with N_2 at -78°C , similar purging here with dry Ar gas at 25°C gave a spectrum identical to that obtained for **1** before adding O_2 (see Figure 4.2).^{12c} This process of adding then removing O_2 could be cycled at least three times, underscoring the ability of the solid-state MOF to enable reversible O_2 binding.

The $\nu_{\text{O-O}}$ vibration in **2** at 984 cm^{-1} is considerably lower than those of $\nu_{\text{O-O}} = 1195$ and 1278 cm^{-1} previously observed for O_2 adducts of $(\text{TPP})\text{Fe}$ and $(\text{TPP})\text{Co}$ at 15 K, which have been unambiguously assigned as superoxometal(III) species.²² This contrast suggests that O_2 binding in $\text{PCN-224Mn}^{\text{II}}$ involves a two-electron transfer from Mn^{II} to O_2 to give a peroxomanganese(IV) species, rather than one-electron transfer to give a superoxomanganese(III) species.^{12a-c,e-n} Here, the weaker O–O bond in **2** relative to superoxo complexes can be primarily attributed to a doubly occupied π^* orbital of an O_2^{2-} ligand compared to singly occupied orbital of $\text{O}_2^{\bullet-}$. Additionally, the $\nu_{\text{O-O}} = 984 \text{ cm}^{-1}$ in **2** is higher than those of $\nu_{\text{O-O}} = 806 \text{ cm}^{-1}$ and 898 cm^{-1} previously reported for the peroxoiron(III) complex^{3a} $[(\text{OEP})\text{FeO}_2]^-$ and the peroxotitanium(IV) complex²³ $(\text{OEP})\text{TiO}_2$ ($\text{H}_2\text{OEP} = 2,3,7,8,12,13,17,18$ -octaethylporphyrin), which both feature side-on coordination of O_2^{2-} . This difference may stem from increasing stabilization of the σ bond of O_2^{2-} with increasing effective nuclear charge

moving from Fe^{III} to Ti^{IV} to Mn^{IV}. In addition, the concomitant increase in Lewis acidity across the series may serve to strengthen this bond by alleviating electron–electron repulsion in O₂²⁻. While the foregoing comparison of data is consistent with the presence of a side-on O₂²⁻ in **2**, analysis of infrared spectra alone cannot definitively confirm this assignment.

Single-Crystal X-ray Diffraction. The stability of the Mn–O₂ adduct in **2** prompted us to investigate both **1** and **2** using single-crystal X-ray diffraction analysis. The structure of **1** exhibits a four-coordinate Mn^{II} center, residing in a square planar coordination environment on a crystallographic special position of *mm2* site symmetry (see Figures 3). Importantly, no significant residual electron density was located in the difference Fourier map, confirming the absence of axial ligation at Mn. The Mn–N distance of 1.998(5) Å is notably shorter than those of 2.082(2)–2.085(2) Å previously reported for the toluene-solvated compound (TPP)Mn·2C₇H₈.^{12b,24}

While this molecular compound features a pseudo four-coordinate Mn^{II} center, weak contacts between Mn and a toluene molecule, with a closest Mn–C_{toluene} distance of 3.04 Å, lead to a 0.19 Å displacement of Mn from the N₄ plane and thus slightly longer Mn–N bonds relative to **1**. As such,

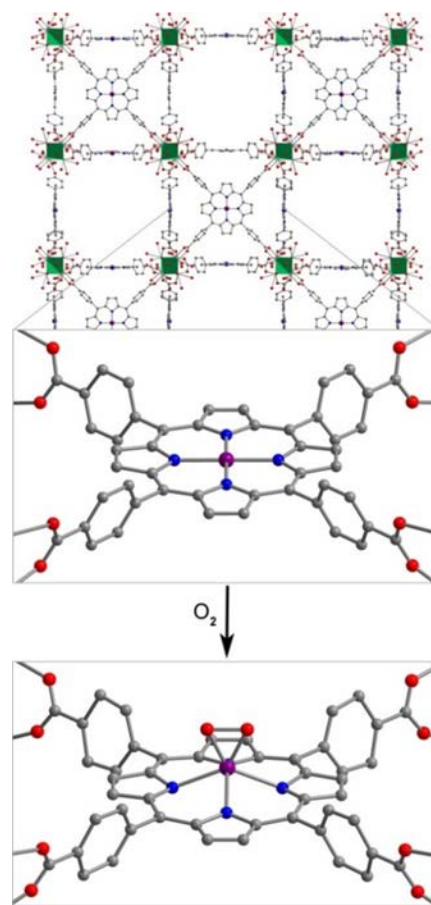


Figure 4.3 Reaction of **1** with O₂ to form **2**. Vertices of the green octahedra represent Zr atoms; purple, red, blue, and gray spheres represent Mn, O, N, and C atoms, respectively; H atoms are omitted for clarity. Selected interatomic distances (Å) for **1**: Mn···N₄ 0, Mn–N 1.998(5); for **2**: Mn···N₄ 0.80(2), Mn–O 1.76(3), Mn–N 2.170(9).

to our knowledge, the structure of **1** provides the first example of a four-coordinate Mn porphyrin species. The isolation of a rigorously four-coordinate Mn center within a porphyrin ligand is remarkable given the relatively large ionic radius of Mn^{II}, and thus its propensity to displace out of the N₄ plane^{12b} to form five-coordinate complexes.^{12g} Indeed, the complex in **1** demonstrates the utility of MOFs to enable isolation of reactive low-coordinate metal complexes.

Exposure of single crystals of **1** to ca. 1 atm of dry O₂ at -78 °C resulted in an immediate color change from purple to black. Subsequent X-ray diffraction analysis at 100 K revealed the formation of **2**. The structure of **2** is globally quite similar to that of **1**, but with key differences in the Mn coordination environment (see Figures 4.3). Most importantly, the structure features a Mn ion that is coordinated to O₂ via a side-on, η² binding mode. In addition, the Mn ion is displaced from the N₄ plane by 0.80(2) Å, slightly longer than the displacement of 0.7640(4) Å observed for the peroxomanganese(III) unit in a potassium cryptate salt of [(TPP)MnO₂]⁻.^{7a} Likewise, the Mn–N and Mn–O distances of 2.170(9) and 1.76(3) Å in **2** are slightly shorter than the analogous mean distances of 2.184(4) and 1.895(4) Å in [(TPP)MnO₂]⁻. While these differences are consistent with the presence of a smaller ionic radius for Mn^{IV} vs Mn^{III}, they should be regarded with caution owing to the positional disorder and large thermal ellipsoids of O atoms in **2**. Finally, this crystallographic disorder also precludes a reliable determination of the O–O distance in **2**. Here, this distance was fixed to a target value of 1.40 ± 0.02 Å, based on other peroxometal complexes with similar values of $\nu_{\text{O-O}}$,^{9,23,25} and subsequent refinement of the structure gave a distance of 1.39(2) Å.

In the structure of **2**, the O_{peroxo} atoms are related through a crystallographic mirror plane. As such, the structure was modeled with an O₂ unit bound symmetrically with respect to Mn.

However, we cannot exclude the possibility of some asymmetry based on the current structure. Indeed, several previously reported crystal structures of η^2 -bound peroxometal complexes feature asymmetric coordination of the peroxo ligand.^{7,9} Nevertheless, the structure of **2** shows that the O–O bond eclipses the pyrrole-based N atoms. This conformation contrasts the results from charge iterative extended Hückel (IEH) calculations on a peroxomanganese(IV) porphyrin complex, which suggested the presence of a staggered peroxo ligand to alleviate electrostatic repulsion.^{12j} However, the eclipsed conformation observed for **2** is consistent with those determined crystallographically for the peroxometal porphyrin complexes (OEP)TiO₂,²³ (TPP)Mo(O₂)₂,²⁶ and [(TPP)MnO₂][−].^{7a}

Despite the large standard deviations in the structure of **2**, this analysis unambiguously reveals the presence of an O₂ adduct coordinated to Mn through a side-on, η^2 binding mode, with the O₂ eclipsing the N atoms of the porphyrin pyrroles. Moreover, the complex in **2** represents a rare example of both a structurally characterized peroxometalloporphyrin^{7a,23,26} and a peroxomanganese(IV) complex.⁹ To our knowledge, **2** provides the first crystal structure of a peroxomanganese(IV) in a porphyrinoid ligand and a rare example of a peroxomanganese(IV) in any ligand environment.^{9,27}

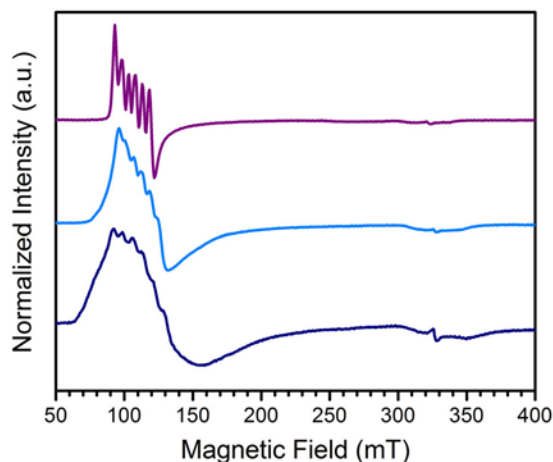


Figure 4.4 Experimental X-band EPR spectra of **1** at 77 K after activation (purple trace, upper), in toluene (blue trace, center), and in a mixture of toluene and pyridine (navy trace, lower).

Table 4.1. Parameters corresponding to simulated EPR spectra for PCN-224Mn species.

Complex	D (cm ^{−1})	λ	A (cm ^{−1} × 10 ⁴)
PCN-224Mn ^{II} (1)	0.55	0	46.032
PCN-224Mn ^{II} + C ₇ H ₈	0.55	0.0267	53.579
PCN-224Mn ^{II} + C ₅ H ₅ N	0.55	0.0410	73.385
PCN-224Mn ^{IV} O ₂ (2)	−1.76	1/3	50.759, 83.659

Electron Paramagnetic Resonance (EPR) Spectroscopy. To further probe the electronic structures of **1** and **2**, as well as the reversibility of O₂ binding, continuous wave X-band EPR spectra were collected on samples at selected temperatures between 298 K and 4.2 K. The spectrum obtained at 77 K for a rigorously activated sample of **1** shows a sharp axial pattern, with observed g values of $g_{\perp} = 6$ and $g_{\parallel} = 2$ that are characteristic of an $S = 5/2$ Mn^{II} ion with zero-field splitting parameters of $D \gg h\nu$, $E/D = \lambda = 0$ (see Figure 4.4, upper). In addition, the low field portion features a well-resolved six-line hyperfine splitting by the $I = 5/2$ ⁵⁵Mn nucleus, with a hyperfine constant of $A_{\perp}^{\text{Mn}} \approx 49$ G (138 MHz).

Addition of toluene to a crystalline sample of **1** led to a broadening of the g region of the spectrum and an increase in the hyperfine coupling (Figure 4.4, middle and Table 4.1). Accordingly, simulating the spectrum with the program Easyspin²⁷ showed that interaction of **1** with toluene lowers the four-fold symmetry of the Mn^{II} ion, as indicated by the introduction of a zero-field splitting rhombicity with $\lambda \approx 0.027$ and an increase in hyperfine coupling to $A_{\perp}^{\text{Mn}} \approx 57$ G (160 mHz). Addition of a three-fold molar excess of pyridine in toluene to **1** appeared to further lower the symmetry, resulting in an increase in rhombicity and hyperfine coupling to $\lambda \approx 0.041$ and $A_{\perp}^{\text{Mn}} \approx 78$ G (219 mHz), respectively (Figure 4.4, lower and Table 4.1). The progressive increase in hyperfine coupling in these three samples reflects an increasing departure of the Mn^{II} from the N₄ plane, which accompanies the progressive departure from four-fold symmetry evident from increases in λ (see Table 4.1). These data strongly support the four-coordinate nature of activated **1**, and the transformation to a five-coordinate complex upon addition of solvent.

Dosing **1** with ca. 1 atm of dry O₂ resulted in conversion to **2**, which features a rhombic

spectrum at 4.2 K (see Figure 4.5). The spectrum was modeled as an $S = 3/2$ spin state with $D = -1.76$ and $\lambda = 1/3$. As zero-field splitting splits the $S = 3/2$ ground state into two doublets, this spectrum comprises an overlap of transitions within each of the two doublets, each with observed g values of $g_x = 5.4$ – 5.5 , $g_y = 2$, and $g_z = 1.45$.^{12c} The feature at $g = 5.4$ corresponds to an overlap of two ^{55}Mn hyperfine sextet patterns, where $A^l = 54$ G (154 MHz) for the lower doublet and $A^u = 89$ G (251 MHz) for the upper doublet (see Figure 4.5 and Table 4.1).^{12a,c} The difference in signal intensities from the two doublets is reproduced by a zero-field splitting of $\Delta = 2(D^2 + E^2)^{1/2} = 2|D|(1 + 3\lambda^2)^{1/2} = 2.35$ cm⁻¹. As the temperature is increased from 4.2 K, the relative populations of the two doublets begin to equalize, causing the spectra to broaden. Finally, when **2** was purged with Ar at 298 K and evacuated for 12 h, a spectrum identical to that for **1** was obtained. This observation corroborates the reversibility of O₂ binding at Mn that was revealed by DRIFTS analysis.

The rhombicity of this spectrum is consistent with O₂ binding, where the symmetry between the d_{yz} and d_{xz} orbitals is broken by the σ interaction between the molecular orbitals of the O₂ and the d_{yz} orbital of the Mn^{IV} ion. Furthermore, unlike Co^{II} porphyrin systems, where binding O₂ causes a significant decrease in the ^{59}Co hyperfine splitting parameter due to the formation of a Co^{III}-superoxo complex, the binding of O₂ to the Mn center does

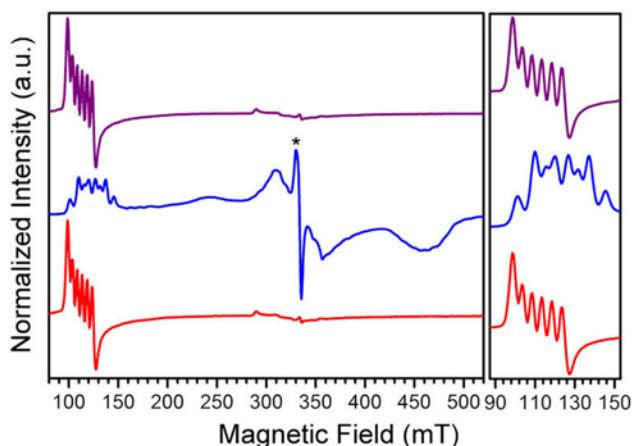


Figure 4.5. Left: X-band EPR spectrum of **1** (purple trace, upper), **2** (blue trace, middle lines), and the restoration of **1** (red trace, lower) from **2** after purge cycles with Ar and evacuation at 4.2 K. Right: Expanded view of the low-field portion of the EPR spectrum. The asterisk denotes an impurity of $S = 1/2$ with $g = 2.00$.

not induce a large decrease in the hyperfine splitting.^{18,28} This contrasting behaviour stems from the formation of a peroxo adduct in the case of Mn, which features minimal unpaired electron density on the O₂ ligand and thus no significant decrease in the overall ⁵⁵Mn hyperfine splitting. Together, these EPR data support O₂ binding to a high-spin four-coordinate $S = 5/2$ Mn^{II} center to form a high-spin Mn^{IV} peroxo species.

O₂ Adsorption. The reversibility of the O₂ interaction enables quantitation of the O₂ binding thermodynamics in PCN-224Mn^{II} through variable temperature O₂ adsorption measurements. Toward this end, O₂ uptake data were collected at selected temperatures between 233 and 298 K, as depicted in Figure 4.6. At 233 K, the O₂ isotherm exhibits an initial steep uptake at low pressure. As the temperature is increased, the slope of this steep region decreases until the isotherm becomes closer to linear at 298 K. To quantify the strength of O₂ binding, the isotherm data were fit to a dual-site Langmuir-Freundlich model, and subsequent treatment of the variable-temperature data with the Clausius-Clapeyron equation revealed a differential enthalpy of adsorption of $h_{\text{ads}} = -49.6(8)$ kJ/mol at low loading, followed by a gradual drop near 1:1 Mn:O₂ to a plateau at $h_{\text{ads}} = -9(2)$ kJ/mol. We assign these values to O₂ binding at the Mn center and physisorption to the remainder of the MOF surface, respectively.

The binding of O₂ to Mn^{II} in PCN-224Mn^{II} is significantly stronger than the analogous values measured for O₂ binding at the four-coordinate metal centers in PCN-224Fe^{II} and PCN-224Co^{II} of -34(4) and -15.2(6) kJ/mol, respectively.^{16,18} As previously discussed, the difference in binding enthalpy can primarily be attributed to the difference in the redox couple at the metal center associated electron transfer reaction upon the binding of O₂.^{12a,29} In line with this relationship, the enthalpy of M–O₂ binding from Mn to Fe to Co in PCN-224M^{II} decreases as $E_{1/2}$ (V vs SCE) of M^{II/III} of the analogous four-coordinate molecular metalloporphyrins becomes less reducing (Mn: -0.230; Fe: -0.047; Co: +0.320).²⁹ Note, however, that binding enthalpy in Mn is further strengthened by the fact that O₂ binding involves a two-electron transfer from Mn to O₂.

4.3 Conclusions

The foregoing results demonstrate the ability of a MOF to enable the isolation and crystallographic characterization of a four-coordinate manganese porphyrin center and its corresponding O₂ adduct. A combined array of single-crystal X-ray diffraction, solid-state infrared, and EPR analysis collectively demonstrate the O₂ complex to comprise a peroxo ligand bound in a side-on, η^2 mode to an $S = 3/2$ Mn^{IV} ion. In addition,

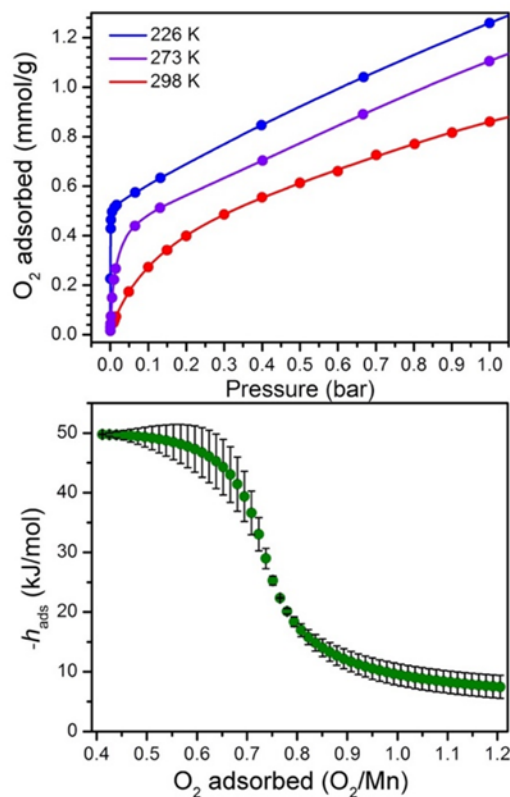


Figure 4.6. Upper: O₂ adsorption data for **1** at 233, 273, and 298 K (blue to red gradient). Circles represent data, and solid lines correspond to fits using a dual-site Langmuir–Freundlich model. Lower: O₂ differential enthalpy of adsorption curve for **1**, plotted as a function of O₂ adsorbed. Green circles represent data, and error bars are shown in black.

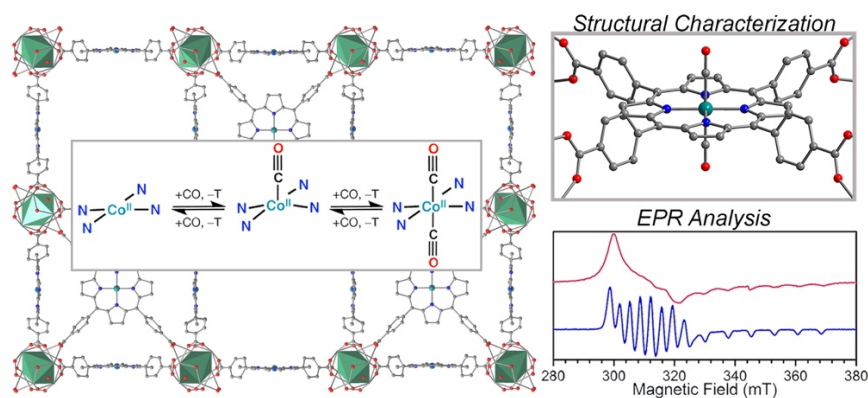
these experiments reveal that O₂ binding is reversible, even at ambient temperature, in stark contrast to behaviour observed in molecular analogues. Finally, O₂ gas adsorption measurements are employed to quantify the enthalpy of O₂ binding as $h_{\text{ads}} = -49.6(8)$ kJ/mol. This value is considerably higher than in the corresponding Fe- and Co-based MOFs, and the strength of binding is found to increase with increasing reductive capacity of the M^{II/III} redox couple. Work is underway to carry out and study the protonation, O–O bond cleavage, and O-atom transfer ability of the peroxo ligand, with emphasis on isolating and structurally characterizing the intermediates involved in these processes.

Chapter 5: CO Binding at a Four-Coordinate Cobaltous Porphyrin Site in a Metal-Organic Framework: Structural, EPR, and Gas Adsorption Analysis

Reprinted with permission from:

Gallagher, A. T.; Kelty, M. L.; Park, J. G.; Anderson, J. S.; Mason, J. A.; Walsh, J. P. S; Collins, S. L.; Harris, T. D. *Inorganic Chemistry* **2017**, *56*, 4654-4661.

Copyright 2017 American Chemical Society.



5.1 Introduction

The interactions of metalloporphyrin centers with small gaseous signaling molecules, such as O₂, CO, and NO, are central to biological processes ranging from neurotransmission to O₂ transport and storage.¹ The diverse functionality of metalloporphyrin-containing proteins is largely dependent upon the ability of the reaction centers to discriminate and selectively interact with these gaseous substrates. As such, there is significant interest in understanding how changes in the electronic structure of both the metal center and gaseous signaling molecules affect the thermodynamics of substrate binding to the metal ions. In particular, a substantial research effort has focused on probing the interaction of CO with metalloporphyrin model complexes, in large part aimed to better understand the factors that govern O₂ vs CO binding in iron(II) porphyrin, or heme, centers of the proteins hemoglobin and myoglobin.² In comparison to hemes, significantly less is known about the dynamics of CO binding to other metalloporphyrins.

In addition to hemes, cobalt porphyrin complexes have also garnered interest, partly owing to their biological relevance as synthetic analogues of vitamin B₁₂ and their ability to form dioxygen adducts in a manner analogous to the hemes.^{3,4} However, previous studies have shown markedly different reactivity of CO with hemoglobin relative to the cobalt(II)-substituted analogue coboglobin.^{4a} For instance, hemoglobin readily binds CO at ambient temperature and pressure, whereas no appreciable binding occurs between CO and the cobalt center of coboglobin under the same conditions. In contrast, cobalt(III) porphyrins behave similarly to their isoelectronic iron(II) analogues, and readily bind CO to form both mono- and dicarbonyl adducts.⁵ Nevertheless, no examples of cobalt porphyrin carbonyl adducts have been structurally characterized.

Carbonyl adducts of cobalt(II) porphyrin complexes have been observed in molecular form, however, their study has been limited to minimal spectroscopic characterization.⁶ More specifically, vibrational spectra at cryogenic temperatures have suggested the presence of both mono- and dicarbonyl adducts.^{6a} Thus far, however, only monocarbonyl cobalt porphyrin complexes have been observed by EPR, and no carbonyl adducts have been crystallographically characterized.^{6b,c} Indeed, the lability of the CO ligand in these complexes presents a key challenge to their isolation and study. Consequently, our knowledge of the nature of CO binding to cobalt(II) porphyrin complexes, particularly in regard to its temperature dependence, remains relatively limited.

As an alternative to employing molecular systems, one can envision probing interactions between Co and CO within a porphyrinic metal-organic framework (MOF). MOFs exhibit porous solid-state structures that enable the facile diffusion of gas-phase substrates to interact with coordinatively-unsaturated metal centers. Furthermore, whereas the thermal lability of the carbonyl adducts to the cobalt porphyrin center presents a tremendous challenge toward crystallographically characterizing molecular species, the crystallinity of MOFs provides an ideal platform to carry out single-crystal-to-single-crystal studies as a function of temperature and gas dosing. As an example, we previously showed that the porphyrinic MOF PCN-224⁷ can be utilized to comprehensively examine the geometric and electronic structures of oxyiron⁸ and oxycobalt⁹ complexes.

Herein, we report a comprehensive analysis of CO binding to Co^{II} in PCN-224, using a combined array of solid-state infrared spectroscopy, single-crystal X-ray diffraction, EPR spectroscopy, and CO adsorption analysis. In particular, this work provides crystallographic

characterization of a cobalt dicarbonyl adduct, spectroscopic evidence for a distinct monocarbonyl analogue at higher temperature, and a quantitation of CO binding thermodynamics.

5.2 Results and Discussion

Infrared Spectroscopy.

As an initial investigation into the interaction of CO with the cobalt porphyrin center, a desolvated sample of PCN-224Co^{II} was exposed to ca. 1 atm of dry CO and monitored by variable-temperature diffuse-reflectance infrared Fourier transform spectroscopy (DRIFTS). At ambient temperature, no significant

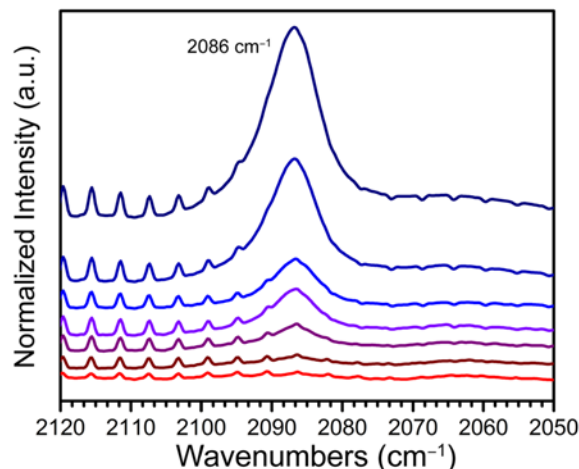


Figure 5.1 Variable-temperature diffuse-reflectance infrared Fourier transform spectra (DRIFTS) for PCN-224Co^{II} plus CO from 213-295 K (blue to red gradient), featuring a strong ν_{CO} vibration at 2086 cm^{-1} .

differences were observed in the infrared spectra of PCN-224Co^{II} before and after addition of CO. However, upon cooling the sample to -35°C , a strong ν_{CO} stretching vibration appeared at 2086 cm^{-1} (Figure 5.1). This feature is relatively close in frequency, albeit slightly higher, to those of 2073 and 2077 cm^{-1} previously assigned to the molecular complexes (TPP)Co(CO) and (TPP)Co(CO)₂ (H_2TPP = 5,10,15,20-tetraphenylporphyrin), respectively, as isolated in a frozen Kr matrix.⁶ Upon warming the sample back to 298 K, this feature disappeared to give a spectrum identical to that obtained before cooling. Together, these results indicate a weak and reversible binding of CO with the cobalt center in PCN-224Co^{II}. Based on the temperature at which these spectra were collected, we postulate this low-temperature species to be a monocarbonyl adduct,

although we note that IR analysis alone cannot distinguish between mono- and dicarbonyl complexes. Notably, the interaction of CO to the cobalt porphyrin center here is distinct from molecular iron(II) heme and cobalt(III) porphyrin complexes, which readily bind two equivalents CO to form mono- and dicarbonyl metalloporphyrin complexes, respectively.^{5,10}

The vibrational frequency of CO provides an important spectroscopic handle to assess how the electronic structure is perturbed upon binding. Overall, the frequency of ν_{CO} results from the combined effects of σ donation from the CO ligand to the metal center, which should increase the frequency of ν_{CO} relative to the 2143 cm^{-1} of free CO, and π back-donation from the metal to the CO ligand π^* orbitals, which should decrease the frequency.¹¹ Accordingly, in the case of the cobalt carbonyl adduct in PCN-224Co^{II}, the decrease in energy of ν_{CO} relative to free CO is consistent with significant π backbonding from the Co-based d_{xz} and d_{yz} orbitals into the CO-based π^* orbitals, which weakens the C \equiv O bond. By comparison, ν_{CO} for the carbonyl complex in PCN-224Co^{II} falls intermediate between the complexes

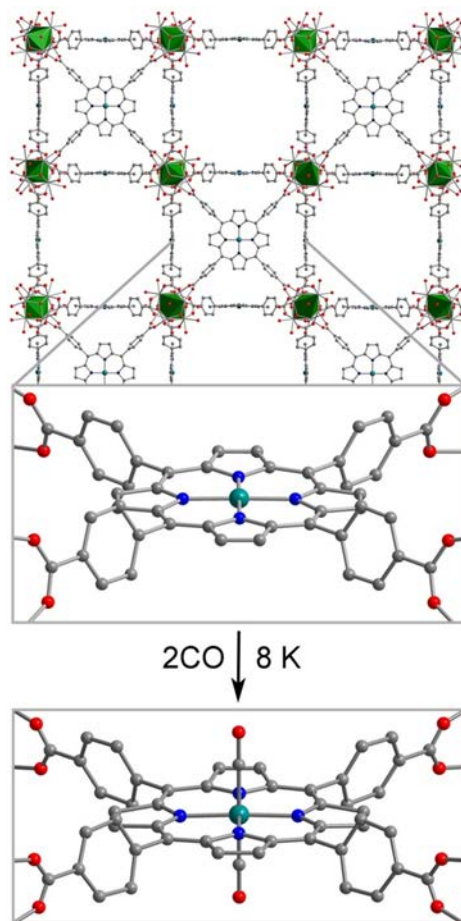


Figure 5.2 Reaction of PCN-224Co^{II} with CO at 8 K to form PCN-224Co(CO)₂. Vertices of the green octahedra represent Zr atoms; teal, red, blue, and gray spheres represent Co, O, N, and C atoms, respectively; hydrogen atoms are omitted for clarity. Selected interatomic distances (Å) and angles (°) for PCN-224Co(CO)₂: Co–C 1.89(4), Co–N 1.993(7), and C–O 1.18(5), Co–C–O 180.

(TPP)Fe^{II}(CO)^{10a} and [(OEP)Co^{III}(CO)]⁺ (H₂OEP = 2,3,7,8,12,13,17,18-octaethylporphyrin)^{5a}, which have been reported to feature ν_{CO} at 1973 and 2110 cm⁻¹, respectively, at ambient temperature. This trend of increasing energy of ν_{CO} in moving from Fe^{II} to Co^{II} to Co^{III} correlates well with increasing effective nuclear charge.¹¹ This increase in nuclear charge density across the series serves to contract electron density at the metal center, such that π backbonding into the CO π^* orbitals is progressively diminished.

Single-Crystal X-ray Diffraction. The difference in CO binding by Co^{II} relative to the analogous d⁶ Fe^{II} and Co^{III} complexes prompted us to investigate this binding by single-crystal X-ray diffraction analysis. MOFs are particularly suitable for such studies, as they often retain single crystallinity upon gas binding. Toward this end, a single crystal of PCN-224Co^{II} was sealed in a thin-walled boron-rich capillary tube under ca. 1 atm of dry CO and was then investigated by variable-temperature X-ray diffraction analysis between 8 and 200 K. At 8 K, the metalloporphyrin unit within the structure features a six-coordinate Co center, residing on a site of approximate four-fold symmetry, coordinated to two *trans*-disposed CO ligands to give PCN-224Co(CO)₂ (see Figure 5.2). Interestingly, this *trans* orientation of the CO ligands contrasts the *cis*-orientation recently observed by scanning tunneling microscopy for (TPP)Co(CO)₂ adsorbed on a Cu(111) substrate, where the TPP²⁻ ligand was structurally restrained in a saddle-like conformation.¹²

At 8 K, the structure of PCN-224Co(CO)₂ features a Co center that is situated within the N₄ plane comprised of the four pyrrole nitrogen atoms, with a Co–C distance of 1.89(4) Å and a C–O distance of 1.18(5) Å. These values are nearly statistically identical to those of 1.856(1) Å and 1.122(1) Å reported for (OEP)Fe(CO)₂ at 100 K,^{10b} albeit with considerably larger estimated

standard deviations. The slightly longer M–C bond Co vs Fe is consistent with weaker CO binding in the former, and perhaps results from the presence of a singly-occupied σ^* molecular orbital of Co d_z^2 character in conjunction with weaker π backbonding. In contrast, the slightly longer C–O bond for Co is unexpected, given the lesser extent of π backbonding as evidenced by IR spectroscopy. However, this value should be considered with caution in view of the large thermal ellipsoid of O. In addition, the structure of PCN-224Co(CO)₂ features a Co–C–O angle of 180°. Again, however, the relatively large thermal parameter of O may indicate the presence of a very slight off-axis tilt of the CO ligands, in particular as an Fe–C–O angle of 173.95(5)° has been reported for (OEP)Fe^{II}(CO).^{10b} Nevertheless, to the best of our knowledge, PCN-224Co(CO)₂ represents the first crystallographically-characterized example of a cobalt porphyrin bound to a CO ligand. Moreover, this compound represents the first dicarbonyl adduct of a non-iron first-row metalloporphyrin to be crystallographically characterized.

Modeling the CO ligand crystallographic site provides a handle through which to assess the extent of CO binding at each temperature. For instance, in the structural data at 8 K, the carbonyl C and

O occupancies were best modeled with a CO occupancy of 100%, which corresponds to a 1:2 Co:CO ratio and thus a dicarbonyl adduct (see Experimental Section). As the

Table 5.1 Selected crystallographic parameters for PCN-224Co^{II} in the presence of CO.

Temperature (K)	8	80	150	200
%CO occupancy	100	97(5)	48(4)	48(4)
Co:CO	1:2	1:1.95	1:0.96	1:0.96

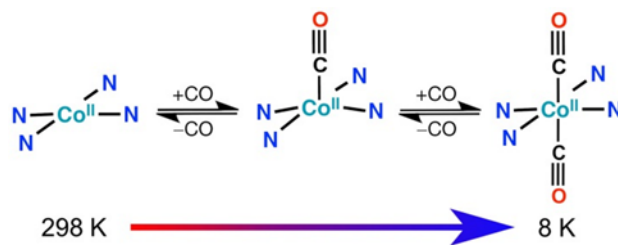


Figure 5.3. Depiction of CO binding to the Co porphyrin center in PCN-224Co^{II}, showing the equilibrium between the four-coordinate, mono- and dicarbonyl species.

temperature was increased, this occupancy was found to decrease upon free refinement (see **Table 5.1**). At 80 K, the occupancy refined to 97(5)%, indicating that still nearly all Co centers bind two CO ligands. In contrast, at 150 and 200 K, the structure refined to an CO occupancy of 48(4)%, which corresponds to a Co:CO ratio of 1:1. Note that data collected above 200 K could not be reliably modeled owing to a combination of thermal motion and the likely presence of multiple species.

The 1:1 Co:CO ratio at 150 and 200 K most likely indicates the presence of an equilibrium mixture whose composition is made up predominantly of a five-coordinate cobalt monocarbonyl adduct (see Figure 5.3). While we would expect for this species a small displacement of the Co center from the N₄ plane, possibly slightly less than that of 0.20(1) Å observed for (OEP)Fe(CO), the axial elongation of the Co thermal ellipsoids at these temperatures may mask such a displacement. Indeed, a similar equilibrium has been observed for mixtures of (TPP)Fe(CO) and (TPP)Fe(CO)₂.^{10a} Nevertheless, X-ray diffraction analysis alone cannot unambiguously identify a cobalt monocarbonyl species in PCN-224Co^{II}.

Electron Paramagnetic Resonance (EPR) Spectroscopy. In order to further probe CO binding in PCN-224Co^{II}, variable-temperature continuous-wave X-band EPR spectra were collected on an activated crystalline sample of PCN-224Co^{II} under an atmosphere of dry CO (see Figure 5.4). As has been previously reported, in the absence of CO, PCN-224Co^{II} exhibits an axial spectrum with an eight-line pattern splitting pattern arising from the hyperfine coupling of the unpaired electron to the $I = 7/2$ ⁵⁹Co nucleus (see Figure 5.4, upper).⁹ Upon dosing PCN-224Co^{II} with ca. 1 atm of CO, the spectrum changed dramatically (see Figure 5.4, lower). In general, at higher temperatures, the spectrum features a single broad resonance, however, lower-

temperature spectra exhibit much more intricate patterns. Indeed, cobalt porphyrin complexes are known for their diagnostic EPR signals, particularly in regard to changes in coordination sphere and local symmetry at the central Co ion.¹³

To model the variable-temperature data, spectral simulations were carried out using the program Easyspin¹⁴ and the Hamiltonian $\hat{H} = (g_{\parallel} + g_{\perp})\mu_B \mathbf{H} \mathbf{S} + \mathbf{I}_{Co} \mathbf{A}_{Co} \mathbf{S}$, where μ_B is the Bohr magneton, \mathbf{H} is the applied dc magnetic field, g_{\parallel} and g_{\perp} are the parallel and perpendicular components of the g -tensor, \mathbf{S} and \mathbf{I}_{Co} are the

electronic and ^{59}Co nuclear spins, respectively, and \mathbf{A}_{Co} is the tensor for hyperfine coupling to the ^{59}Co nucleus. At all temperatures, data collected for PCN-224Co^{II} in the presence of CO exhibit an axial signal and were best modeled as a single, $S = 1/2$ species (see Figures 5.3). The key simulation parameters for selected temperatures of PCN-224Co^{II}, both in the absence and the presence of CO, are enumerated in Table 5.2, with the parallel direction taken to be the axis normal to the porphyrin N₄ plane.

The electronic structure of the square planar low-spin Co^{II} complex in PCN-224Co^{II} exhibits significant 4s-3d_{z²} orbital mixing,¹⁵ which induces an increased electronic spin density at the metal nucleus to result in an unusually large degree of hyperfine coupling. In contrast, upon axial

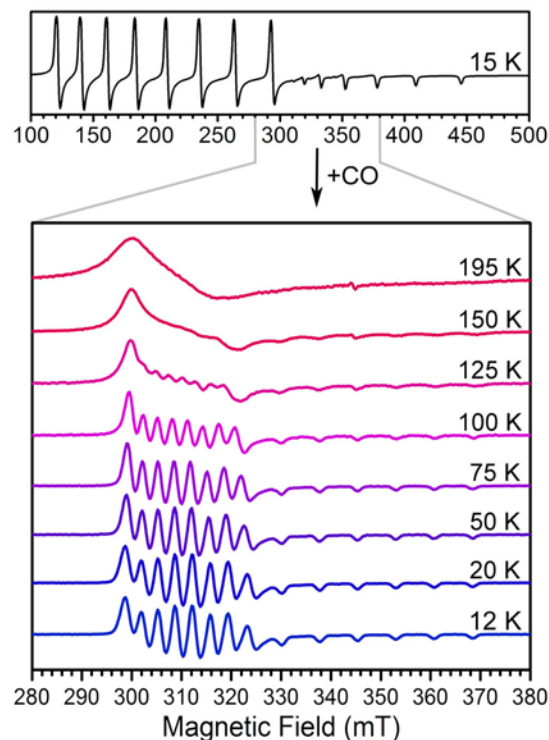


Figure 5.4 X-band EPR spectra for activated PCN-224Co^{II} before (upper, ref 9b) and after (lower) dosing with 1 atm CO at selected temperatures. Microwave frequency = 9.632 GHz; microwave power = 0.199 mW.

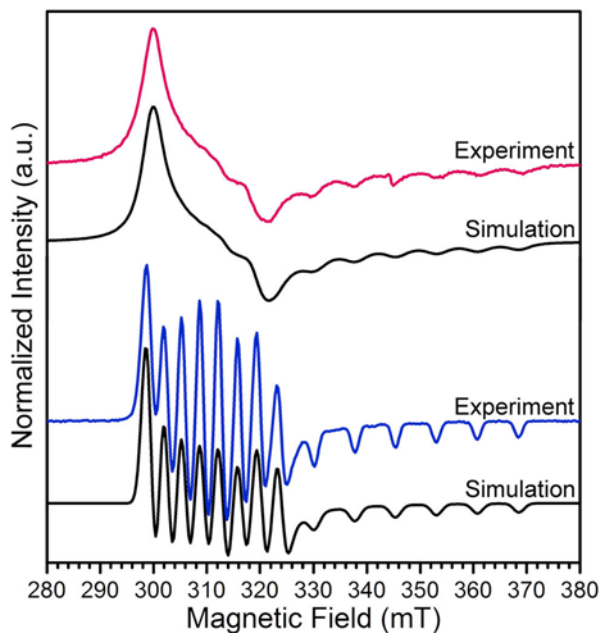


Figure 5.5 Experimental and simulated X-band EPR spectra for PCN-224Co^{II} dosed with ca. 1 atm CO at 125 K (upper) and 12 K (lower).

Table 5.2. Parameters corresponding to simulated EPR spectra for PCN-224Co^{II} in the absence and presence of CO.

T/K	g_{\perp}	A_{\perp} /MHz	g_{\parallel}	A_{\parallel} /MHz
evacuated ^a				
15	3.271(4)	1122(4)	1.783(3)	480(5)
under CO				
12	2.208(1)	108(1)	2.012(1)	215(2)
20	2.208(1)	108(1)	2.012(1)	215(1)
50	2.210(1)	104(1)	2.012(1)	215(2)
75	2.210(1)	100(2)	2.012(1)	215(1)
100	2.215(1)	93(1)	2.012(1)	215(2)
125	2.219(1)	79(3)	2.012(1)	215(1)
150	2.220(1)	79(1)	2.012(1)	215(3)
195	2.220(4)	79(6)	2.012(5)	215(5)

^aData obtained from reference 9.

induces a substantial decrease in the hyperfine coupling.

In the absence of significant changes to the electronic structure of a paramagnetic metal, the g -tensor value should remain relatively constant as a function of temperature.¹⁶ In the case of cobalt porphyrin complexes, perturbation of the electronic structure through axial ligand binding

ligation, covalency effects lead to partial transfer of the spin density from the Co^{II} nucleus onto the axial ligand(s) so as to decrease the strength of hyperfine coupling. This scenario was observed in the case of PCN-224Co^{II} in the presence of CO at 12 K, where the data were best modeled with hyperfine coupling constants of $A_{\parallel} = 215(2)$ MHz and $A_{\perp} = 108(1)$ MHz, representing a significant decrease relative to the values of $A_{\parallel} = 480(5)$ MHz and $A_{\perp} = 1122(4)$ MHz associated with the compound at 15 K in the absence of CO. These observations indicate a strong σ interaction between Co and CO ligand(s), which shifts spin density from the singly-occupied Co d_z^2 orbital onto the CO ligand and thus

often manifests as significant changes to g_{\perp} .¹⁷ As such, the temperature dependence of g_{\perp} extracted from the data collected in the range 195–12 K for PCN-224Co^{II} in CO could imply the presence of distinct cobalt mono- and dicarbonyl species. At 12 K, the spectrum was best modeled with $g_{\parallel} = 2.012(1)$ and $g_{\perp} = 2.208(1)$ (Figure 5.5). With increasing temperature, g_{\parallel} remains constant, whereas g_{\perp} increases to a maximum value of $g_{\perp} = 2.220(1)$ at 150 K (see Table 5.2 and Figure 5.5). The significant difference in g_{\perp} , in conjunction with the identical value of g_{\parallel} , suggests an equilibrium between two distinct species within this temperature range. As ascertained through X-ray diffraction above, a dicarbonyl complex can be unambiguously assigned at 8 K. From these EPR data, we postulate that a monocarbonyl species predominates at 150 K. Indeed, these data are nearly identical to those previously reported for a 1:1 (TPP)Co:CO adduct trapped in a frozen toluene solution at 123 K.^{6bc} Note that spectral broadening with increasing temperature has impeded our efforts to simulate the spectra using multiple spin centers.

Moreover, in cobalt porphyrin systems, the value of g_{\perp} varies largely as a function of the energy separation between $d_{xz,yz}$ and d_z^2 orbitals, where increasing this separation causes g_{\perp} to approach the free electron value of 2.0023.¹⁸ Upon moving from a mono- to dicarbonyl complex within PCN-224Co^{II}, one would expect an overall increase in separation between the $d_{xz,yz}$ and d_z^2 orbitals, stemming from a combination increased π backbonding and σ interactions between Co and CO. The temperature dependence of g_{\perp} observed here is therefore consistent with conversion of a dicarbonyl to monocarbonyl with increasing temperature.

Finally, the larger value of $A_{\perp} = 108(1)$ MHz at 12 K vs 79(1) MHz at 150 K is also

consistent with the foregoing assignment. In a monocarbonyl complex, the Co^{II} center adopts a five-coordinate geometry, where the Co^{II} ion is expected to be slightly displaced from the N_4 plane. In contrast, upon binding a second equivalent of CO, the six-coordinate Co center returns to a site of local D_{4h} symmetry. This effect in turn increases the degree of $4s-3d_z^2$ orbital mixing in the six- vs five-coordinate complex, and thus leads to a stronger hyperfine coupling. Nevertheless, the value of A_{\perp} for the dicarbonyl complex is still much lower than that for the four-coordinate Co^{II} prior to CO

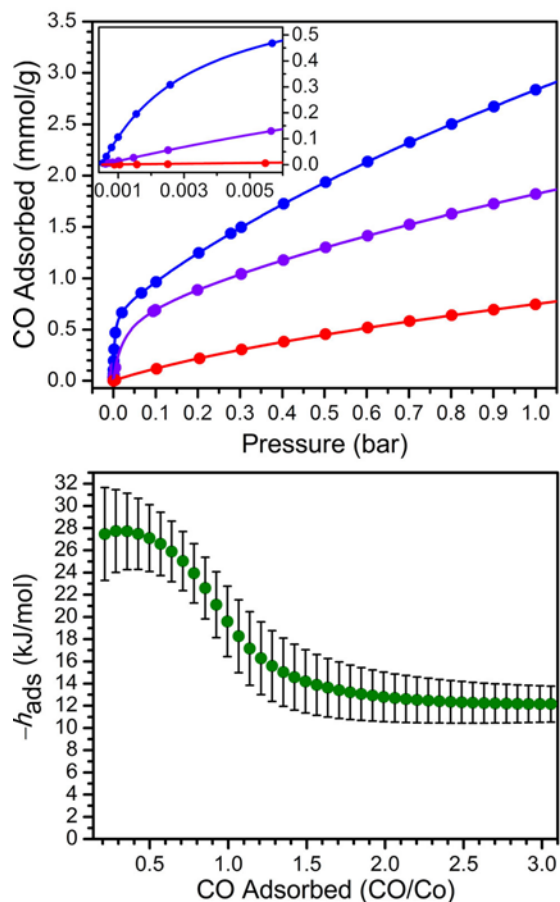


Figure 5.6 Upper: CO adsorption data for PCN-224Co^{II} at 195, 226, and 273 K (blue to red gradient), including an expanded view of the low-pressure region (inset). Circles represent data, and solid lines correspond to fits using a dual-site Langmuir–Freundlich model. Lower: CO differential enthalpy of adsorption curve for PCN-224Co^{II}, plotted as a function of CO adsorbed. Green circles represent data, and error bars are shown in black.

addition, and this observation is reflective of spin density being transferred from the Co^{II} center onto the CO ligands.

CO Adsorption. In order to quantitatively assess the thermodynamics of CO binding in PCN-224Co^{II}, CO adsorption measurements were carried out. These data were collected at selected temperatures between 195 and 273 K, and are depicted in Figures 5.6. At 195 K, the CO isotherm exhibits an initial step uptake at low pressure. As the temperature is increased, the

slope of this steep region decreases until the isotherm becomes nearly linear at 273 K. To quantify the strength of CO binding, the isotherm data at each temperature were fit to a dual-site Langmuir-Freundlich model. Subsequent treatment of the variable-temperature data with the Clausius-Clapeyron equation revealed a differential enthalpy of adsorption of $h_{\text{ads}} = -29(2)$ kJ/mol at low loading, followed by a gradual drop near 1:1 Co:CO to a plateau at $h_{\text{ads}} = -12(2)$ kJ/mol. We respectively assign these distinct values to CO binding to the Co center and physisorption to the remainder of the MOF surface.

The binding enthalpy of CO to the cobalt porphyrin center is significantly stronger than the previously characterized interaction of O₂ with PCN-224Co^{II} of $-15.2(6)$ kJ/mol.⁹ This difference in binding enthalpy can primarily be attributed to the stronger σ interaction of Co with CO vs O₂. This trend is consistent with previously reported studies for Fe centers in hemoglobin and model complexes, where CO and O₂ binding enthalpies fall in the range of 68–73 kJ/mol and 63–65 kJ/mol, respectively.¹⁹ However, the difference between O₂ and CO binding strengths in PCN-224Co^{II} is much larger than the corresponding values for Fe. This discrepancy may stem from the fact that the Co complex in PCN-224Co^{II} does not feature an axial ligand, whereas the Fe compounds whose enthalpies are cited above do.

As discussed above, the much weaker CO binding for Co^{II} vs Fe^{II} likely stems in large part from the singly-occupied d_z^2 -based σ^* orbital for Co, in conjunction with the decreased π backbonding arising from a higher effective nuclear charge for Co. In addition, consideration of metal spin state may also help to rationalize the weak CO binding.²⁰ For example, four-coordinate ferrous heme species feature an $S = 1$ ground state, and binding of CO induces a spin state change to $S = 0$.^{10,21,22} In contrast, the $S = 1/2$ four-coordinate cobaltous porphyrin does not

undergo a spin state upon binding CO. Indeed, just such a spin state transition has been recently demonstrated to facilitate selective CO binding over other gases in an iron(II) triazolate MOF.²³

5.3 Conclusion

The foregoing results demonstrate the ability of MOFs to enable a comprehensive study of CO binding at coordinatively-unsaturated metalloporphyrins complexes. Variable-temperature single-crystal X-ray diffraction analysis revealed the formation of a cobalt dicarbonyl adduct at low temperature, representing the first crystallographically-characterized cobalt porphyrin carbonyl species. This dicarbonyl complex was also observed at low temperature by EPR spectroscopy, and warming of the sample showed the conversion of this species to a monocarbonyl analogue. In addition, the CO binding at the Co^{II} center was quantified through variable-temperature CO gas adsorption measurements, with a fit to the data providing a differential enthalpy of adsorption of $h_{\text{ads}} = -29(2)$ kJ/mol. Finally, this work provides only the second example of a MOF wherein multiple gas molecules bind a single coordinatively-unsaturated metal center, and therefore represents a step toward developing porous materials that can facilitate selective gas binding through fine-tuning the electronic structure of metal centers.²⁴

EXPERIMENTAL SECTION

General Considerations. Unless otherwise noted, all materials and chemicals were purchased from commercial suppliers and used without further purification. Additionally, unless otherwise stated, all manipulations were carried out under an atmosphere of dinitrogen using either standard Schlenk techniques or in a Vacuum Atmospheres Nexus II glovebox. All glassware was dried at 150 °C and allowed to cool under vacuum prior to use. All solvents were dried on a solvent purification system from Pure Process Technology and stored under N₂ over 4 Å

molecular sieves. Effective removal of O₂ and H₂O from solvents was verified using a standard solution of Na benzophenone ketyl radical anion. The material PCN-224Co^{II} was prepared as previously reported.⁹

Diffuse-Reflectance Infrared Fourier Transform Spectroscopy (DRIFTS). Samples were prepared as a 10-fold dilution of PCN-224Co^{II} in KBr and pulverized with a mortar and pestle to make a smooth, homogenous powder. Samples was then transferred to a Praying MantisTM low-temperature reaction chamber under a dinitrogen atmosphere. Data collections were performed on a Thermo Nicolet 6700 FT-IR spectrometer with a tabletop 110v Harrick temperature controller rated for 25 to -150 °C at the Northwestern Clean Catalysis (CleanCat) Core Facility. The data was collected under a constant flow of CO.

Variable-Temperature X-ray Structure Determination. A single crystal of PCN-224Co^{II} was added to a 0.3 mm boron-rich X-ray capillary (Charles-Supper Company), which was then evacuated at 150 °C for 12 h on a Schlenk line. The capillary was dosed with ca. 1 atm CO at ambient temperature and flame-sealed under reduced pressure at -78 °C. The capillary was then fixed to a goniometer head with a PELCO[®] water based colloidal graphite epoxy.

Variable-temperature analysis for PCN-224Co^{II} in the presence of CO was performed at 8, 80, 150, and 200 K. All successive data collections at the various temperatures were obtained on the same crystal. Data obtained at 80, 150, and 200 K were collected on a Bruker APEX II diffractometer equipped with CuK α microsource (MX optics), where the temperature was controlled with a Cryostream 700 liquid nitrogen cryostat from Oxford Cryosystems. The 8 K data were collected on a Bruker Kappa Apex II diffractometer equipped with an APEX-II detector and MoK α microsource (QuazarTM optics) and cooled by a Cryocool-LHe cryostat

from Cryo Industries.

Raw data obtained from the data collections at 8, 80, 150, and 200 K were integrated and corrected for Lorentz and polarization effects using Bruker APEX2 v. 2009.1.4 Absorption corrections were applied using SADABS.²⁵ Space group assignments were determined by examination of systematic absences, E-statistics, and successive refinement of the structures. Structures at 80, 150, and 200 K were solved and refined with SHELXL²⁶ operated with the Olex2 interface with the aid of standard restraints.^{27,28} Disorder in the structure was modeled by splitting the atomic coordinates, and residual electron density found in the difference Fourier map was removed using the solvent mask protocol included in Olex2. This residual electron density likely arises from either residual solvent or partial occupation of a separate morphology of the closely related MOF-525.²⁹

The occupancies of the CO ligands of the data collected at 80, 150, and 200 K were freely refined. The occupancy obtained from the free refinement of the CO ligands was then fixed prior to the application of the solvent mask to prevent any redistribution of electron density. C-O bonds were restrained to prevent their artificial elongation or contraction, due to the potential presence of a various species in these structures i.e. monocarbonyl, dicarbonyl, and the unbound Co^{II} porphyrin centers. Bond metrics from these structures represent an average of the species present at each temperature. Multiple diffraction intensity data sets were collected at 8 K due to the unavoidable formation of ice on the capillary containing PCN-224Co^{II} plus CO gas. Data sets were merged, scaled, and reflections of the sample that overlapped with reflections from the ice were omitted. The Jana2006 software was then used to combine all of the intensity data collected at 8 K.³⁰

Electron Paramagnetic Resonance (EPR) Spectroscopy. A polycrystalline sample of PCN-224Co^{II} was loaded into a quartz EPR tube under a dinitrogen atmosphere. The quartz EPR tube was then evacuated and dosed with ca. 1 atm CO at ambient temperature and flame-sealed under reduced pressure at 77 K. Continuous-wave EPR spectra were collected on this sample at 12, 20, 50, 75, 100, 125, 150, and 195 K. Measurements were performed at the University of Chicago EPR facility using a Bruker Elexsys 500 X-band EPR spectrometer. Temperatures were held constant using an Oxford Systems continuous-flow helium cryostat coupled with a 10 K helium stinger from Bruker. Spectra were acquired with the Bruker Win-EPR software suite. The spectrometer was equipped with a dual mode cavity, operating in perpendicular mode. Data were collected using the following instrumental parameters: radiation frequency = 9.632 GHz; microwave power = 0.199 mW; modulation amplitude = 5 G; modulation frequency = 100 kHz. Spectral simulations were carried out using the program Easyspin.¹²

Gas Adsorption Measurements. Crystalline material of PCN-224 or PCN-224Co^{II} was transferred into a pre-weighed analysis tube which was then sealed with a TranSealTM. Activation and analysis was then performed on a Micromeritics ASAP 2020 instrument. The samples were activated at 150 °C until an outgas rate of less than 1 mTorr/minute was observed. After activation, the samples were weighed to determine the final mass of analyte. The sample was checked to ensure the outgas rate remained below 1 mTorr/minute. Carbon monoxide uptake was measured using volumetric methods and the free space of all samples was determined with UHP He prior to analysis. The analysis was performed on both PCN-224 and PCN-224Co^{II} to demonstrate that the cobalt center is responsible for the strong, initial uptake of CO. Temperature control was provided with a variety of cold baths: dry ice/isopropanol for 195 K, dry

ice/acetonitrile for 226 K, and ice bath for 273 K.

Differential Enthalpies of Adsorption Calculations. The variable-temperature CO adsorption isotherms at 195, 226 and 273 K were independently fit with a dual-site Langmuir-Freundlich model (Eqn 1), where n is the amount adsorbed in mmol/g, P is the pressure in bar, $n_{\text{sat},i}$ is the saturation capacity in mmol/g, v_i is the Freundlich parameter, and b_i is the Langmuir parameter in bar^{-v} for two sites 1 and 2.

$$n = \frac{n_{\text{sat},1} b_1 P^{v_1}}{1 + b_1 P^{v_1}} + \frac{n_{\text{sat},2} b_2 P^{v_2}}{1 + b_2 P^{v_2}} \quad (1)$$

Note that the Langmuir-Freundlich model was simply used to mathematically fit each adsorption isotherm in preparation for isosteric heat of adsorption calculations using the Clausius-Clapeyron equation, and we do not intend to attribute any physical meaning to the obtained parameters. The fitted parameters for each adsorption isotherm can be found in Table S5.

The Clausius-Clapeyron equation (Eqn 2) was used to calculate the differential enthalpies of adsorption, $-h_{\text{ads}}$, using the dual-site Langmuir-Freundlich fits at each temperature. Here, P is the pressure, n is the amount of gas adsorbed, T is the temperature, R is the universal gas constant, and C is a constant.

$$\ln P = \frac{h_{\text{ads}}}{R} \left(\frac{1}{T} \right) + C \quad (2)$$

The isosteric heats of adsorption were obtained from the slope of plots of $(\ln P)_n$ versus $1/T$. An error in the isosteric heat for a given loading can be calculated from the standard error in the slope of the best-fit line. Fundamentally, this error describes the quality of agreement between the fitted isotherms and the Clausius-Clapeyron relation.

Powder X-ray Diffraction (PXRD) Analysis. An activated powder sample of PCN-224Co^{II} was loaded into two 0.7 mm boron-rich X-ray capillaries (Charles-Supper Company). The tubes were capped with a septum and both evacuated on a Schlenk line at 150 °C for 12 h. The first sample was sealed under reduced pressure at 77 K while the second sample was dosed with 1 atm of CO prior to sealing at 77 K. PXRD data were collected at room temperature on a STOE-STADIMP powder diffractometer equipped with an asymmetric curved Germanium monochromator (Cu K α 1 radiation, $\lambda = 1.54056 \text{ \AA}$). The samples were measured in a transmission geometry utilizing a rotating capillary holder.

Chapter 6: Efforts Towards the Generation of a High-Valent Iron(V) Nitride in a Metal-Organic Framework

6.1 Introduction

Metal-ligand multiple bonds are understood to play crucial roles in both synthetic and biological catalysis.¹ Molecular model complexes of high-valent transition metal species have shown to facilitate group and atom transfer reactions for the functionalization of organic molecules.² In nature, metal-ligand multiple bonds are speculated to be involved in the mechanistic pathways of metalloenzymes. For example, experimental evidence has corroborated a mechanism wherein Cytochrome P450 catalyzes the oxidation of saturated alkanes by way of a highly reactive Fe(IV) oxo intermediate.³ In addition, high-valent iron nitrides have been studied for their potential as key intermediates in the nitrogen-fixing pathway of the metalloenzyme nitrogenase.⁴ In addition to the innate value in investigating the electronic structure and reactivity of these intermediates, the design of more efficient catalysts depends on understanding the intermediates that participate in these overall catalytic processes.

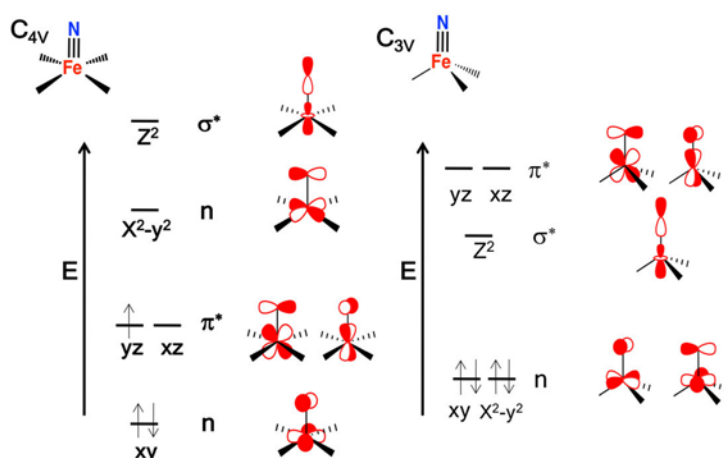


Figure 6.1 Frontier orbitals of an iron(V) nitride in four (left) and three (right) fold symmetry assuming a low spin state for iron.

Owing in part to the difficulties associated with studying these reactive intermediates within the protein native structure, researchers have turned towards synthesizing molecular model complexes. These efforts have

resulted in the isolation of myriad species relevant to synthetic and biological catalysis, including high-valent Fe-oxo⁵, -nitrido⁶, and -imido⁷ functionalities. One compound of particular interest is the porphyrin iron nitride, which is highly reactive largely as a result of the four-fold symmetry enforced by the ligand scaffold (**Fig. 1**). Nakamoto observed the first iron nitride in 1988 by the photolysis of a porphyrin iron azido precursor at ca. 30 K; iron nitride formation was characterized solely by resonance Raman spectroscopy with a $\nu_{\text{FeN}}^{\text{NN}}$ stretching frequency of 876 cm^{-1} .^{6a,b,c} Owing to their instability, iron nitrides in four-fold symmetry are transient in nature and have only been observed in frozen matrices. Under ambient conditions, iron nitrides in four-fold symmetry undergo bimolecular condensation reactions that arrest catalytic activity and prevent comprehensive characterization (**Fig. 1**). Such bimolecular condensation reactions are common as exemplified by bridging oxo species obtained from transiently formed terminal iron oxos.⁸ A key development in the investigation of iron nitrides involved the use of ligands that enforce three-fold symmetry to increase the stability of the reactive species. In a trigonal ligand field, the orbitals of dominant anti-bonding character remain unoccupied for low spin

systems. In four-fold symmetry however, the highest occupied molecular orbitals are the degenerate $d_{yz,xz}$ (Figure 6.1). This provides three-fold symmetric complexes with an overall larger bond order and increased stability. This strategy allowed for these reactive species to be studied under ambient conditions and resulted in the first crystallographically characterized terminal iron nitride.⁹ The increased stability, however, decreases the reactivity of the iron nitride functionality that is inherent to the tetragonal ligand field. Although iron nitrides in four-fold symmetry have been studied by a suite of spectroscopic techniques, they have yet to be crystallographically characterized owing to their intrinsic instability.

To overcome the challenges associated with studying these chemical species in solution, this work focuses on sequestration of metal reaction sites in metal-organic frameworks (MOFs), thereby preventing unwanted side reactions without sacrificing inherent reactivity. This approach will enable stabilization of reactive species, allowing their solid-state and electronic structure to be studied at an unprecedented level. MOFs serve as suitable candidates for this aim due to their high degree of crystallinity, which will enable characterization of the catalytic site with atomic precision. While a substantial amount of research in the past several years has focused on MOF reactivity, the use of MOFs or the stabilization and characterization of reactive species remains relatively unexplored.¹⁰

6.2 Results and Discussion

Initial synthetic work has focused on stabilization of high-valent iron nitrides in porphyrin based framework PCN-224.¹¹ PCN-224 is a highly robust framework featuring $[\text{Zr}^{\text{IV}}_6\text{O}_8(\text{H}_2\text{O})_{12}]^{8+}$ cores as structural building units linked by tetracarboxyphenylporphyrin (TCPP) organic struts. Incorporation of transition metal ions into the scaffold has been demonstrated with both pre- and

post-synthetic strategies. In addition, sizable pores of 19 Å allow for facile diffusion of substrates into the framework, providing a pathway for chemical manipulations within the superstructure. Furthermore, the large crystallite size of PCN-224 is suitable for single crystal X-ray analysis. As such, current work is focused on generating and studying highly reactive porphyrin iron nitrides using the PCN-224 framework. A commonly used method for the synthesis of iron nitrides involves the thermolysis of iron azido complexes;¹² as such the first manipulation of the

framework involved the introduction of azide functionality to the iron metal center.

The porphyrinic MOF PCN-224 was synthesized as previously described.¹¹ Subsequent metalation of the porphyrin with Fe^{III}Cl was carried out by heating single crystals of PCN-224 under N₂ in a DMF solution containing excess anhydrous FeCl₃ and 2,6-lutidine, followed by evacuation at 150 °C for 12 h, to give the compound PCN-224Fe^{III}Cl. Complete metalation of porphyrin within the bulk crystalline material was confirmed by solid-state diffuse reflectance UV/Visible spectroscopy and Mössbauer Spectroscopy (see Figure 6.2).

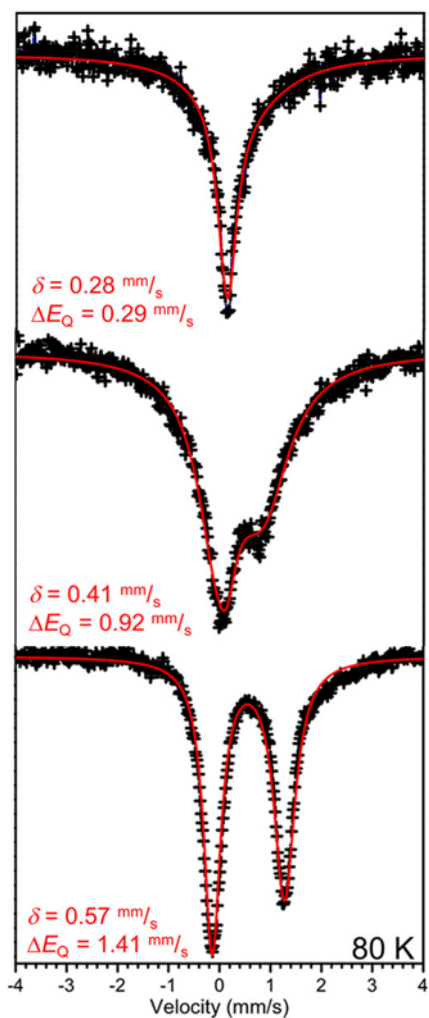


Figure 6.2 Mössbauer spectra and corresponding fit parameters for PCN-224FeCl, PCN-224FeN₃, and the thermolysis product of PCN-224FeN₃.

Next, trimethylsilylazide (Me₃SiN₃) was

used for the chemical exchange of the iron-bound chloride ligand for an azide. Soaking PCN-224FeCl with Me_3SiN_3 in THF for 24 h at 25 °C results in a new feature in the infrared spectrum at $\nu = 2050 \text{ cm}^{-1}$, consistent with the ν_{FeN} vibration of Fe- N_3 units previously reported in molecular complexes (Figure 6.3).^{6a,b,c} This suggests that some fraction of chloride has been

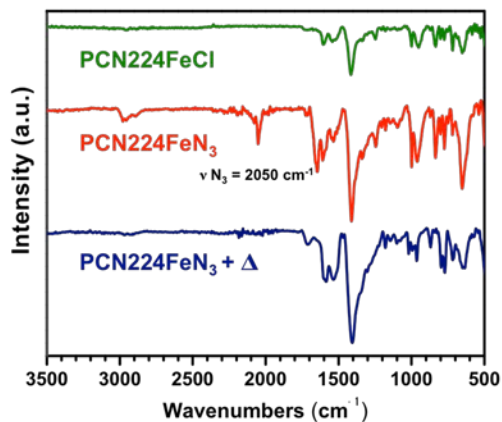


Figure 6.3 Infrared spectra for PCN-224FeCl, PCN-224FeN₃, and the thermolysis product of PCN-224FeN₃.

replaced by the azide, resulting in the formation of PCN-224FeN₃. To further confirm the substitution of the chloride for the azide, Mössbauer spectroscopy was performed on the resulting azide complex, PCN-224FeN₃ (Figure 6.2). The Mössbauer spectra shows an expected high-spin Fe(III) complex that is distinct from the Fe(III)-Cl.

Having established the complete substitution of the chloride ligand for an azide, we next turned our attention towards decomposing the azide to generate the terminal Fe(V) nitride. PCN-224FeN₃ was thermolyzed at 120 °C for 24 h, which resulted in the loss of the azide stretch at 2050 cm^{-1} in the infrared spectrum (Figure 6.3). However, subsequent inspection of the thermolysis product by Mössbauer spectroscopy revealed that the thermolytic decomposition of the heme-azide functionality provides a signal consistent with the formation of an intermediate-spin, four-coordinate iron porphyrin center (Figure 6.2). The reduction of the metal center indicates that thermolysis of the iron-azide complex results in a homolytic cleavage of the Fe-N bond, resulting in the formation of an Fe(II) center and a corresponding $\bullet\text{N}_3^-$ radical. The homolytic cleavage of the Fe- N_3 functionality upon thermolysis suggests that the most effective

route towards generating the Fe(V)-nitride will involve photolysis at cryogenic temperatures. Indeed, no molecular iron-nitride functionality has been generated through thermolytic decomposition. However, the strongly absorbing nature of the porphyrin unit has impeded efforts to photolyze this complex. After irradiation at 77 K over the course of 15 hours using various light sources, the azide functionality remains as judged by infrared spectroscopy.

6.3 Conclusion

One potential pathway to overcome the challenges associated with the photolysis experiments, involves a move towards smaller MOF particle sizes. Our group has recently demonstrated the high-throughput synthesis of nanoscale porphyrin zirconium MOFs.¹³ The use of nanoMOFs may enable more thorough light penetration into the frameworks and therefore, serve as a potential pathway to photolytically cleave the iron-azide functionality. However, for this method to be successful, the nanoMOFs must be suspended in a homogenous frozen solvent matrix with minimal aggregation of the crystallites.

Chapter 7: O₂ Binding to a Chlorine Ligated Heme Complex in Metal-Organic Framework

7.1 Introduction

Chapters 3-4 detail investigations into how the identity of metalloporphyrin center influences the thermodynamics of O₂ binding. Importantly, this work provides experimental evidence to corroborate a hypothesis that an increase in reductive capacity of the M^{II/III} redox couple correlates to a stronger enthalpy of O₂ binding.¹ Having demonstrated this trend using Mn, Fe, and Co metalloporphyrin centers, current work is now directed towards more thoroughly understanding another factor that influences O₂ binding strength, the identity of the axial ligand. In chapter 2, section 2.2, variable temperature O₂ adsorption studies show that O₂ binding in the four-coordinate heme center in PCN-224Fe^{II} is much weaker than that observed in 6-coordinate analogues featuring an axial histidine ligand.^{1a} This observation highlights the critical importance of the axial ligand on heme sites in globin proteins, as the absence of this ligand would lead to ineffectual O₂ transport properties due to a drastically weakened O₂ binding enthalpy. The difference in the enthalpy of O₂ binding is attributed to a change in the redox potential of 0.250 V between 4-coordinate and imidazole-ligated 5-coordinate heme complexes.² To further explore the role axial ligation plays in engendering changes in O₂ binding strength, our current efforts are directed towards isolating and studying heme centers in PCN-224 featuring axial ligands with various electronic properties. Here, the porous, solid-state structure of the MOF not only prevents bimolecular condensation reactions and enables introduction of gas-phase substrates in the absence of exogenous solvent, but also offers synthetic tunability, where the unsaturated heme center provides a platform by which we can introduce a variety of axial ligands.

7.2 Results and Discussion

Initial efforts have focused on studying the interaction of O₂ with a chloride ligated high-spin Fe^{II} center in PCN-224 due to the shift in the redox potential as compared to both the 4-coordinate and imidazole bound heme centers (see

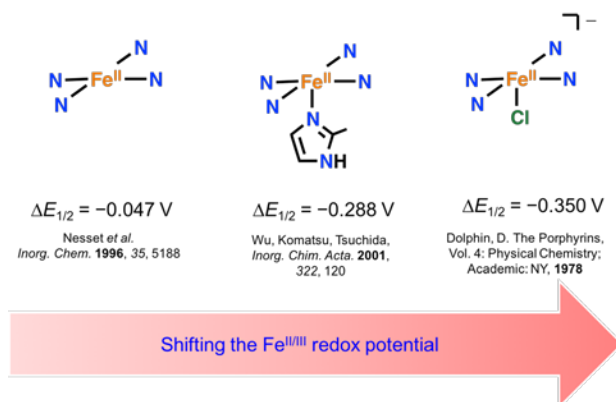


Figure 7.1 Depiction of a 4-coordinate, imidazole, and chloride ligated heme center with the corresponding $\Delta E_{1/2}$ (V vs SCE) for each species.

Figure 7.1).^{2,3} Based on these reported redox potentials, the chloride bound high-spin Fe^{II} center should engender a stronger interaction between the metal center and the O₂ ligand. Subsequent metalation of the porphyrin with Fe^{III}Cl was carried out by heating single crystals of PCN-224 under N₂ in a DMF solution containing excess anhydrous FeCl₃ and 2,6-lutidine, followed by evacuation at 150 °C for 12 h, to give the compound PCN-224FeCl. Complete metalation of porphyrin within the bulk crystalline material was confirmed by solid-state diffuse reflectance UV/Visible spectroscopy and Mössbauer Spectroscopy (see Figure 6.2). Soaking PCN-224FeCl in ten-fold molar excess of CoCp₂ in Et₂O for 12 h, resulted in the formation of a new species featuring a high-spin Fe^{II} center as judged by Mössbauer spectroscopy (see Figure 7.2). The Mössbauer spectrum of the reduced species at 80 K exhibits an isomer shift of $\delta = 0.999$ mm/s and a quadrupole splitting $\Delta E_Q = 4.636$ mm/s, consistent with previously characterized anionic high-spin iron(II) heme complexes.⁴ Having successfully synthesized this species, current work is directed towards studying its reactivity towards O₂ with an emphasis on ascertaining the strength of O₂ binding with variable temperature O₂ adsorption measurements.

7.3 Conclusion

The four-coordinate, imidazole, and chloride ligated heme complexes in PCN-224, provide an important data point in a growing series that has focused on understanding how changes in the electronic structure of the metal center influences the thermodynamics of O₂ binding. Based on the hypothesis that the strength of O₂ binding correlates to the ease of oxidation of the metal center, the high-spin Fe(II) center in PCN-224Fe^{II}-Cl⁻ should result in an O₂ binding enthalpy stronger than both that observed in both the four-coordinate and imidazole-bound heme centers. Importantly, this provides an avenue towards the formation of a stable Fe-O₂ adduct under ambient conditions, which will then open new pathways to generate reactive oxygenated heme species derived from the heme-O₂ complex.

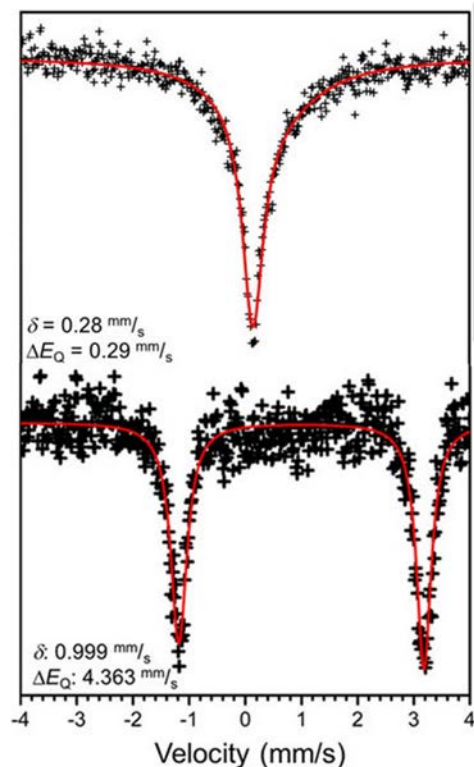


Figure 7.2 Mössbauer spectra and corresponding fit parameters of PCN-224FeCl and PCN-224Fe^{II}Cl⁻ at 80 K.

References

References for Chapter 1

- (1) (a) Sono, M.; Roach, M. P.; Coulter, E. D.; Dawson, J. H. *Chem. Rev.* **1996**, *96*, 2841-2888. (b) Meunier, B.; de Visser, S. P.; Shaik, S. *Chem. Rev.* **2004**, *104*, 3947. (c) Poulos, T. L. *Chem. Rev.* **2014**, *114*, 3919. (d) Addison, A. W.; Stephanos, J. J. **1986**, *25*, 4104. (e) Giardina, B.; Messina, I.; Scatena, R.; Castagnola, M. *Crit. Rev. Biochem. Mol. Biol.* **1995**, *30*, 165. (f) Kim, H. P.; Ryter, S. W.; Choi, A. M. K. *Annu. Rev. Pharmacol. Toxicol.* **2006**, *46*, 411.
- (2) (a) Poulos, T. L.; Finzel, B. C.; Howard, A. J. *J. Mol. Biol.* **1987**, *195*, 687. (b) Lieberman, R. L.; Rosenzweig, A. C. *Nature* **2005**, *434*, 177. (c) Rittle, J.; Green, M. T. *Science* **2010**,

330, 933.

- (3) (a) Groves, J. T.; Nemo, T. E.; Myers, R. S. *J. Am. Chem. Soc.* **1979**, *101*, 1032-1033. (b) Hill, C. L.; Schardt, B. C. *J. Am. Chem. Soc.* **1980**, *102*, 6374. (c) Groves, J. T.; Kruper, Jr., W. J.; Haushalter, R. C. *J. Am. Chem. Soc.* **1980**, *102*, 6375. (d) Watanabe, Y.; Fujii, H. *Structure and Bonding* **2000**, *97*, 61. (e) Nam, W.; Kim, I.; Kim, Y.; Kim, C. *Chem. Commun.* **2001**, 1262-1263.
- (4) (a) Momenteau, M.; Reed C. A. *Chem. Rev.* **1994**, *94*, 659. (b) Collman, J. P.; Fu, L. *Acc. Chem. Res.* **1999**, *32*, 455. (c) Collman, J. P.; Boulatov, R.; Sunderland, C. J.; Fu, L. *Chem. Rev.* **2004**, *104*, 561. (d) Suslick, K. S.; Reinert, T. J. *J. Chem. Educ.* **1985**, *62*, 974. (e) Weschler, C. J.; Hoffman, B. M.; Basolo, F. *J. Am. Chem. Soc.* **1975**, *97*, 5278. (f) Gonzalez, B.; Kouba, J.; Yee, S.; Reed, C. A.; Kirner, J. F.; Scheidt, W. R. *J. Am. Chem. Soc.* **1975**, *97*, 3247. (g) Hoffman, B. M.; Weschler, C. J.; Basolo, F. *J. Am. Chem. Soc.* **1976**, *98*, 5473. (h) Dedieu, A.; Rohmer, M. M. *J. Am. Chem. Soc.* **1977**, *99*, 8050. (i) Hoffman, B. M.; Szymanski, T.; Brown, T. G.; Basolo, F. *J. Am. Chem. Soc.* **1978**, *100*, 7253. (j) Lawrence, G. D.; Sawyer, D. T. *Coord. Chem. Rev.* **1978**, *27*, 173. (k) Jones, R. D.; Summerville, D. A.; Basolo, F. *J. Am. Chem. Soc.* **1978**, *100*, 4416. (l) Fleishcer, E. B.; Ferra, R. V. *J. Inorg. Biochem.* **1979**, *10*, 91. (m) Coleman, W. M.; Taylor, L. T. *Coord. Chem. Rev.* **1980**, *32*, 1. (n) Hanson, L. K.; Hoffman, B. M. *J. Am. Chem. Soc.* **1980**, *102*, 4602. (o) Shirazi, A.; Goff, H. M. *J. Am. Chem. Soc.* **1982**, *104*, 6318. (p) Urban, M. W.; Nakamoto, K.; Basolo, F. *Inorg. Chem.* **1982**, *21*, 3407. (q) Weselucha-Birczynska, A.;

- Proniewicz, L. M.; Bajdor, K.; Nakamoto, K. *J. Raman Spectrosc.* **1991**, *22*, 315. (r)
- Pecoraro, V. L.; Baldwin, M. J.; Gelasco, A. *Chem. Rev.* **1994**, *94*, 807. (s) Kurtikyan, T. S.; Stepanyan, T. H.; Martirosyan, G. G.; Kazaryan, R. K.; Madakyan, V. N. *Russ. Chem. Bull., Int. Ed.*, **2000**, *49*, 1540. (t) Wayland, B. B.; Mohajer, D. *J. Am. Chem. Soc.* **1971**, *93*, 5295. (u) Wayland, B. B.; Minkiewicz, J. V.; Abd-Elmageed, M. E. *J. Am. Chem. Soc.* **1974**, *96*, 2795. (v) Kozuka, M.; Nakamoto, K. *J. Am. Chem. Soc.* **1981**, *103*, 2162.
- (5) (a) Hoffman, A. B.; Collins, D. M.; Day, V. W.; Fleischer, E. B.; Srivastava, T. S.; Hoard, J. L. *J. Am. Chem. Soc.* **1972**, *94*, 3620. (b) Chin, D.-H.; La Mar, G. N.; Balch, A. L. *J. Am. Chem. Soc.* **1980**, *102*, 4344.
- (6) (a) Eddaoudi, M.; Kim, J.; Rosi, N.; Vodak, D.; Wachter, J.; O’Keeffe, M.; Yaghi, O. M. *Science* **2002**, *295*, 469. (b) Kitagawa, S.; Kitaura, R.; Noro, S.-I. *Angew. Chem. Int. Ed.* **2004**, *43*, 2334. (c) Millward, A. R.; Yaghi, O. M. *J. Am. Chem. Soc.* **2005**, *127*, 17998. (d) Ma, S.; Sun, D.; Simmons, J. M.; Collier, C. D.; Yuan, D.; Zhou, H.-C. *J. Am. Chem. Soc.* **2008**, *130*, 1012. (e) Morris, R. E.; Wheatley, P. S. *Angew. Chem. Int. Ed.* **2008**, *47*, 4966. (f) Llewellyn, P. L.; Bourrelly, S.; Serre, C.; Vimont, A.; Daturi, M.; Hamon, L.; De Weireld, G.; Chang, J.-S.; Hong, D.-Y.; Hwang, Y. K.; Jhung, S. H.; Férey, G. *Langmuir* **2008**, *24*, 7245. (g) Murray, L. J.; Dinca, M.; Long, J. R. *Chem. Soc. Rev.* **2009**, *38*, 1294. (k) Chen, B.; Xiang, S.; Qian, G. *Acc. Chem. Res.* **2010**, *43*, 1115. (h) Li, B.; Wen, H.-M.; Cui, Y.; Zhou, W.; Qian, G.; Chen, B. *Adv. Mater.* **2016**, *28*, 8819.
- (7) (a) Li, J.-R.; Kuppler, R. J.; Zhou, H.-C. *Chem. Soc. Rev.* **2009**, *38*, 1477. (b) Furukawa,

- H.; Cordova, K. E.; O'Keefe, M.; Yaghi, O. M. *Science* **2013**, *341*, 974. (c) Cui, Y.; Li, B.; He, H.; Zhou, W.; Chem, B.; Qian, G. *Acc. Chem. Res.* **2016**, *49*, 483-493. (d) Nandasin, M. I.; Jambovane, S. R.; McGrail, B. P.; Schaef, H. T.; Nune, S. K. *Coord. Chem. Rev.* **2016**, *311*, 38-52.
- (8) (a) Chen, B. L.; Xiang, S. C.; Qian, G. D. *Acc. Chem. Res.* **2010**, *43*, 1115. (b) Kreno, L. E.; Leong, K.; Farha, O. K.; Allendorf, M.; Van Duyne, R. P.; Hupp, J. T. *Chem. Rev.* **2012**, *112*, 1105. (c) Xu, R. Y.; Wang, Y. F.; Duan, X. P.; Lu, K. D.; Micheroni, D.; Hu, A. G.; Lin, W. B. *J. Am. Chem. Soc.* **2016**, *138*, 2158.
- (9) (a) Morozan, A.; Jaouen, F. *Energy Environ. Sci.* **2012**, *5*, 9269. (b) Horike, S.; Umeyama, D.; Kitagawa, S. *Acc. Chem. Rev.* **2013**, *46*, 2376. (c) Talin, A. A.; Centrone, A.; Ford, A. C.; Foster, M. E.; Stavila, V.; Haney, P.; Kinney, R. A.; Szalai, V.; El Gabaly, F.; Yoon, H. P.; Leondard, F.; Allendorf, M. D. *Science* **2014**, *343*, 66.
- (10) (a) Ferey, G. *Chem. Soc. Rev.* **2008**, *37*, 191-214. (b) Horcajada, P.; Greg, R.; Baati, T.; Allan, P. K.; Maurin, G.; Courvreur, P.; Ferey, G.; Morris, R. E.; Serre, C. *Chem. Rev.* **2012**, *112*, 1232. (c) Yu, J.; Mu, C.; Yan, B. Y.; Qin, X. Y.; Shen, C.; Xue, H. G.; Pang, H. *Mater. Horiz.* **2017**, *4*, 557.
- (11) (a) Lee, J. Farha, O. K.; Roberts, J.; Scheidt, K. A.; Nguyen, S. T.; Nguyen, J. T. *Chem Soc. Rev.* **2009**, *38*, 1450. (b) Ma, L.; Abney, C.; Lin, W. *Chem. Soc. Rev.* 2009, *38*, 1248-1256. (c) Alkordi, M. H.; Liu, Y.; Larsen, R. W.; Eubank, J. F.; Eddaoudi, M. *J. Am. Chem. Soc.* **2008**, *130*, 12639.

- (12) (a) Morris, W.; Voloskiy, B.; Demir, S.; Gándara, F.; McGrier, P. L.; Furukawa, H.; Cascio, D.; Stoddart, J. F.; Yaghi, O. M. *Inorg. Chem.* **2012**, *51*, 6443. (b) Feng, D.; Gu, Z.-Y.; Li, J.-R.; Jiang, H.-L.; Wei, Z.; Zhou, H.-C. *Angew. Chem. Int. Ed.* **2012**, *51*, 10307. (c) Chen, Y.; Hoang, T.; Ma, S. *Inorg. Chem.* **2012**, *51*, 12600. (d) Jiang, H.-L.; Feng, D.; Wang, K.; Gu, Z.-Y.; Wei, Z.; Chen, Y.-P.; Zhou, H.-C. *J. Am. Chem. Soc.* **2013**, *135*, 13934. (e) Feng, D.; Chung, W.-C.; Wei, Z.; Gu, Z.-Y.; Jiang, H.-L.; Chen, Y.-P.; Darensbourg, D. J.; Zhou, H.-C. *J. Am. Chem. Soc.* **2013**, *135*, 17105. (f) Feng, D.; Jiang, H.-L.; Chen, Y.-P.; Gu, Z.-Y.; Wei, Z.; Zhou, H.-C. *Inorg. Chem.* **2013**, *52*, 12661. (g) Feng, D.; Gu, Z.-Y.; Chen, Y.-P.; Park, J.; Wei, Z.; Sun, Y.; Bosch, M.; Yuan, S.; Zhou, H.-C. *J. Am. Chem. Soc.* **2014**, *136*, 17714. (h) Lu, K.; He, C.; Lin, W. *J. Am. Chem. Soc.* **2014**, *136*, 16712. (i) Liu, T.-F.; Feng, D.; Chen, Y.-P.; Zou, L.; Bosch, M.; Yuan, S.; Wei, Z.; Fordham, S.; Wang, K.; Zhou, H.-C. *J. Am. Chem. Soc.* **2015**, *137*, 413. (j) Lin, Q.; Bu, X.; Kong, A.; Mao, C.; Zhao, X.; Bu, F.; Feng, P. *J. Am. Chem. Soc.* **2015**, *137*, 2235. (k) Wang, T. C.; Bury, W.; Gómez-Gualdrón, D. A.; Vermeulen, N. A.; Mondloch, J. E.; Deria, P.; Zhang, K.; Moghadam, P. Z.; Sarjeant, A. A.; Snurr, R. Q.; Stoddart, J. F.; Hupp, J. T.; Farha, O. K. *J. Am. Chem. Soc.* **2015**, *137*, 3585. (l) Zheng, J.; Wu, M.; Jiang, F.; Su, W.; Hong, M. *Chem. Sci.* **2015**, *6*, 3466.
- (13) Cavka, J. H.; Jakobsen, S.; Olsbye, U.; Guillou, N.; Lamberti, C.; Bordiga, S.; Lillerud, K. *J. Am. Chem. Soc.* **2008**, *130*, 13850.
- (14) (a) Kandaih, M.; Nilsen, M. H.; Usseglio, S.; Jakobsen, S.; Olsbye, U.; Tilset, M.; Larabi,

- C.; Quadrelli, E. A.; Bonino, F.; Lillerud, K. P. *Chem. Mater.* **2010**, *22*, 6632. (b) DeCoste, J. B.; Peterson, G. W.; Jasuja, H.; Glover, T. G.; Huang, Y.-G.; Walton, K. S. *J. Mater. Chem. A* **2013**, *1*, 5642. (c) Liu, C.; Demir, N. K.; Wu, Z.; Li, K. *J. Am. Chem. Soc.* **2015**, *137*, 6999. (d) Valenzano, L.; Civalleri, B.; Chavan, S.; Bordiga, S.; Nilsen, M. H.; Jakobsen, S.; Lillerud, K. P. *Chem. Mater.* **2011**, *23*, 1700. (b) Bai, Y.; Dou, Y.; X, L.-H.; Rutledge, W.; Li, J.-R.; Zhou, H.-C. *Chem. Soc. Rev.* **2016**, *45*, 2327.
- (15) (a) Choi, E.-Y.; Wray, C. A.; Hu, C.; Choe, W. *CrystEngCommun* **2009**, *11*, 553. (b) Kosal, M. E.; Chou, J.-H.; Wilson, S. R.; Suslick, K. S. *Nat. Mater.* **2002**, *1*, 118. (c) Fateeva, A.; Devautour-Vinot, S.; Heymans, N.; Devic, T.; Grenèche, J.-M.; Wuttke, S.; Miller, S.; Lago, A.; Serre, C.; De Weireld, G.; Maurin, G.; Vimont, A.; Férey, G. *Chem. Mater.* **2011**, *23*, 4641.
- (16) (a) Nakagaki, S.; Ferreira, G. K. B.; Ucoski, G. A.; de Freitas Castro, K. A. D. *Molecules* **2013**, *18*, 7279. (b) Zhao, M.; Ou, S.; Wu, C. D. *Acc. Chem. Res.* **2014**, *47*, 1199. (c) Gu, Z.-Y.; Park, J.; Raiff, A.; Wei, Z.; Zhou, H.-C. *ChemCatChem* **2014**, *6*, 67.
- (17) (a) Demel, J.; Kubát, P.; Millange, F.; Marrot, J.; Císarová, I.; Lang, K. *Inorg. Chem.* **2013**, *52*, 2779. (b) Kuangda, L.; He, C.; Lin, W. *J. Am. Chem. Soc.* **2014**, *136*, 16712.
- (18) (a) Spoerke, E. D.; Small, L. J.; Foster, M. E.; Wheeler, J.; Ullman, A. M.; Stavila, V.; Rodriguez, M.; Allendorf, M. D. *J. Phys. Chem. C* **2017**, *121*, 4816. (b) Rajnish, K.; Kim, K.-H.; Paul, A. K.; Deep, A. *J. Mater. Chem. A* **2016**, *4*, 3991.

References for Chapter 2

- (1) (a) Sono, M.; Roach, M. P.; Coulter, E. D.; Dawson, J. H. *Chem. Rev.* **1996**, *96*, 2841. (b) Meunier, B.; de Visser, S. P.; Shaik, S. *Chem. Rev.* **2004**, *104*, 3947. (c) Poulos, T. L. *Chem. Rev.* **2014**, *114*, 3919.
- (2) Giardina, B.; Messina, I.; Scatena, R.; Castagnola, M. *Crit. Rev. Biochem. Mol. Biol.* **1995**, *30*, 165.
- (3) (a) Suslick, K. S.; Reinert, T. J. *J. Chem. Educ.* **1985**, *62*, 974. (b) Momenteau, M.; Reed C. A. *Chem. Rev.* **1994**, *94*, 659. (c) Collman, J. P.; Fu, L. *Acc. Chem. Res.* **1999**, *32*, 455. (c) Collman, J. P.; Boulatov, R.; Sunderland, C. J.; Fu, L. *Chem. Rev.* **2004**, *104*, 561.
- (4) (a) Hoffman, A. B.; Collins, D. M.; Day, V. W.; Fleischer, E. B.; Srivastava, T. S.; Hoard, J. L. *J. Am. Chem. Soc.* **1972**, *94*, 3620. (b) Chin, D.-H.; La Mar, G. N.; Balch, A. L. *J. Am. Chem. Soc.* **1980**, *102*, 4344.
- (5) (a) Collman, J. P.; Gagne, R. R.; Halbert, T. R.; Marchon, J. C.; Reed, C. A. *J. Am. Chem. Soc.* **1973**, *95*, 7868. (b) Collman, J. P.; Gagne, R. R.; Reed, C. A.; Robinson, W. T.; Rodley, G. A. *Proc. Natl. Acad. Sci. U.S.A.* **1974**, *71*, 1326. (c) Jameson, G. B.; Rodley, G. A.; Robinson, W. T.; Gagne, R. R.; Reed, C. A.; Collman, J. P. *Inorg. Chem.* **1978**, *17*, 850. (d) Schappacher, M.; Ricard, L.; Fischer, J.; Weiss, R.; Bill, E.; Montiel-Montoya, R.; Winkler, H.; Trautwein, A. X. *Eur. J. Biochem.* **1987**, *168*, 419. (e) Yeh, C.-Y.; Chang, C. J.; Nocera, D. G. *J. Am. Chem. Soc.* **2001**, *123*, 1513. (f) Chang, C. J.; Chng, L. L.; Nocera, D. G. *J. Am. Chem. Soc.* **2003**, *125*, 1866.

- (6) (a) Collman, J. P.; Brauman, J. I.; Doxsee, K. M.; Sessler, J. L.; Morris, R. M.; Gibson, Q. H. *Inorg. Chem.* **1983**, *22*, 1427. (b) Chang, C. K.; Traylor, T. G. *J. Am. Chem. Soc.* **1973**, *95*, 8477.
- (7) (a) Latos-Grazynski, L.; Cheng, R. J.; La Mar, G. N.; Balch, A. L. *J. Am. Chem. Soc.* **1982**, *104*, 5992. (b) Nakamoto, K.; Watanabe, T.; Ama, T.; Urban, M. W. *J. Am. Chem. Soc.* **1982**, *104*, 3744. (c) Nakamoto, K. *Coord. Chem. Rev.* **1990**, *100*, 363. (d) Proniewicz, L. M.; Paeng, I. R.; Nakamoto, K. *J. Am. Chem. Soc.* **1991**, *113*, 3294.
- (8) (a) Lee, J.; Farha, O. K.; Roberts, J.; Scheidt, K. A.; Nguyen, S. T.; Hupp, J. T. *Chem. Soc. Rev.* **2009**, *38*, 1450. (b) Ma, L. Q.; Abney, C.; Lin, W. B. *Chem. Soc. Rev.* **2009**, *38*, 1248. (c) Farha, O. K.; Hupp, J. T. *Acc. Chem. Res.* **2010**, *43*, 1166. (d) Cohen, S. M. *Chem. Rev.* **2011**, *112*, 970. (e) Furukawa, H.; Cordova, K. E.; O’Keeffe, M.; Yaghi, O. M. *Science* **2013**, *341*, 123044. (f) Evans, J. D.; Sumby, C. J.; Doonan, C. J. *Chem. Soc. Rev.* **2014**, *43*, 5933. (g) Li, L.; Matsuda, R.; Tanaka, I.; Sato, H.; Kanoo, P.; Jeon, H. J.; Foo, M. L.; Wakamiya, A.; Murata, Y.; Kitagawa, S. *J. Am. Chem. Soc.* **2014**, *136*, 7543.
- (9) (a) Abrahams, B. F.; Hoskins, B. F.; Robson, R. *J. Am. Chem. Soc.* **1991**, *113*, 3606. (b) Abrahams, B. F.; Hoskins, B. F.; Michail, D. M.; Robson, R. *Nature* **1994**, *369*, 727. (c) Suslick, K. S.; Bhyrappa, P.; Chou, J. H.; Kosal, M. E.; Nakagaki, S.; Smithenry, D. W.; Wilson, S. R. *Acc. Chem. Res.* **2005**, *38*, 283. (d) Shultz, A. M.; Farha, O. K.; Hupp, J. T.; Nguyen, S. T. *J. Am. Chem. Soc.* **2009**, *131*, 4204. (e) Fateeva, A.; Devautour-Vinot, S.; Heymans, N.; Devic, T.; Grenèche, J.-M.; Wuttke, S.; Miller, S.; Lago, A.; Serre, C.; De

- Weireld, G.; Maurin, G.; Vimont, A.; Férey, G. *Chem. Mat.* **2011**, *23*, 4641. (f) Farha, O. K.; Shultz, A. M.; Sarjeant, A. A.; Nguyen, S. T.; Hupp, J. T. *J. Am. Chem. Soc.* **2011**, *133*, 5652. (g) Wang, X. S.; Meng, L.; Cheng, Q.; Kim, C.; Wojtas, L.; Chrzanowski, M.; Chen, Y.-S.; Zhang, X. P.; Ma, S. *J. Am. Chem. Soc.* **2011**, *133*, 16322. (h) Morris, W.; Voloskiy, B.; Demir, S.; Gándara, F.; McGrier, P. L.; Furukawa, H.; Cascio, D.; Stoddart, J. F.; Yaghi, O. M. *Inorg. Chem.* **2012**, *51*, 6443. (i) Feng, D.; Gu, Z.-Y.; Li, J.-R.; Jiang, H. L.; Wei, Z.; Zhou, H.-C. *Angew. Chem. Int. Ed.* **2012**, *41*, 10307. (j) Jiang, H.-L.; Feng, D.; Wang, K.; Gu, Z.-Y.; Wei, Z.; Chen, Y.-P.; Zhou, H.-C. *J. Am. Chem. Soc.* **2013**, *135*, 13934. (k) So, M. C.; Jin, S.; Son, H.-J.; Wiederrecht, G. P.; Farha, O. K.; Hupp, J. T. *J. Am. Chem. Soc.* **2013**, *135*, 15698. (l) Wang, K.; Feng, D.; Liu, T.-F.; Su, J.; Yuan, S.; Chen, Y.-P.; Bosch, M.; Zou, X.; Zhou, H.-C. *J. Am. Chem. Soc.* **2014**, *136*, 13983.
- (10) Feng, D.; Chung, W.-C.; Wei, Z.; Gu, Z.-Y.; Jiang, H.-L.; Chen, Y.-P.; Darensbourg, D. J.; Zhou, H.-C. *J. Am. Chem. Soc.* **2013**, *135*, 17105.
- (11) Collman, J. P.; Basolo, F.; Bunnenberg, E.; Collins, T. J.; Dawson, J. H.; Ellis, P. E.; Marrocco, M. L.; Moscovitz, A.; Sessler, J.; Szymanski, T. *J. Am. Chem. Soc.* **1981**, *103*, 5636.
- (12) (a) Collman, J. P.; Hoard, J. L.; Kim, N.; Lang, G.; Reed, C. A. *J. Am. Chem. Soc.* **1975**, *97*, 2676. (b) Li, N.; Su, Z.; Coppens, P.; Landrum, J. *J. Am. Chem. Soc.* **1990**, *112*, 7294. (c) Hu, C.; Noll, B. C.; Schulz, C. E.; Scheidt, W. R. *Inorg. Chem.* **2007**, *46*, 619.
- (13) (a) Hagrman, D.; Hagrman, P.J.; Zubieta, J. *Angew. Chem. Int. Ed.* **1999**, *38*, 3165. (b) Pan,

- L.; Kelly, S.; Huang, X.; Li, J. *Chem. Commun.* **2002**, 2334. (c) Zou, C.; Zhang, T.; Xie, M.-H.; Yan, L.; Kong, G.-Q.; Yang, X.-L.; Ma, A.; Wu, C.-D. *Inorg. Chem.* **2013**, *52*, 3620.
- (14) (a) Jameson, G. B.; Rodley, G. A.; Robinson, W. T.; Gagne, R. R.; Reed, C.; Collman, J. P. *Inorg. Chem.* **1978**, *17*, 850. (b) Jameson, G. B.; Molinaro, F. S.; Ibers, J. A.; Collman, J. P.; Brauman, J. I.; Rose, E.; Suslick, K. S. *J. Am. Chem. Soc.* **1980**, *102*, 3224.
- (15) According to a search of the Cambridge Structural Database Version 5.35.0. Allen, F. *Acta Crystallogr. B* **2002**, *58*, 380.
- (16) Würtele, C.; Gaoutchenova, E.; Harms, K.; Holthausen, M. C.; Sundermeyer, J.; Schindler, S. *Angew. Chem. Int. Ed.* **2006**, *45*, 3867.
- (17) (a) Cai, X.; Majumdar, S.; Fortman, G. C.; Cazin, C. S. J.; Slawin, A. M. Z.; Lhermitte, C.; Prabhakar, R.; Germain, M. E.; Palluccio, T.; Nolan, S. P.; Rybak-Akimova, E. V.; Temprado, M.; Captain, B.; Hoff, C. D. *J. Am. Chem. Soc.* **2011**, *133*, 1290. (b) Huacuja, R.; Graham, D. J.; Fafard, C. M.; Chen, C.-H.; Foxman, B. M.; Herbert, D. E.; Alliger, G.; Thomas, C. M.; Ozerov, O. V. *J. Am. Chem. Soc.* **2011**, *133*, 3820.
- (18) Mason, J. A.; Sumida, K.; Herm, K. R.; Krishna, R.; Long, J. R. *Energy Environ. Sci.* **2011**, *4*, 3030.
- (19) Bloch, E. D.; Murray, L. J.; Queen, W. L.; Chavan, S.; Maximoff, S. N.; Bigi, J. P.; Krishna, R.; Peterson, V. K.; Grandjean, F.; Long, G. J.; Smit, B.; Bordiga, S.; Brown, C. M.; Long, J. R. *J. Am. Chem. Soc.* **2011**, *133*, 14814.

- (20) Dolphin, D. *The Porphyrins, Vol. 3: Physical chemistry*; Academic: New York, 1978.
- (21) Spartalian, K.; Lang, G.; Collman, J. P.; Gagne, R. R.; Reed, C. A. *J. Chem. Phys.* **1975**, *63*, 5375.
- (22) (a) Five-coordinate: Wayland, B. B.; Mehne, L. F.; Swartz, J. *J. Am. Chem. Soc.* **1978**, *100*, 2379. (b) Six-coordinate: Silvernail, N. J.; Roth, A.; Schulz, C. E.; Noll, B. C.; Scheidt, W. *J. Am. Chem. Soc.* **2005**, *127*, 14422.
- (23) (a) Nasset, M. J. M.; Shokhirev, N. V.; Enemark, P. D.; Jacobson, S. E.; Walker, F. A. *Inorg. Chem.* **1996**, *35*, 5188. (b) Wu, Y.; Komatsu, T.; Tsuchida, E. *Inorg. Chim. Acta* **2001**, *322*, 120.

References for Chapter 3

- (1) Sono, M.; Roach, M. P.; Coulter, E. D. J. H. Dawson, *Chem. Rev.* **1996**, *96*, 2841.
- (2) J. P. Collman, R. Boulatov, C. J. Sunderland, L. Fu, *Chem. Rev.* **2004**, *104*, 561.
- (3) T. L. Poulos, *Chem. Rev.*, **2014**, *114*, 3919.
- (4) J. P. Collman, *Acc. Chem. Res.*, **1977**, *10*, 265.
- (5) B. Giardina, I. Messana, R. Scatena, M. Castagnola, *Crit. Rev. Biochem. Mol. Biol.*, **1995**, *30*, 165.
- (6) B. M. Hoffman, D. H. Petering, *Proc. Natl. Acad. Sci. USA*, **1970**, *67*, 637.
- (7) T. D. Smith, J. R. Pilbrow, *Coord. Chem. Rev.*, **1981**, *39*, 295.
- (8) R. D. Jones, D. A. Summerville, F. Basolo, *Chem. Rev.*, **1979**, *79*, 139.
- (9) A. B. Hoffman, D. M. Collins, V. W. Day, E. B. Fleischer, T. S. Srivastava, J. L. Hoard, *J.*

Am. Chem. Soc., **1972**, *94*, 3620.

- (10) D.-H. Chin, G. N. La Mar, A. L. Balch, *J. Am. Chem. Soc.* 1980, **102**, 4344.
- (11) L. Latos-Grazynski, R. J. Cheng, G. N. La Mar, A. L. Balch, *J. Am. Chem. Soc.*, 1982, **104**, 5992.
- (12) K. Nakamoto, T. Watanabe, T. Ama, M. W. Urban, *J. Am. Chem. Soc.*, 1982, **104**, 3744.
- (13) K. Nakamoto, *Coord. Chem. Rev.*, 1990, **100**, 363.
- (14) L. M. Proniewicz, I. R. Paeng, K. Nakamoto, *J. Am. Chem. Soc.*, 1991, **113**, 3294.
- (15) M. Kozuka, K. Nakamoto, *J. Am. Chem. Soc.*, 1981, **103**, 2162.
- (16) A. Wesełucha-Birczyńska, K. Nakamoto, L. M. Proniewicz, *J. Mol. Struct.*, 1992, **275**, 95.
- (17) L. M. Proniewicz, A. Kulczycki, A. Wesełucha-Birczyńska, H. Majcherczyk, K. Nakamoto, *New J. Chem.*, 1999, **23**, 71.
- (18) J. M. Assour, *J. Chem. Phys.*, 1965, **43**, 2477.
- (19) F. A. Walker, *J. Am. Chem. Soc.*, 1970, **92**, 4235.
- (20) S. Van Doorslaer, A. Schweiger, *Phys. Chem. Chem. Phys.*, 2001, **3**, 159.
- (21) A. Ozarowski, H. M. Lee, A. L. Balch, *J. Am. Chem. Soc.*, 2003, **125**, 12606.
- (22) J. S. Anderson, A. T. Gallagher, J. A. Mason, T. D. Harris, *J. Am. Chem. Soc.*, 2014, **136**, 16489.
- (23) K. S. Suslick, T. J. Reinert, *J. Chem. Ed.*, 1985, **62**, 974.
- (24) M. Momenteau, C. A. Reed, *Chem. Rev.*, 1994, **94**, 659.
- (25) J. P. Collman, L. Fu, *Acc. Chem. Res.*, 1999, **32**, 455.

- (26) D. Feng, W.-C. Chung, Z. Wei, Z.-Y. Gu, H.-L. Jiang, Y.-P. Chen, D. J. Darensbourg, H.-C. Zhou, *J. Am. Chem. Soc.*, 2013, **135**, 17105.
- (27) A. M. Shultz, A. A. Sarjeant, O. K. Farha, J. T. Hupp, S. T. Nguyen, *J. Am. Chem. Soc.*, 2011, **133**, 13252.
- (28) X.-S. Wang, M. Chrzanowski, L. Wojitas, Y.-S. Chen, S. Ma, *Chem. Eur. J.*, 2013, **19**, 3297.
- (29) W. M. Bloch, A. Burgun, C. J. Coghlan, R. Lee, M. L. Coote, C. J. Doonan, C. J. Sumby, *Nat. Chem.*, 2014, **6**, 906.
- (30) K. Manna, T. Zhang, M. Carboni, C. W. Abney, W. Lin, *J. Am. Chem. Soc.*, 2014, **136**, 13182.
- (31) C.-W. Kung, T.-H. Chang, L.-Y. Chou, J.T. Hupp, O.K. Farha, K.-C. Ho, *Chem. Commun.*, 2015, **51**, 2414.
- (32) M. I. Gonzalez, E. D. Bloch, J. A. Mason, S. J. Teat, J. R. Long, *Inorg. Chem.*, 2015, **54**, 2995.
- (33) According to a search of the Cambridge Structural Database Version 5.35.0. F. Allen, *Acta Crystallogr. B*, 2002, **58**, 380.
- (34) D. Feng, H.-L. Jiang, Y.-P. Chen, Z.-Y. Gu, Z. Wei, H.-C. Zhou, *Inorg. Chem.*, 2013, **52**, 12661.
- (35) J. Li, B.C. Noll, A.G. Oliver, W.R. Scheidt, *J. Am. Chem. Soc.*, 2012, **134**, 10595.
- (36) P. Doppelt, J. Fischer, L. Ricard, R. Weiss, *New J. Chem.*, 1987, **11**, 357.

- (37) T. Sakurai, K. Yamamoto, J. Naito, N. Nakamoto, *Bull. Chem. Soc. Jpn.*, 1976, **49**, 3042.
- (38) J. Li, B.C. Noll, A.G. Oliver, G. Ferraudi, A.G. Lappin, W.R. Scheidt, *Inorg. Chem.*, 2010, **49**, 2398.
- (39) S. Stoll, A. Schweiger, *J. Magn. Reson.*, 2006, **178**, 42.
- (40) J. S. Griffith, *Discuss. Faraday Soc.*, 1958, **26**, 81.
- (41) A. H. Maki, N. Edelstein, A. Davidson, R. H. Holm, *J. Am. Chem. Soc.*, 1964, **86**, 4580.
- (42) L. M. Engelhardt, M. Green, *J. Chem. Soc., Dalton Trans.*, 1972, 4724.
- (43) B. R. McGarvey, *Can. J. Chem.*, 1975, **53**, 2498.
- (44) R.S. Drago, B.B. Corden, *Acc. Chem. Res.*, 1980, **13**, 353.
- (45) T. D. Smith, J. R. Pilbrow, *Coord. Chem. Rev.*, 1981, **39**, 295.
- (46) F. A. Walker, *J. Magn. Reson.*, 1974, **15**, 201.
- (47) J. A. Mason, K. Sumida, Z. R. Herm, R. Krishna, J. R. Long, *Energy Environ. Sci.*, 2011, **4**, 3030.
- (48) S. Ma, H.-C. Zhou, *J. Am. Chem. Soc.*, 2006, **128**, 11734.
- (49) H. C. Stynes, J. A. Ibers, *J. Am. Chem. Soc.*, 1972, **94**, 1559.
- (50) F. A. Walker, *J. Am. Chem. Soc.*, 1973, **95**, 1154.
- (51) J. P. Collman, J. I. Brauman, K. M. Doxsee, T. R. Halbert, S. E. Hayes, K. S. Suslick, *J. Am. Chem. Soc.*, 1978, **100**, 2761.
- (52) M.-Y. R. Wang, B. M. Hoffman, S. J. Shire, F. R. N. Gurd, *J. Am. Chem. Soc.*, 1979, **101**, 7394.

- (53) J. E. Linard, P. E. Ellis, Jr., J. R. Budge, R. D. Jones, F. Basolo, *J. Am. Chem. Soc.*, 1980, **102**, 1896.
- (54) B. A. Friesen, A. Bhattarai, U. Mazur, K. W. Hipps, *J. Am. Chem. Soc.*, 2012, **134**, 14897.

References for Chapter 4

- (1) (a) M. Sono, M. P. Roach, E. D. Coulter, J. H. Dawson, *Chem. Rev.*, 1996, **96**, 2841. (b) B. Meunier, S. P. de Visser, S. Shaik, *Chem. Rev.*, 2004, **104**, 3947. (c) M. Costas, M. P. Mehn, M. P. Jensen, L. Que, Jr., *Chem. Rev.*, 2004, **104**, 939. (d) A. Decker, E. I. Solomon, *Curr. Opin. Chem. Biol.*, 2005, **9**, 152. (e) M. M. Abu-Omar, A. Loaiza, N. Hontzeas, *Chem. Rev.*, 2005, **105**, 2227. (f) T. L. Poulos, *Chem. Rev.*, 2014, **114**, 3919.
- (2) (a) C. Bull, E. C. Niederhoffer, T. Yoshida, J. A. Fee, *J. Am. Chem. Soc.*, 1991, **113**, 4069. (b) J. A. Kovacs, L. M. Brines, *Acc. Chem. Res.*, 2007, **40**, 501. (c) I. G. Denisov, P. J. Mark, T. M. Makris, S. G. Sligar, J. R. Kincaid, *J. Phys. Chem. A.*, 2008, **112**, 13172. (d) W. A. Gunderson, A. I. Zatsman, J. P. Emerson, E. R. Farquhar, L. Que, Jr., J. D. Lipscomb, M. P. Hendrich, *J. Am. Chem. Soc.*, 2008, **130**, 14465. (e) G. Renger, T. Renger, *Photosynth. Res.*, 2008, **98**, 53. (f) D. J. Vinyard, G. M. Ananyev, G. C. Dismukes, *Annu Rev. Biochem.*, 2013, **82**, 577. (g) E. I. Solomon, D. E. Heppner, E. M. Johnston, J. W. Ginsbach, J. Cirera, M. Qayyum, M. T. Kieber-Emmons, C. H. Kjaergaard, R. G. Hadt, L. Tian, *Chem. Rev.*, 2014, **114**, 3659. (g) S. Sahu, D. P. Goldberg, *J. Am. Chem. Soc.*, 2016, **138**, 11410.
- (3) (a) E. McCandlish, A. R. Miksztal, M. Nappa, A. Q. Sprenger, J. S. Valentine, J. D. Stong,

- T. G. Spiro, *J. Am. Chem. Soc.*, 1980, **102**, 4268. (b) C. H. Welborn, D. Dolphin, B. R. James, *J. Am. Chem. Soc.*, 1981, **103**, 2869. (c) C. A. Reed, in *Electrochemical and Spectrochemical Studies of Biological Redox Components*, ed. K. M. Kadish, American Chemical Society, Washington, D.C. 201, 1982, ch. 15, pp. 333-356. (d) K. Bajdor, K. Nakamoto, *J. Am. Chem. Soc.*, 1984, **106**, 3045. (e) P. Friant, J. Goulon, J. Fischer, L. Ricard, M. Schappacher, R. Weiss, M. Momenteau, *Nouv. J. Chim.*, 1985, **9**, 33.
- (4) Selected examples of peroxoheme species: (a) R. A. Ghiladi, R. M. Kretzer, I. Guzei, A. L. Rheingold, Y.-M. Neuhold, K. R. Hatwell, A. D. Zuberbühler, K. D. Karlin, *Inorg. Chem.*, 2001, **40**, 5754. (b) E. Kim; M. E. Helton, I. M. Wasser, K. D. Karlin, S. Lu, H. W. Huang, P. Moenne-Loccoz, C. D. Incarvito, A. L. Rheingold, M. Honecker, S. Kaderli, A. D. Zuberbühler, *Proc. Natl. Acad. Sci. U. S. A.*, 2003, **100**, 3623. (c) K. Mitra, S. Chatterjee, S. Samanta, K. Sengupta, H. Bhattacharjee, A. Dey, *Chem. Commun.*, 2012, **48**, 10535. (d) M. F. Sisemore, M. Selke, J. N. Burstyn, J. S. Valentine, *Inorg. Chem.*, 1997, **36**, 979. (e) M. F. Sisemore, M. Selke, J. N. Burstyn, J. S. Valentine, *Inorg. Chem.*, 1997, **36**, 979.
- (5) Selected examples of non-heme peroxo species: (a) J. Cho, S. Jeon, S. A. Wilson, L. V. Liu, E. A. Kang, J. J. Braymer, M. H. Lim, B. Hedman, K. O. Hodgson, J. S. Valentine, E. I. Solomon, W. Nam, *Nature*, 2011, **478**, 502. (b) E. D. Bloch, L. J. Murray, W. L. Queen, S. Chavan, S. N. Maximoff, J. P. Bigi, R. Krishna, V. K. Peterson, F. Grandjean, G. J. Long, B. Smit, S. Bordiga, C. M. Brown, J. R. Long, *J. Am. Chem. Soc.*, 2011, **133**, 14814. (c) L. V. Liu, S. Hong, J. Cho, W. Nam, E. I. Solomon, *J. Am. Chem. Soc.*, 2013, **135**,

3286. (d) W. Nam, *Acc. Chem. Res.*, 2015, **48**, 2415.
- (6) Selected examples of isolated peroxomanganese(III) species: (a) D. L. Werz, J. S. Valentine, *Struct. Bonding* (Berlin), 2000, **97**, 37. (b) R. L. Shook, W. A. Gunderson, J. Greaves, J. W. Ziller, M. P. Hendrich, A. S. Borovik, *J. Am. Chem. Soc.*, 2008, **130**, 8888. (c) R. A. Geiger, S. Chattopadhyay, V. W. Day, T. A. Jackson, *J. Am. Chem. Soc.*, 2010, **132**, 2821. (d) R. L. Shook, A. S. Borovik, *Inorg. Chem.*, 2010, **49**, 3646. (e) R. A. Geiger, S. Chattopadhyay, V. W. Day, T. A. Jackson, *Dalton Trans.*, 2011, **40**, 1707. (f) R. L. Shook, S. M. Peterson, J. Greaves, C. Moore, A. L. Rheingold, A. S. Borovik, *J. Am. Chem. Soc.*, 2011, **133**, 5810. (g) H. So, Y. J. Park, K.-B. Cho, Y.-M. Lee, M. S. Seo, J. Cho, R. Sarangi, W. Nam, *J. Am. Chem. Soc.*, 2014, **136**, 12229. (h) K. Ray, F. F. Pfaff, B. Wang, W. Nam., *J. Am. Chem. Soc.*, 2014, **136**, 13942. (i) D. F. Leto, T. A. Jackson, *J. Biol. Inorg. Chem.*, 2014, **19**, 1. (j) H. E. Colmer, A. W. Howcroft, T. A. Jackson, *Inorg. Chem.*, 2016, **55**, 2055. (k) P. Barman, P. Upadhyay, A. S. Faponle, J. Kumar, S. S. Nag, D. Kumar, C. V. Sastri, S. P. de Visser, *Angew. Chem.*, 2016, **128**, 11257.
- (7) Examples of structurally-characterized peroxomanganese(III) species: (a) R. B. VanAtta, C. E. Strouse, L. K. Hanson, J. S. Valentine, *J. Am. Chem. Soc.*, 1987, **109**, 1425. (b) N. Kitajima, H. Komatsuzaki, S. Hikichi, M. Osawa, Y. Moro-oka, *J. Am. Chem. Soc.*, 1994, **116**, 11596. (c) U. P. Singh, A. K. Sharma, S. Hikichi, H. Komatsuzaki, Y. Moro-oka, M. Akita, *Inorg. Chim. Acta.*, 2006, **359**, 4407. (d) M. S. Seo, J. Y. Kim, J. Annaraj, Y. Kim, Y.-M. Lee, S.-J. Kim, J. Kim, W. Nam, *Angew. Chem. Int. Ed.*, 2007, **46**, 377. (e) J.

- Annaraj, J. Cho, Y.-M. Lee, S. Y. Kim, R. Latifi, S. P. de Visser, W. Nam, *Angew. Chem. Int. Ed.*, 2009, **48**, 4150. (f) H. Kang, J. Cho, K.-B. Cho, T. Nomura, T. Ogura, W. Nam, *Chem. Eur. J.*, 2013, **19**, 14119. (g) H. E. Colmer, R. A. Geiger, D. F. Leto, G. B. Wijeratne, V. W. Day, T. A. Jackson, *Dalton Trans.*, 2014, **43**, 17949.
- (8) Examples of isolated peroxomanganese(IV) species: (a) U. Bossek, T. Weyhermueller, K. Wieghardt, B. Nuber, J. Weiss, *J. Am. Chem. Soc.*, 1990, **112**, 6387. (b) S. H. Kim, H. Park, M. S. Seo, M. Kubo, T. Ogura, J. Klajn, D. T. Gryko, J. S. Valentine, W. Nam, *J. Am. Chem. Soc.*, 2010, **132**, 14030.
- (9) (a) C.-M. Lee, C.-H. Chuo, C.-H. Chen, C. C. Hu, M. -H. Chiang, Y.-J. Tseng, C.-H. Hu, G.-H. Lee, *Angew. Chem. Int. Ed.*, 2012, **124**, 5523. (b) S. Hong, K. D. Sutherlin, J. Park, E. Kwon, M. A. Siegler, E. I. Solomon, W. Nam, *Nat. Commun.*, 2014, **5**, 5440.
- (10) (a) N. M. Senozan, *J. Chem. Educ.*, 1974, **51**, 503. (b) E. C. Neiderhoffer, J. H. Timmons, A. E. Martell, *Chem. Rev.*, 1984, **84**, 137.
- (11) (a) I. Tabushi, N. Koga, *J. Am. Chem. Soc.*, 1979, **101**, 6456. (b) I. Tabushi, A. Yazaki, *J. Am. Chem. Soc.*, 1981, **103**, 7371. (c) M. Perrée-Fauvet, A. Gaudemer, *J. Chem. Soc., Chem. Commun.*, 1981, 874. (d) D. Mansuy, M. Fontecave, J.-F., Bartoli, *J. Chem. Soc., Chem. Commun.*, 1983, 253. (e) M. Fontecave, D. Mansuy, *Tetrahedron*, 1984, **40**, 4297. (f) S. E. Creager, S. A. Raybuck, R. W. Murray, *J. Am. Chem. Soc.*, 1986, **108**, 4225. (g) S. E. Creager, R. W. Murray, *Inorg. Chem.*, 1987, **26**, 2612. (h) P. Battioni, J. F. Bartoli, P. Leduc, M. Fontecave, D. Mansuy, *J. Chem. Soc., Chem. Commun.*, 1987, 791. (i) I.

- Tabushi, *Coord. Chem. Rev.*, 1988, **86**, 1. (j) H. Sakurai, Y. Mori, M. Shibuya, *Inorg. Chim. Acta.*, 1989, **162**, 23. (k) H. Nishihara, K. Pressprich, R. W. Murray, J. P. Collman, *Inorg. Chem.*, 1990, **29**, 1000.
- (12) (a) C. J. Weschler, B. M. Hoffman, F. Basolo, *J. Am. Chem. Soc.*, 1975, **97**, 5278. (b) B. Gonzalez, J. Kouba, S. Yee, C. A. Reed, J. F. Kirner, W. R. Scheidt, *J. Am. Chem. Soc.*, 1975, **97**, 3247. (c) B. M. Hoffman, C. J. Weschler, F. Basolo, *J. Am. Chem. Soc.*, 1976, **98**, 5473. (d) A. Dedieu, M. M. Rohmer, *J. Am. Chem. Soc.*, 1977, **99**, 8050. (e) B. M. Hoffman, T. Szymanski, T. G. Brown, F. Basolo, *J. Am. Chem. Soc.*, 1978, **100**, 7253. (f) G. D. Lawrence, D. T. Sawyer, *Coord. Chem. Rev.*, 1978, **27**, 173. (g) R. D. Jones, D. A. Summerville, F. Basolo, *J. Am. Chem. Soc.*, 1978, **100**, 4416. (h) E. B. Fleischer, R. V. Ferra, *J. Inorg. Biochem.*, 1979, **10**, 91. (i) W. M. Coleman, L. T. Taylor, *Coord. Chem. Rev.*, 1980, **32**, 1. (j) L. K. Hanson, B. M. Hoffman, *J. Am. Chem. Soc.*, 1980, **102**, 4602. (k) A. Shirazi, H. M. Goff, *J. Am. Chem. Soc.*, 1982, **104**, 6318. (l) M. W. Urban, K. Nakamoto, F. Basolo, *Inorg. Chem.*, 1982, **21**, 3406. (m) A. Weselucha-Birczynska, L. M. Proniewicz, K. Bajdor, K. Nakamoto, *J. Raman Spectrosc.*, 1991, **22**, 315. (n) V. L. Pecoraro, M. J. Baldwin, A. Gelasco, *Chem. Rev.*, 1994, **94**, 807. (o) T. S. Kurtikyan, T. H. Stepanyan, G. G. Martirosyan, R. K. Kazaryan, V. N. Madakyan, *Russ. Chem. Bull., Int. Ed.*, 2000, **49**, 1540.
- (13) (a) A. B. Hoffman, D. M. Collins, V. W. Day, E. B. Fleischer, T. S. Strivastava, J. L. Hoard, *J. Am. Chem. Soc.* 1972, **94**, 3620. (b) D.-H. Chin, G. N. La Mar, A. L. Balch, *J.*

- Am. Chem. Soc.*, 1980, **102**, 4344. (c) G. C. Dismukes, J. E. Sheats, J. A. Smegal, *J. Am. Chem. Soc.*, 1987, **109**, 7202.
- (14) Iron: (a) G. B. Jameson, G. A. Rodley, W. T. Robinson, R. R. Gagne, C. A. Reed, J. P. Collman, *Inorg. Chem.*, 1978, **17**, 850. (b) G. B. Jameson, F. S. Molinaro, J. A. Ibers, J. P. Collman, J. I. Brauman, E. Rose, K. S. Suslick, *J. Am. Chem. Soc.*, 1980, **102**, 3224. (c) M. Schnappcher, L. Ricard, J. Fischer, R. Weiss, E. Bill, R. Montiel-Montoya, H. Winkler, A. X. Trautwein, *Eur. J. Biochem.*, 1987, **168**, 419. (d) J. Li, B. C. Noll, A. G. Oliver, C. E. Schulz, W. R. Scheidt, *J. Am. Chem. Soc.*, 2013, **135**, 15627. Cobalt: (e) P. Doppelt, J. Fischer, L. Ricard, R. Weiss, *New. J. Chem.*, 1987, **11**, 357. (f) J. Li, B. C. Noll, A. G. Oliver, W. R. Scheidt, *J. Am. Chem. Soc.*, 2012, **134**, 10595.
- (15) D. Feng, W.-C. Chung, Z. Wei, Z. Y. Gu, H.-L. Jiang, Y.-P. Chen, D. J. Darensbourg, H.-C. Zhou, *J. Am. Chem. Soc.*, 2013, **135**, 17105.
- (16) J. S. Anderson, A. T. Gallagher, J. A. Mason, T. D. Harris, *J. Am. Chem. Soc.*, 2014, **136**, 16489.
- (17) A. T. Gallagher, M. L. Kelty, J. G. Park, J. S. Anderson, J. A. Mason, J. P. S. Walsh, S. L. Collins, T. D. Harris, *Inorg. Chem. Front.*, 2016, **3**, 536
- (18) A. T. Gallagher, C. D. Malliakas, T. D. Harris, *Inorg. Chem.*, 2017, **56**, 4654.
- (19) J. M. Zadrozny, A. T. Gallagher, T. D. Harris, D. E. Freedman, *J. Am. Chem. Soc.*, 2017, **139**, 7089.
- (20) (a) X.-L Lv, K. Wang, B. Wang, J. Su, X. Zou, Y. Xie, J.-R. Li, H.-C Zhou, *J. Am. Chem.*

- Soc.*, 2017, **139**, 211. (b) J. W. Brown, Q. T. Nguyen, T. Otto, N. N. Jarenwattananon, S. Glöggler, L.-S. Bouchard, *Catal. Commun.*, 2015, **59**, 50. (c) K. S. Suslick, P. Bhyrappa, J.-H Chou, M. E. Kosal, S. Nakagaki, D. W. Smithenry, S. R. Wilson, *Acc. Chem. Res.*, 2005, **38**, 283. (d) D. H. Lee, S. Kim, M. Y. Hyun, J.-Y. Hong, S. Huh, C. Kim, S. J. Lee, *Chem. Commun.*, 2012, **48**, 5512. (e) Z. Guo, D. Yan, H. Wang, D. Tesfagaber, X. Li, Y. Chen, W. Huang, B. Chen, *Inorg. Chem.*, 2015, **54**, 200. (f) M.-H Xie, X.-L. Yang, Y. He, J. Zhang, B. L. Chen, C.-D. Wu, *Chem. Eur. J.*, 2013, **19**, 14316. (h) C. Zhou, T. Zhang, M.-H. Xie, J. Yan, G.-Q Kong, X.-L. Yang, A. Ma, C.-D. Wu, *Inorg. Chem.*, 2013, **52**, 3620. (i) P. M. Barron, H.-T Son, C. Hu, W. Choe, *Cryst. Growth Des.*, 2009, **9**, 1960. (j) W. Zhang, P. Jiang, Y. Wang, J. Zhang, J. Zheng, P. Zhang, *Chem. Eng. J.*, 2014, **257**, 28.
- (21) (a) K. S. Suslick, R. A. Watson, *New. J. Chem.*, 1992, **16**, 633. (b) D. Dolphin, in *Volume III, Physical Chemistry*, Part C, Academic Press, New York, 1978.
- (22) (a) Iron: K. Nakamoto, T. Watanabe, T. Ama, M. W. Urban, *J. Am. Chem. Soc.*, 1982, **104**, 3744. (b) Cobalt: M. Kozuka, K. Nakamoto, *J. Am. Chem. Soc.*, 1981, **103**, 2162.
- (23) R. Guillard, M. Fontesse, P. Fournari, *J. Chem. Soc., Chem. Commun.*, 1976, 161.
- (24) J. F. Kirner, C. A. Reed, W. R. Scheidt, *J. Am. Chem. Soc.*, 1977, **99**, 1093.
- (25) J. S. Valentine, *Chem Rev.*, 1973, **73**, 235. (b) L. Vaska, *Acc. Chem. Res.*, 1976, **9**, 175.
- (26) B. Chevrier, T. Diebold, R. Weiss, *Inorg. Chimica. Acta.*, 1976, **19**, 57.
- (27) A peroxo-bridged Mn^{IV}_2 complex: U. Bossek, T. Weyhermueller, K. Wieghardt, B. Nuber, J. Weiss, *J. Am. Chem. Soc.*, 1990, 112, 6387.

- (28) (a) J. M. Assour, *J. Chem. Phys.*, 1965, **43**, 2477. (b) F. A. Walker, *J. Am. Chem. Soc.*, 1970, **92**, 4235. (c) S. Van Doorslaer, A. Schweiger, *Phys. Chem. Chem. Phys.*, 2001, **3**, 159.
- (29) (a) D. Dolphin, in *The Porphyrins Volume V, Physical Chemistry*, Part C, Academic Press, New York, 1978. (b) L. H. Vogt, Jr., H. M. Faigenbaum, S. E. Wiberley, *Chem. Rev.*, 1963, **63**, 269.

References for Chapter 5

- (1) (a) Addison, A. W.; Stephanos, J. J. Nitrosyliron(III) Hemoglobin: Autoreduction and Spectroscopy. *Biochem.* **1986**, *25*, 4104-4113. (b) Giardina, B.; Messina, I.; Scatena, R.; Castagnola, M. The Multiple Functions of Hemoglobin. *Crit. Rev. Biochem. Mol. Biol.* **1995**, *30*, 165-196. (c) Kim, H. P.; Ryter, S. W.; Choi, A. M. K. CO as a Cellular Signaling Molecule. *Annu. Rev. Pharmacol. Toxicol.* **2006**, *46*, 411-449.
- (2) (a) Collman, J. P.; Brauman, J. I.; Halbert, T. R.; Suslick, K. E. Nature of O₂ and CO Binding to Metalloporphyrins and Heme Proteins. *Proc. Natl. Acad. Sci. USA* **1976**, *73*, 3333-3337.
- (b) Alberding, N.; Austin, R. H.; Chan, S. S.; Eisenstein, L.; Frauenfelder, H.; Good, D.; Kaufmann, K.; Marden, M.; Nordlund, T. M.; Reinisch, L.; Reynolds, A. H.; Sorensen, L. B.; Wagner, G. C.; Yue, K. T. Fast Reactions in Carbon Monoxide Binding to Heme Proteins. *Biophys. J.* **1978**, *24*, 319-334. (c) Olson, J. S.; Phillips Jr.; G. N. Myoglobin

- Discriminates Between O₂, NO, and CO by Electrostatic Interactions with the Bound Ligand. *J. Biol. Inorg. Chem.* **1997**, *2*, 544-552. (d) Collman, J. P.; Fu, L. Synthetic Models for Hemoglobin and Myoglobin. *Acc. Chem. Res.* **1999**, *32*, 455-463. (e) McMahon, B. H.; Stojkovic, B. P.; Hay, P. J.; Martin, R. L.; García, A. E. Microscopic Model of Carbon Monoxide Binding to Myoglobin. *J. Chem. Phys.* **2000**, *113*, 6831-6850. (f) Blumenthal, I. Carbon Monoxide Poisoning. *J. R. Soc. Med.* **2001**, *94*, 270-272.
- (3) Vitamin B12 (a) Bayston, J. H.; Winfield, M. E. Catalysis of the Autoxidation of Carbon Monoxide by Cobalt Corrins. *J. Catal.* **1967**, *9*, 217-224. (b) Lee, L.-P.; Schrauzer, G. N. The Reaction of Vitamin B12a and of Cobaloximes with Carbon Monoxide. Evidence for Self-Reduction of Vitamin B12a in Neutral Solution. *J. Am. Chem. Soc.* **1968**, *90*, 5274-5276. (c) Schrauzer, G. N. New Developments in the Field of Vitamin B12: Reactions of the Cobalt Atom in Corrins and in Vitamin B12 Model Compounds. *Angew. Chem. Int. Ed. Engl.* **1976**, *15*, 417-426.
- (4) Cobalt porphyrin O₂ adducts: (a) Hoffman, B. M.; Petering, D. H. Coboglobins: Oxygen-Carrying Cobalt-Reconstituted Hemoglobin and Myoglobin. *Proc. Natl. Acad. Sci. U.S.A.* **1970**, *67*, 637-643. (b) Jones, R. D.; Summerville, D. A.; Basolo F. Synthetic Oxygen Carriers Related to Biological Systems. *Chem. Rev.* **1970**, *79*, 139-179. (c) Smith, T. D.; Pilbrow, J. R. Recent Developments in the Studies of Molecular Oxygen Adducts of Cobalt(II) Compounds and Related Systems. *Coord. Chem. Rev.* **1981**, *39*, 295-383.
- (5) (a) Mu, X. H.; Kadish, K. M. Oxidative Electrochemistry of Cobalt Tetraphenylporphyrin

- under a CO Atmosphere. Interaction between Carbon Monoxide and Electrogenerated [(TPP)Co]⁺ in Nonbonding Media. *Inorg. Chem.* **1989**, *28*, 3743-3747. (b) Hu, Y.; Han, B. C.; Bao, L. Y.; Mu, X. H.; Kadish, K. M. Electrochemistry of (octaethylporphinato)cobalt(II), (OEP)Co, under a Carbon Monoxide Atmosphere. Electrogeneration and Characterization of [(OEP)CoIII(CO)]⁺. *Inorg. Chem.* **1991**, *30*, 2444-2446. (c) Schmidt, E.; Zhang, H.; Chang, C. K.; Babcock, G. T.; Oertling, W.A. Room Temperature Binding of CO to Cobaltous Porphyrin π Cation Radical: Spectroscopic Characterization of Mono and Bis CO Complexes with Cobaltic Porphyrin. *J. Am. Chem. Soc.* **1996**, *118*, 2954-296. (d) Kadish, K. M.; Li, J.; Caemelbecke, E. V.; Ou, Z.; Guo, N.; Auret, M.; D'Souza, F.; Tagliatesta, P. Electrooxidation of Cobalt(II) β -Brominated-Pyrrole Tetraphenylporphyrins in CH₂Cl₂ under and N₂ or a CO Atmosphere. *Inorg. Chem.* **1997**, *36*, 6292-6298. (e) Shi, C.; Anson, F. C. Catalysis of the Electro-Oxidation of Carbon Monoxide by Cobalt Octaethylporphyrin. *Inorg. Chem.* **2001**, *40*, 5829-5833.
- (6) (a) Wayland, B. B.; Mohajer, D. Cobalt(II)-tetraphenylporphyrin Complex with Carbon Monoxide. *J. Am. Chem. Soc.* **1971**, *93*, 5295-5296. (b) Wayland, B. B.; Minkiewicz, J. V.; Abd-Elmageed, M. E. Spectroscopic Studies for Tetraphenylporphyrincobalt(II) Complexes of Carbon Monoxide, Nitrogen Oxide, Molecular Oxygen, Methylisonitrile, and Trimethyl Phosphite, and a Bonding Model for Complexes of Carbon Monoxide, Nitrogen Oxide, and Molecular Oxygen with Cobalt(II) and Iron(II) Porphyrins. *J. Am. Chem. Soc.* **1974**, *96*, 2795-2801. (c) Kozuka, M.; Nakamoto, K. Vibrational Studies of

- (tetraphenylporphyrinato)cobalt(II) and its Adducts with Carbon Monoxide, Nitric Oxide, and Oxygen in Gas Matrixes. *J. Am. Chem. Soc.* **1981**, *103*, 2162-2168.
- (7) Feng, D.; Chung, W.-C.; Wei, Z.; Gu, Z. Y.; Jiang, H.-L.; Chen, Y.-P.; Darensbourg, D. J.; Zhou, H.-C. Construction of Ultrastable Porphyrin Zr Metal-Organic Frameworks through Linker Elimination. *J. Am. Chem. Soc.* **2013**, *135*, 17105-17110.
- (8) Anderson, J. S.; Gallagher, A. T.; Mason, J. A.; Harris, T. D. A Five-Coordinate Heme Dioxygen Adduct Isolated within a Metal-Organic Framework. *J. Am. Chem. Soc.* **2014**, *136*, 16489-16492.
- (9) Gallagher, A. T.; Kelty, M. L.; Park, J. G.; Anderson, J. S.; Mason, J. A.; Walsh, J. P. S.; Collins, S. L.; Harris, T. D. Dioxygen Binding at a Four-Coordinate Cobaltous Porphyrin Site in a Metal-Organic Framework: Structural, EPR, and O₂ Adsorption Analysis. *Inorg. Chem. Front.* **2016**, *3*, 536-540.
- (10) (a) Wayland, B. B.; Mehne, L. F.; Swartz, J. Mono- and Biscarbonyl Complexes of Iron(II) Tetraphenylporphyrin. *J. Am. Chem. Soc.* **1978**, *100*, 2379-2383. (b) Silvernail, N. J.; Noll, B. C.; Schulz, C. E.; Scheidt, W. R. Coordination of Diatomic Ligands to Heme: Simply CO. *Inorg. Chem.* **2006**, *45*, 7050-7052.
- (11) Housecroft, C.E.; Sharped, A.G. *Inorganic Chemistry*, 4th ed.; Pearson Education Limited: England, 2001.
- (12) Seufert, K.; Bocquet, M.-L.; Auwarter, W.; Weber-Bargioni, A.; Reichert, J.; Lorente, N.; Barth, J. V. *Cis*-dicarbonyl Binding at Cobalt and Iron Porphyrins with Saddle-Shape

- Conformation. *Nat. Chem.* **2011**, *3*, 114-119.
- (13) Dolphin, D. *The Porphyrins, Vol. 3: Physical Chemistry*; Academic: New York, 1978.
- (14) Stoll, S.; Schweiger, A. EasySpin, a Comprehensive Software Package for Spectral Simulation and Analysis in EPR. *J. Magn. Reson.*, **2006**, *178*, 42-55.
- (15) (a) McGarvey, B. R. Theory of the Spin Hamiltonian Parameters of Low Spin Cobalt(II) Complexes. *Can. J. Chem.* **1975**, *53*, 2498-2511. (b) Ceulemans, A.; Dendooven, M.; Vanquickenborne, L. G. Unusual Ligand Field Effects in Square-Planar Cobalt(II) Complexes of Quadridentate Schiff Bases. *Inorg. Chem.* **1985**, *24*, 1159-1165.
- (16) Abraham, A.; Bleaney, B. *Electron Paramagnetic Resonance of Transition Ions*; Dover Publications, Inc: New York, 1968.
- (17) (a) Griffith, J. S. The Electronic Structures of Some First Transition Series Metal Porphyrins and Phthalocyanines. *Discuss. Faraday Soc.* **1958**, *26*, 81-86. (b) Maki, A. H.; Edelstein, N.; Davidson, A.; Holm R. H. Electron Paramagnetic Resonance Studies of the Electronic Structures of Bis(maleonitriledithiolato)copper(II), -nickel(III), -cobalt(II), and -rhodium(II) Complexes. *J. Am. Chem. Soc.* **1964**, *86*, 4580-4587. (c) Engelhardt, L. M.; Green, M. Ligand-Field Calculations for Cobalt(II) Compounds. *J. Chem. Soc., Dalton Trans.* **1972**, 724-728. (d) Poulos, T. L. Heme Enzyme Structure and Function. *Chem. Rev.* **2014**, *114*, 3919-3962.
- (18) Van Doorslaer, S.; Schweiger, A. A Continuous Wave and Pulse Electron Paramagnetic Resonance Study of Co(II) (tetraphenylporphyrin) in Different Matrices. *Phys. Chem.*

- Chem. Phys.* **2001**, *32*, 159-166.
- (19) Traylor, T. G.; Berzins, A.P. Binding of O₂ and CO to Heme and Hemoproteins. *Proc. Natl. Acad. Sci. USA* **1980**, *77*, 3171-3175.
- (20) Benito-Garagorri, D.; Lagoja, I.; Veiros, L. F.; Kirchner, K. A. Reactivity of Coordinatively Unsaturated Iron Complexes Towards Carbon Monoxide: to Bind or Not to Bind? *Dalton Trans.* **2011**, *40*, 4778-4792.
- (21) Rovira, C.; Kunc, K.; Hutter, J.; Ballone, P.; Parrinello, M. Equilibrium Geometries and Electronic Structure of Iron-Porphyrin Complexes: A Density Functional Study. *J. Phys. Chem. A* **1997**, *101*, 8914-8925.
- (22) (a) Williams, R. J. P. Nature and Properties of Metal Ions of Biological Interest and their Coordination Compounds. *Fred. Proc. Am. Soc. Exp. Biol.* **1961**, *20*, 5. (b) Hoard, J. L.; Hoard, M. J.; Hamor, T. A.; Caughey, W. S. The Crystal Structure of Molecular Stereochemistry of Methoxyiron(III) Mesoporphyrin-IX Dimethyl Ester. *J. Am. Chem. Soc.* **1965**, *87*, 2312-2319. (c) Scheidt, W. R.; Reed, C. A. Spin-state/Stereochemical Relationships in Iron Porphyrins: Implications for the Hemoproteins. *Chem. Rev.* **1981**, *81*, 543-555. (d) Meunier, B.; de Visser, S. P.; Shaik, S. Mechanism of Oxidation Reactions Catalyzed by Cytochrome P450 Enzymes. *Chem. Rev.* **2004**, *104*, 3947-3980.
- (23) Reed, D. A.; Xiao, D. J.; Gonzalez, M. I.; Darago, L. E.; Herm, Z. R.; Grandjean, F.; Long, J. R. Reversible CO Scavenging via Adsorbate-Dependent Spin State Transitions in an Iron(II)-Triazolate Metal-Organic Framework. *J. Am. Chem. Soc.* **2016**, *138*, 5594-5602.

- (24) Runčevski, T.; Kapelewski, M. T.; Torres-Gavosto, R. T.; Tarver, J. D.; Brown, C. M.; Long, J. R. Adsorption of Two Gas Molecules at a Single Metal Site in a Metal-Organic Framework. *Chem. Commun.* **2016**, *52*, 8251-8254.
- (25) Sheldrick, G. M. SADABS (Version 2.03), Bruker Analytical X-Ray Systems, Madison, WI, 2000.
- (26) Sheldrick, G. M. SHELXTL (Version 6.12), Bruker Analytical X-ray Systems Inc., Madison, WI, 2000.
- (27) Dolomanov, O.V.; Bourhis, L. J.; Gildea, R. J.; Howard, J. A. K.; Puschmann, H. OLEX2: A Complete Structure Solution, Refinement and Analysis Program. *J. Appl. Crystallogr.* **2009**, *42*, 339-341.
- (28) Muller, P.; Herbst-Irmer, R.; Spek, A.; Schneider T.; Sawaya, M. Crystal Structure Refinement: A Crystallographer's Guide to SHELXL, OUP, Oxford, 2006.
- (29) Morris, W.; Voloskiy, B.; Demir, S.; Gándara, F.; McGrier, P.L.; Furukawa, H.; Cascio, D.; Stoddart, J.F.; Yaghi, O.M. Synthesis, Structure, and Metalation of Two New Highly Porous Zirconium Metal-Organic Frameworks. *Inorg. Chem.* **2012**, *51*, 6443-6445.
- (30) Petricek, V.; Dusek, M.; Palatinus, L. Crystallographic Computation Systems JANA2006: General Features. *Z. Kristallogr.* **2014**, *229*, 345-352.

References for Chapter 6

- (1) Abu-Omar, M. M. In Physical Inorganic Chemistry; Bakac, A., Ed.; Wiley: Hoboken, NJ, 2010; Chapter 3.

- (2) (a) Scepaniak, J.J.; Margarit, C.G.; Harvey, J.N.; Smith, J.M. Nitrogen atom transfer from iron(IV) nitrido complexes: a dual-nature transition state for atom transfer. *Inorganic Chemistry* **2011**, *50*, 9508-9517.
- (3) (a) Groves, J. T. In *Cytochrome P450 Structure, Mechanism, and Biochemistry*, 3rd ed.; Ortiz de Montellano, P. R., Ed.; Kluwer, New York, 2005. (b) Ortiz de Montellano, P. R. Hydrocarbon hydroxylation by Cytochrome P450 enzymes. *Chemical Reviews* **2010**, *110*, 932. (c) Rittle, J.; Green, M. T. Cytochrome P450 compound I: capture, characterization, and C-H bond activation kinetics. *Science* **2010**, *330*, 933.
- (4) (a) Eady, R. R. Structure-function relationships of alternative nitrogenases. *Chemical Reviews* **1996**, *96*, 3013-3030. (b) Hoffman, B.M.; Deam, D.R.; Seefeldt, L.C. Climbing nitrogenase: toward a mechanism of enzymatic nitrogen fixation. *Accounts of Chemical Research* **2009**, *42*, 609-619. (c) Anderson, J.S.; Rittle, J.; Peters, J.C. Catalytic conversion of nitrogen to ammonia by an iron model complex. *Nature* **2013**, *501*, 84-87.
- (5) (a) MacBeth, C. E.; Golombek, A. P.; Young, V. G.; Yang, C.; Kuczera, K.; Hendrich, M. P.; Borovik, A. S. O₂ activation by nonheme iron complexes: monomeric Fe(III)-oxo complex derived from O₂. *Science* **2000**, *289*, 938-941. (b) Bigi, J. P.; Harman, W. H.; Lassalle-Kaiser, B.; Robles, D. M.; Stich, T. A.; Yano, J.; Britt, R. D.; Chang, C. J. A high-spin iron(IV)-oxo complex supported by a trigonal nonheme pyrrolide platform. *Journal of American Chemical Society* **2012**, *134*, 1536-1542.
- (6) (a) Wagner, W.-D.; Nakamoto, K. Formation of nitridoiron(V) porphyrins detected by

- resonance Raman spectroscopy. *Journal of American Chemical Society* **1988**, *110*, 4044-4045. (b) Wagner, W.-D.; Nakamoto, K. Resonance Raman spectra of nitridoiron(V) porphyrin intermediates produced by laser photolysis. *Journal of American Chemical Society* **1989**, *111*, 1590-1598. (c) Nakamoto, K. Resonance Raman spectra and biological significance of a high-valent iron(IV,V) porphyrins. *Coordination Chemistry Reviews* **2002**, *226*, 153-165. (d) Alcalde, A.N.; George, S.D.; Mienert, B., Bill, E.; Wieghardt, K.; Neese, F. The geometric and electronic structure of [(cyclam-acetato)Fe(N)]⁺: A genuine iron(V) species with a ground-state spin $S = \frac{1}{2}$. *Angewandte Chemie International Edition* **2005**, *44*, 2908-2912. (e) Berry, J.F.; Bill, E.; George, S.D.; Mienert, B.; Neese, F.; Wieghardt, K. Complex of iron(VI). *Science* **2006**, *312*, 1937-1941.
- (7) (a) Berry, J. F. Terminal nitrido and imido complexes of the late transition metals. *Comments Inorganic Chemistry* **2009**, *30*, 28-66. (b) Verma, A. K.; Nazif, T. N.; Achim, C.; Lee, S. C. A stable terminal imide on iron. *Journal of American Chemical Society* **2000**, *122*, 11013-11014.
- (8) Chin, D.H.; La Mar, G.N.; Blach, A.L. Mechanism of autoxidation of iron(II) porphyrins. Detection of peroxo-bridged iron(III) porphyrin dimer and the mechanism of its thermal decomposition to the oxo-bridged iron(III) porphyrin dimer. *Journal of American Chemical Society* **1980**, *102*, 4344-4350.
- (9) (a) Vogel, C., Heinemann, F.W., Sutter, J., Anthone. C., and Meyer, K. An iron nitride complex. *Angewandte Chemie International Edition*, **2008**, *47*, 2681-2684. (b) Scepaniak,

- J.J., Fulton, M.D., Bontchev, R.P., Duesler, E.N., Kirk, M.L., Smith, J.M. Structural and spectroscopic characterization of an electrophilic iron nitrido complex. *Journal of American Chemical Society* **2008**, *130*, 10515-10517.
- (10) (a) Cho, S.H.; Ma, B.; Nguyen, S. Y.; Hupp, J.T.; Albercht-Schmitt, T.E.; A metal-organic framework material that functions as an enantioselective catalyst for olefin epoxidation. *Chemical Communications* **2006**, 2563-2565. (b) Horike, S.; Dincă, M.; Tamaki, K.; Long, J.R. Size-selective lewis acid catalysis in a microporous metal-organic framework with exposed Mn²⁺ coordination sites. *Journal of American Chemical Society* **2008**, *130*, 5854-5855. (c) Liu, D.; Lu, K.; Poon, C.; Lin, W. Metal-organic frameworks as sensory materials and imaging agent. *Inorganic Chemistry* **2014**, *53*, 1916-1924.
- (11) Feng, D.; Chung, W.-C.; Wei, Z.; Gu, Z.-Y.; Jiang, H.-L.; Chen, Y.-P.; Darenbourg, D. J.; Zhou, H.-C. Construction of ultrastable porphyrin Zr metal-organic framework through linker elimination. *Journal of the American Chemical Society* **2013**, *135*, 17105-17110.
- (12) Cohen, I.A.; Summerville, D.A. Metal-metal interactions involving metalloporphyrins. III. Conversion of a tetraphenylporphyrinatoiron(III) azide to a N-bridged hemin dimer. *Journal of American Chemical Society* **1976**, *98*, 1747-1752.
- (13) Kelty, M. L.; Morris, W.; Gallagher, A. T.; Anderson, J. S.; Brown, K. A.; Mirkin, C. A.; Harris, T. D. High-Throughput Synthesis and Characterization of Nanocrystalline Porphyrinic Zirconium Metal-Organic Framework. *Chemical Communications* **2016**, *52*, 7854-7857.

Chapter 7 References

- (1) (a) Anderson, J. S.; Gallagher, A. T.; Mason, J. A.; Harris, T.D. *J. Am. Chem. Soc.* **2014**, *136*, 16489. (b) Gallagher, A. T.; Kelty, M. L.; Park, J. G.; Anderson, J. S.; Mason, J. A.; Walsh, J. P. S.; Collins, S. L.; Harris, T. D. *Inorg. Chem. Front.* **2016**, *3*, 536.
- (2) (a) Nasset, M. J. M.; Shokhirev, N. V.; Enemark, P. D.; Jacobson, S. E.; Walker, F. A. *Inorg. Chem.* **1996**, *35*, 5188. (b) Wu, Y.; Komatsu, T.; Tsuchida, E. *Inorg. Chim. Acta* **2001**, *322*, 120.
- (3) Dolphin, D. *The Porphyrins, Vol. 3: Physical chemistry*; Academic: New York, 1978.
- (4) Hu, C.; An, J.; Noll, B. C.; Schulz, C. E.; Schedit, W. R. *Inorg. Chem.* **2006**, *45*, 4177.